Molecular dynamics simulations of thermodynamic and dynamical properties of liquids and supercritical fluids

Ling Wang

Submitted in partial fulfillment
of the requirements of the Degree of
Doctor of Philosophy

21 Jan 2019

School of Physics and Astronomy
Queen Mary, University of London

Queen Mary
University of London

Statement of originality

I, Ling Wang, confirm that the research included within this thesis is my own work or that where it has been carried out in collaboration with, or supported by others, that this is duly acknowledged below and my contribution indicated. Previously published material is also acknowledged below.

I attest that I have exercised reasonable care to ensure that the work is original, and does not to the best of my knowledge break any UK law, infringe any third party's copyright or other Intellectual Property Right, or contain any confidential material.

I accept that the College has the right to use plagiarism detection software to check the electronic version of the thesis.

I confirm that this thesis has not been previously submitted for the award of a degree by this or any other university.

The copyright of this thesis rests with the author and no quotation from it or information derived from it may be published without the prior written consent of the author.

.....

Ling Wang

21 Jan 2019

Abstract

Liquid is the least understood state of matter from theoretical point of view among solids, liquids and gases. This is due to the strong interactions and large displacement in liquids compared to solids and gases and, consequently, the absence of a small parameter in liquids. The aim in this thesis is to gain some fundamental understanding of liquids and supercritical fluids on the basis of extensive molecular dynamics simulations.

The work begins with revisiting the solid-like approach to liquid thermodynamics based on collective modes. The simulations provide the direct evidence that liquid energy and specific heat are well described by the temperature dependence of the Frenkel frequency. The agreement between predicted and calculated thermodynamic properties is seen in both subcritical and supercritical states. I subsequently detect the structural crossover of the medium-range order at the Frenkel line seen from the behaviour of the peaks of the pair distribution function. The results offer insights into inter-relationships between structure, dynamics and thermodynamics in liquids and supercritical fluids.

I subsequently calculate the Grüneisen parameter (GP) in the supercritical state and find that it decreases with temperature from 3 to 1 on isochores depending on the density. The wide range GP results which includes the solid-like values - an interesting finding in view of the common perception of the supercritical state as being an intermediate state between gases and liquids. GP is also found nearly constant at the Frenkel line above the critical point.

Collective modes above the Frenkel line at extreme supercritical conditions are studied. Direct evidence is presented for propagating longitudinal phonon-like excitations with wavelengths extending to interatomic separations deep in the supercritical state. Finally, I address the thermodynamic crossover seen as the change of most important system properties such as energy and heat

capacity at the Frenkel line.

Acknowledgements

First of all, I would like to thank my supervisors Dr. Kostya Trachenko and Prof. Martin Dove for offering me this research opportunity and their guidance during my PhD study. I am grateful to Kostya for his close and patient guidance, various effort and leading the project. I thank Martin for being a problem solver when I was stuck with simulation and his contribution to the experimental work. It is my honour and great pleasure to work with them both.

I thank our long-term collaborator Prof. Vadim Brazhkin for useful suggestions and discussion to this project and generously acting as a third supervisor sometimes.

I am grateful to all academics in CCMMP group for discussion. I thank Dr. Chenxing Yang for teaching me how to run a simulation at the beginning of my PhD and many other helps. I thank former and current group members Dr. Eleftherios Andritsos, Dr. Yuanpeng Zhang, Dr. Dabiao Liu, Dr. Oliver Dicks, Jiaxun Liu, Aaron Diver and Guanqun Cai for useful and interesting discussion.

Finally, special thanks to my parents and brother. Thanks for their support and love.

This work was supported by the China Scholarship Council.

Contents

List of Figures

List of Abbreviations

MD	molecular dynamics
FL	Frenkel line
IXS	inelastic X-ray scattering
NMR	nuclear magnetic resonance
GP	Grüneisen parameter
DD	Domain Decomposition
VV	Velocity Verlet
NVE	microcanonical ensemble
NPT	isothermal-isobaric ensemble
LJ	Lennard-Jones
EAM	embedded atom model
VAF	velocity autocorrelation function
VFT	Vogel-Fulcher-Tammann
DOS	density of states
PDFs	Pair distribution functions
BZ	Brillouin zone

MFP	mean free path
NIST	National Institute of Standards and Technology

Chapter 1

Introduction

1.1 Challenge in studying liquid theory

It is an interesting fact that the liquid state has proven to be difficult to describe theoretically throughout the history of condensed matter research [1, 2, 3, 4, 5, 6, 7, 8, 9, 10, 11, 12].

In a weakly-interacting system such as a dense gas, the potential energy is much smaller than the kinetic energy. These systems are amenable to perturbation treatment giving corrections to the non-interacting case [5]. Perturbation approaches have been widely studied in calculating liquid thermodynamic properties but have not been able to agree with experiments. For example, the analysis of tractable models such as van der Waals or hard-spheres systems returns the gas-like result for the liquid constant-volume specific heat $c_v = \frac{3}{2}k_B$ [12, 13, 14]. This is in contrast to experimental results showing that c_v of monatomic liquids close to the melting point is nearly identical to the solid-like result, $c_v = 3k_B$ and decreases to about $2k_B$ at high temperature [15, 16]. As expected on general grounds, the perturbation approach does not work for strong interacting systems.

Strong interactions are successfully treated in solids, crystals or glasses,

where the harmonic model is a good starting point and gives the most of the system's energy. However, this approach requires fixed reference points around which the energy expansion can be made. With small vibrations around mean atomic positions, solids meet this requirement but liquids seemingly do not: liquid ability to flow implies that the reference lattice is not existing.

Therefore, liquids seemingly have no simplifying features such as small interactions of gases or small displacements of solids [12]. In other words, liquids have no small parameter that could simplify their theoretical description.

1.2 History of liquid research

In view of the liquid fluidity, the thermodynamic properties of liquids was first approached from the gas state. This approach combines the kinetic energy of the gas and the potential energy calculated by the perturbation theory where using liquids interatomic potentials. As we all know, one of the most difficulties in understanding liquids is that the interactions in liquids are strong and system-dependent. For this reason, it is impossible to derive a general equation of liquid thermodynamics from this approach [17].

The approach from the gas state is destined as a failure, therefore liquids was treated as general strong interacting disordered systems. A lot of work was focused on the structure and dynamics of liquids afterwards. In the phase diagram, liquids not far from the melting points have the similar properties as in solids. These properties include density, heat capacity, bulk moduli, and other main properties. Among these solid-like liquids research, Frenkel's phonon theory plays a significant role in the history of liquid research. In 1932, Frenkel used the term phonon as the first time in his publications. As mentioned in [17], many liquid theories when stripped in details, are essentially due to Frenkel to a large amount.

In this work, based on Frenkel's ideas, we use phonon theory to calculate liquid thermodynamics and study supercritical fluids.

1.3 Supercritical fluids

1.3.1 Motivation of studying supercritical fluids

A supercritical fluid is any substance at its temperature and pressure exceed the critical point [18]. No differences between liquids and gases are believed to exist in the supercritical state and the supercritical fluids show the properties of both liquids and gases.

Since the discovery in 1822 of supercritical state, supercritical fluid technology has been widely used in extraction and purification in the food and pharmaceuticals industry and for techniques such as removing actinides in nuclear waste. It is widely considered that more efficient use of supercritical fluids is limited by the lack of fundamental understanding of the supercritical state and theoretical guidance [18, 19]. To enhance the use of supercritical liquids as effective cleaning and dissolving agents in the future, we need to understand atomic dynamics in the supercritical region. Such an understanding has been absent until now.

1.3.2 The idea of Frenkel line

It was generally agreed that in supercritical region a distinction between liquid and gas phases does not exist, and that changing pressure or temperature gives monotonic property changes only. It was proposed that this is not the case and there is a new dynamical line above the critical point [13, 20]. This new line separates two states with qualitatively distinct physical properties. The new line is called the "Frenkel line (FL)" and it exists at arbitrarily high

pressure and temperature above the critical point. This will be discussed in more details later on.

Frenkel line corresponds to the qualitative changes of the particle dynamics. It changes from combined oscillatory and diffusive motion below the line to purely diffusive motion above the line. Some key physical properties change as well across the Frenkel line in the supercritical region, including diffusion, viscosity, thermal conductivity, specific heat and speed of sound as well as structure. In addition, the combination of gas-like dynamics and high density on the new Frenkel line gives the largest diffusion constants and dissolution rates, and therefore near the Frenkel line the supercritical fluids have the most effective cleaning and dissolving ability [18, 19].

This work focuses on the thermodynamic, dynamical and structural properties change across the Frenkel line including heat capacity, pair distribution function and so on.

1.3.3 Widom line

Another popular study in the supercritical state is the Widom line. Some thermo-physical properties have maxima in the vicinity of a critical point, for example, heat capacity, isothermal compression, heat expansion coefficients etc [21]. These maxima define a line emanating from the critical point, named the "Widom line" [22]. The Widom line is the continuation of the line of maxima and was proposed to demonstrate the crossover between liquid-like and gas-like behaviour in the supercritical fluids [23].

From the study of inelastic X-ray scattering (IXS) and molecular dynamics simulation, the Widom line can only be measured by 2 to 3 times the critical temperature and pressure [23]. On the other hand, the Frenkel line can exist on the phase diagram above the critical point at arbitrarily high pressure and

temperature [13] as long as the chemical bonding does not change (e.g. due to ionization).

1.4 Thesis outline

The work in this thesis aims to gain some fundamental understanding of liquids and supercritical fluids. This is mostly achieved by classical molecular dynamics (MD) simulation.

Molecular dynamics simulation is introduced in Chapter 2. Firstly, I briefly introduce the simulation package DL_POLY which is used in my simulations. This is followed by the discussion of algorithms, ensembles and interatomic potentials in DL_POLY.

In Chapter 3, I revisit the solid-like approach to liquid thermodynamics based on collective modes. I perform molecular dynamics simulations of noble, molecular and metallic liquids and provide the direct evidence that liquid energy and specific heat are well described by the temperature dependence of the Frenkel frequency. I demonstrate the agreement between predicted and calculated thermodynamic properties in a wide range of temperature spanning tens of thousands of Kelvin. The simulated temperature range includes both subcritical liquids and supercritical fluids.

In Chapter 4, I detect the structural crossover of the medium-range order at the Frenkel line. I observe the slope change of the peaks height of the pair distribution function (PDF) and the disappearance of the higher order peaks of the PDF in different systems. The results offer insights into inter-relationships between structure, dynamics and thermodynamics in liquids and supercritical fluids.

I subsequently study the thermo-mechanical properties of matter at extreme conditions deep in the supercritical state. In Chapter 5, I calculate the

Grüneisen parameter γ in the supercritical state and find that on isochores it decreases with temperature from 3 to 1, depending on the density. The wide range of γ includes the solid-like values, which is an interesting finding in view of the common perception of the supercritical state as being an intermediate state between gases and liquids. This result is rationalized by considering the relative weights of oscillatory and diffusive components of the supercritical system below the Frenkel line. γ is also found nearly constant at the Frenkel line above the critical point and this universality has been explained in terms of pressure and temperature scaling of system properties along the lines where the particle dynamics changes qualitatively.

In Chapter 6, I extend the work to study the collective modes above the Frenkel line at extreme supercritical conditions. Direct evidence is presented for propagating solid-like longitudinal phonon-like excitations with wavelengths extending to interatomic separations deep in the supercritical state at temperatures up to 3,300 times the critical temperature. I observe a crossover from the phonon regime to the mean free path (MFP) regime of particle motion which moves to lower k-points with temperature.

In Chapter 7, the evidence has been provided for the thermodynamic crossover seen as the change of the energy and heat capacity in liquids and supercritical fluids and attribute the crossover to the Frenkel line.

In Chapter 8, I make a conclusion of the presented results in this thesis and list some remaining questions to explore in the future.

Chapter 2

Molecular dynamics simulation

Molecular dynamics is the method based on solving classical equations of motion (Newton's equations) for a set of molecules. This was first accomplished by Alder and Wainwright (1957, 1959) for a system of hard spheres [24, 25, 26]. Computer simulation developed rapidly afterwards. In 1964, Rahman achieved the next major advance by using a realistic potential for liquid argon for the first time [27]. This is extended to more complicated systems such as water by Rahman and Stillinger in 1974 [28]. The first protein simulations was reported in 1977 with the simulation of the bovine pancreatic trypsin inhibitor [29].

Computer simulation of liquid state is important in view of the difficulties of their theoretical description [11]. One of the major topics in this study is the supercritical state where the temperature and pressure can be extremely high. It would be difficult or impossible to carry out experiments under extremes of temperature and pressure. Therefore, physical properties from experimental point of view are limited. Computer simulations can provide microscopic details and macroscopic properties directly even at very high temperature and pressure.

2.1 DL_POLY

There are two forms of DL_POLY MD packages available, DL_POLY Classic and DL_ POLY 4. DL_POLY 4 is a general purpose MD package developed at Daresbury Laboratory by W. Smith and I. T. Todorov. The most important difference between DL_POLY Classic and DL_ POLY 4 is that their parallelism are achieved by different strategies. DL_POLY Classic parallelism is based on replicated data strategy and DL_POLY 4 is based on the Domain Decomposition (DD) strategy [30, 31, 32, 33, 34, 35] which makes DL_ POLY 4 more suitable for large molecular simulations systems from 10^4 to 10^9 atoms. I use DL_POLY 4 in my simulations.

2.2 Velocity Verlet algorithm

There are several ways to integrate classical equations of motion. I describe one of them, the Velocity Verlet (VV) algorithm, which is the default integration algorithm of DL_ POLY 4 and it is simple and time reversible [36]. The VV algorithm has two steps (VV1 and VV2). At the first step the simulation requires the initial values of position $r(t)$, velocity $v(t)$ and force $f(t)$ at time t. The first step is to calculate the velocities at half timestep $t + (1/2)\Delta t$ based on Newton's second law:

$$v(t + \frac{1}{2}\Delta t) = v(t) + \frac{\Delta t}{2}\frac{f(t)}{m} \tag{2.1}$$

Where Δt is the timestep, m is the mass. Substituting the above equation into position function, gives new positions as

$$r(t + \Delta t) = r(t) + v(t + \frac{1}{2}\Delta t)\Delta t \tag{2.2}$$

The second step is to advance the velocities to a full step $t + \Delta t$ using the new half-step velocities. Between the first and the second stage, it should be

noted that the forces have changed from $f(t)$ to $f(t+\Delta t)$ since the positions have changed. The velocities at $t+\Delta t$ are

$$v(t+\Delta t) = v(t+\frac{1}{2}\Delta t) + \frac{\Delta t}{2}\frac{f(t+\Delta t)}{m} \tag{2.3}$$

Therefore, the VV algorithm is using the half timestep method to increase the accuracy in simulation. The timestep plays an important role in the accuracy and should be chosen carefully. For example, if smaller timestep is used to increase the accuracy, it would result in the increase of computational cost.

2.3 Thermodynamic ensembles

The energy, volume and the number of particles are constant in microcanonical (NVE) ensemble [11]. Classical mechanics conserve energy by using Newton's equations of motion. In microcanonical ensemble, the probability density is proportional to

$$\delta(\mathcal{H}(\Gamma) - E) \tag{2.4}$$

where Γ is the particle positions and momenta and $\mathcal{H}$ is the Hamiltonnian.

Another popular ensemble is isothermal-isobaric (NPT) ensemble where pressure is constant [11]. The probability density for the NPT ensemble is proportional to

$$exp(-(\mathcal{H} + PV)/k_B T) \tag{2.5}$$

2.4 Interatomic potentials

The interatomic forces are the cause of atoms moving around [37]. The details of all liquid properties depend on the intermolecular potential. There are two main methods to derive an interatomic potential. One method is fitting to

experiment data, and the other one is to the results of *ab initio* simulations. Three types of potentials have been used in my simulation, Lennard-Jones (LJ) potential [38], Buckingham potential [39] and embedded atom model (EAM) potential [40].

The Lennard-Jones potential is commonly used for simple solids such as Argon and has been proved to work well in liquid state:

$$\phi(r_{ij}) = \frac{A}{r_{ij}^{12}} - \frac{B}{r_{ij}^{6}} \tag{2.6}$$

where A and B are parameters and r_{ij} is the distance between atoms i and j. The first term in Eq. (2.6) is the short-ranged repulsive term due to Pauli exclusion and the second term is the long-ranged attractive term.

In Buckingham potential, the repulsive term is replaced by the more accurate Born-Mayer term:

$$\phi(r_{ij}) = Aexp(\frac{-r_{ij}}{\rho}) - \frac{B}{r_{ij}^{6}} \tag{2.7}$$

where ρ is an adjustable parameter.

EAM potential is one type of density dependent potentials where each interaction depends on the local environment. EAM potential is designed to simulate metallic systems. The general form of the EAM potential is as follows [40]:

$$E_i = \frac{1}{2} \sum_{j=1, j\neq i}^{N} \phi(r_{ij}) + F(\rho_i) \tag{2.8}$$

with

$$\rho_i = \sum_{j=1, j\neq i}^{N} \rho(r_{ij}) \tag{2.9}$$

where N is the number of atoms, E_i is the potential energy of atom i, $\phi(r_{ij})$ is the pairwise potential function between atoms i and j, r_{ij} is the distance between

them, F is the embedding function describing the energy of embedding an atom, and $\rho(r_{ij})$ is another pairwise interaction leading to the density term ρ_i. It should be noted that the density is calculated by the coordination number of the atom defined by *pairs* of atoms, which makes the metal potential depend on the local density.

2.5 Ewald Sum

Ewald Sum is one of the several techniques for dealing with long ranged electrostatic potentials. It is the best method of choice for periodic systems while other techniques can be used with either periodic or non-periodic systems. The Ewald method divides the Coulomb interaction into short-range term which is calculated in real space and long-range term which is calculated in reciprocal space.

In Ewald model, firstly, each ion is effectively neutralised by a spherical gaussian cloud with opposite charge centred on the ion. The combined gathering of point ions and gaussian charges is the real space term of the Ewald sum. Secondly, a gaussian cloud with the same charges as the original point ions centres on the point ions. This is the model of the reciprocal space term in Ewald sum [41].

The Coulomb energy can be calculated by:

$$E_C = \frac{1}{2}\sum_{l}\sum_{i,j}\frac{Q_iQ_j}{2\pi^{3/2}\epsilon_0}\int_0^\infty exp(-r_{ij}^2(l)\rho^2)d\rho \tag{2.10}$$

where r_{ij} is the distance between atoms i and j. Q is the charge of that atom and l is the label of the periodic configuration. We separate the integral into two parts:

$$\int_0^\infty exp(-r^2\rho^2)d\rho = \int_0^g exp(-r^2\rho^2)d\rho + \int_g^\infty exp(-r^2\rho^2)d\rho \tag{2.11}$$

where g is the convergence parameter, we can rewrite Eq. (2.11) with so called complementary error function $erfc(m)$ as:

$$\int_0^\infty exp(-r^2\rho^2)d\rho = \int_0^g exp(-r^2\rho^2)d\rho + \frac{\sqrt{\pi}}{2}\frac{erfc(gr)}{r} \tag{2.12}$$

$$erfc(m) = \frac{2}{\sqrt{\pi}}\int_m^\infty exp(-n^2)dn \tag{2.13}$$

The first term in Eq. (2.12) demonstrates that a gaussian cloud with the same charges of the point ions centres on the point ions. The second term represents the point ion surrounded by the opposite charge cloud, which decreases to zero quickly with increasing r. We transform the first term into the reciprocal space:

$$\frac{2}{\sqrt{\pi}}\sum_l exp(-r_{ij}^2(l)\rho^2) = \frac{2\pi}{V}\sum_G \rho^{-3}exp(-G^2/4\rho^2)exp(iG\cdot r_{ij}) \tag{2.14}$$

The integral in the first term of Eq. (2.12) gives:

$$\int_0^g \rho^{-3}exp(-G^2/4\rho^2)exp(iG\cdot r_{ij})d\rho = \frac{2exp(-G^2/4g^2)}{G^2}exp(iG\cdot r_{ij}) \tag{2.15}$$

where r_{ij} is the vector between atoms i and j, V is the volume of the box, and G is a reciprocal lattice vector.

The above calculations give the real space and reciprocal space term of Ewald sum, the complete Ewald sum requires an additional correction, known as the self-energy correction. The self-energy term arises from a gaussian acting on its own site. The self-energy term can write as:

$$E_{self} = -\frac{1}{4\pi\epsilon_0}\sum_i \frac{g{Q_i}^2}{\sqrt{\pi}} \tag{2.16}$$

The total electrostatic energy with the self-energy term is the sum of Eq. (2.13), Eq. (2.15) and Eq. (2.16):

$$\begin{aligned} E_C = & \frac{1}{2}\sum_{i,j}\frac{Q_iQ_j}{4\pi\epsilon_0}\frac{4\pi}{V}\sum_{G}\frac{exp(-G^2/4g^2)}{G^2}exp(iG\cdot r_{ij}) \\ & +\frac{1}{2}\sum_{i,j}\frac{Q_iQ_j}{4\pi\epsilon_0}\sum_{l}\frac{erfc(gr_{ij}(l))}{r_{ij}(l)} - \frac{1}{4\pi\epsilon_0}\sum_{i}\frac{g{Q_i}^2}{\sqrt{\pi}} \end{aligned} \tag{2.17}$$

Chapter 3

Thermodynamical properties of liquids and supercritical fluids

The discussion of liquids thermodynamic properties has remained scarce and physics textbooks have very little to describe about liquid specific heat, including textbooks dedicated to liquids [1, 2, 3, 4, 5, 6, 7, 8, 9, 10, 11, 12]. This is because in contrast to solids and gases, the interactions in liquids are both strong and system-dependent [12]. This meets the challenge in directly calculating energy and other thermodynamic properties in liquids as the interactions and structure are not known.

As recently reviewed [17], emerging evidence advances our understanding of the thermodynamics of the liquid state. The start point is the early theoretical idea of J. Frenkel [1] who proposed that liquids can be considered as solids at times smaller than liquid relaxation time, τ, the average time between two particle rearrangements at one point in space. This implies that the liquid energy can be calculated similarly as solids. In this Chapter, I provide direct computational evidence of the agreement in calculating liquid thermodynamics (the energy and heat capacity) between phonon theory and MD simulation. Part of the material in this Chapter was previously published in Ref. [42].

3.1 Introduction

Based on the idea of Frenkel, if the observation time is smaller than the liquid relaxation time, liquids can be considered as solids. In terms of the frequency, the phonons in liquids will be similar to those in solids for frequencies above the Frenkel frequency ω_{F}:

$$\omega > \omega_{\mathrm{F}} = \frac{1}{\tau} \tag{3.1}$$

The above argument predicts that liquids are capable of supporting shear modes, the property hitherto attributable to solids only, it should be noted that this statement only applies for the frequencies above ω_{F} in liquids.

Low-frequency modes in liquids, sound waves, are well-understood in the hydrodynamic regime $\omega\tau < 1$ [43], however Eq. (3.1) denotes a distinct, solid-like elastic regime of wave propagation where $\omega\tau > 1$. In essence, this implies the existence of a cutoff frequency ω_{F} above which particles in the liquid can be described by the same equations of motion as in, for example, solid glass. Therefore, liquid collective modes include both longitudinal and transverse modes with frequency above ω_{F} in the solid-like elastic regime and one longitudinal hydrodynamic mode with frequency below ω_{F} (shear mode is not propagating below frequency ω_{F}).

Recall the earlier textbook assertion [12] that a general thermodynamic theory of liquids can not be developed because liquids have no small parameter. How is this fundamental problem addressed here? According to Frenkel's idea, liquids behave like solids with small oscillating particle displacements serving as a small parameter. Large-amplitude diffusive particle jumps continue to play an important role, but do not destroy the existence of the small parameter. Instead, the jumps serve to modify the phonon spectrum: their frequency, ω_{F}, sets the minimal frequency above which the small-parameter description

applies and solid-like modes propagate.

It has taken a long time to verify this picture by experiments. The experimental evidence supporting the propagation of high-frequency (solid-like) modes in liquids currently includes inelastic X-ray, neutron and Brillouin scattering experiments but most important evidence is recent and follows the deployment of powerful synchrotron sources of X-rays [23, 44, 45, 46, 47, 48, 49, 50, 51, 52, 53, 54, 55, 56, 57, 58, 59].

Early experiments found the presence of high-frequency longitudinal acoustic propagating modes and mapped dispersion curves which were in striking resemblance to those in solids [44]. These and similar results were generated at temperature just above the melting. The measurements were later extended to high temperatures considerably above the melting point, confirming the same result. It is now well established that liquids support propagating modes with wavelengths extending down towards interatomic separations, comparable to the wave vectors of phonons in crystals at the Brillouin zone boundaries [23, 45, 46, 47, 48, 49, 50, 51, 52, 53, 54, 55]. More recently, the same result has been asserted for the supercritical fluids [23, 49, 55]. Importantly, the propagating modes in liquids include acoustic transverse modes. These were first seen in highly viscous fluids (see, e.g., Refs. [56, 57]), but were then studied in low-viscosity liquids on the basis of positive dispersion [45, 46, 47] (the presence of high-frequency transverse modes increases sound velocity from the hydrodynamic to the solid-like value). These studies included water [58], where it was found that the onset of transverse excitations coincides with the inverse of liquid relaxation time [59], as predicted by Frenkel [1].

More recently, high-frequency transverse modes in liquids were directly measured in the form of distinct dispersion branches and verified on the basis of computer modelling [50, 51, 52, 53, 54], and the striking similarity between dispersion curves in liquids and their crystalline (poly-crystalline) counterparts

was noted. It should also be noted that the contribution of high-frequency modes is particularly important for liquid thermodynamics because these modes make the largest contribution to the energy due to quadratic density of states (DOS).

The above discussion calls for an important question about liquid thermodynamics. In solids, collective modes, phonons, play a central role in the theory, including the theory of thermodynamic properties. Can collective modes in liquids play the same role, in view of the earlier Frenkel proposal and recent experimental evidence? This question has been started to explore [60] just before the high-frequency transverse modes were directly measured and subsequently developed in a number of ways [17]. This involves calculating the liquid energy as the phonon energy where transverse modes propagate above ω_{F} in Eq. (3.1).

The main aim of this Chapter is to provide direct computational evidence to the phonon theory of liquid thermodynamics and its predictions. This is achieved by calculating the liquid energy and ω_{F} in extensive molecular dynamics simulations. In this Chapter, I briefly discuss the main steps involved in calculating the liquid energy. I then proceed to calculating the liquid energy and Frenkel frequency independently from molecular dynamics simulations using several methods which agree with each other. This is done for three systems chosen from different classes of liquids: noble, metallic and molecular, and find good agreement between predicted and calculated results in the wide range of temperature and pressure. The range includes both subcritical liquids and supercritical state below the Frenkel line where transverse modes propagate.

3.2 Phonon approach to liquid thermodynamics

3.2.1 Liquid energy calculation

The main result of calculation of the liquid energy on the basis of propagating modes is summarized here. A detailed discussion can be found in a recent review [17].

According to the previous discussion, in liquids there are two transverse modes propagating in the solid-like elastic regime with frequency $\omega > \omega_F$. The energy of these transverse modes, together with the energy of the longitudinal mode gives the liquid vibrational energy. In addition to vibrations, particles in the liquids move as diffusive jumps between quasi-equilibrium positions as discussed above. Adding the energy of these jumps to the phonon energy in the Debye model gives the total energy of thermal motion in the liquid [17, 60]:

$$E_T = NT\left(3 - \left(\frac{\omega_F}{\omega_D}\right)^3\right) \tag{3.2}$$

where N is the number of particles and ω_D is transverse Debye frequency and the subscript T refers to thermal motion. Here and below, $k_B = 1$.

At low temperature, $\tau \gg \tau_D$, where τ_D is the Debye vibration period, or $\omega_F \ll \omega_D$. In this case, Eq. (3.3) gives the specific heat $c_v = \frac{1}{N}\frac{dE}{dT}$ close to 3, the solid-like result. At high temperature when $\tau \to \tau_D$ and $\omega_F \to \omega_D$, Eq. (3.3) gives c_v close to 2. The decrease of c_v from 3 to 2 with temperature is consistent with experimental results in monatomic liquids [15, 16]. The decrease of c_v is also seen in complex liquids [61].

Eq. (3.3) attributes the experimental decrease of c_v with temperature to the decrease of the number of transverse modes above the frequency $\omega_F = \frac{1}{\tau}$. The comparison of this effect with experiments can be more detailed if c_v is compared in the entire temperature range where it decreases from 3 to 2. This

meets the challenge that ω_{F} in Eq. (3.3) is not directly available in the cases of interest. ω_{F} (or τ) is measured in dielectric relaxation or nuclear magnetic resonance (NMR) experiments in systems responding to electric or magnetic fields only. These liquids are often complex and do not include simple model systems that are widely studied theoretically such as liquid Ar. Importantly, the range of measured ω_{F} does not extend to high frequency comparable to ω_{D}, and it is in this range where liquid c_v undergoes an important change from 3 to 2 as discussed above. ω_{F} can be calculated from the Maxwell relationship $\omega_{\mathrm{F}} = \frac{G_\infty}{\eta}$, where G_∞ is the instantaneous shear modulus and η is viscosity taken from a different experiment [17]. More recently, it has been suggested [63] that taking the shear modulus at a finite high frequency (rather than infinite frequency) agrees better with the modelling data. Apart from rare estimations [62, 63], G_∞ is not available. In practice, the comparison of experimental c_v and c_v predicted as $\frac{dE}{dT}$ with E given by Eq. (3.3) is done by keeping G_∞ as a free parameter, obtaining a good agreement between experimental and predicted c_v and observing that G_∞ lies in the range of several GPa typical for liquids [17, 60]. In the last few years, Eq. (3.3) and its extensions including the phonon anharmonicity and quantum effects of phonon excitations were demonstrated to account for the experimental c_v of over 20 different systems, including metallic, noble, molecular and network liquids [17].

In view of the persisting problem of liquid thermodynamics, it is important to test Eq. (3.3) directly by linking the liquid energy (and c_v) on one hand and ω_{F} on the other and testing the theory in a precise way. This, together with achieving consistency with other approaches (like, energy fluctuations) to calculate the liquid energy and heat capacity, is what I will discuss later on.

3.2.2 Thermodynamics of supercritical fluids

If the system is below the critical point (see Figure 3.1), the temperature increase eventually results in boiling and the first-order transition, with c_v discontinuously decreasing to about $\frac{3}{2}$ in the gas phase. The intervening phase transition excludes the state of the liquid where c_v can gradually reduce to $\frac{3}{2}$ and where interesting physics operates. However, this becomes possible above the critical point. This brings us to the interesting discussion of the supercritical state of matter. As discussed above, theoretically, little is known about the supercritical state, apart from the general assertion that supercritical fluids can be thought of as high-density gases or high-temperature fluids whose properties change smoothly with temperature or pressure and without qualitative changes of properties. This assertion followed from the known absence of a phase transition above the critical point. It has been recently proposed that this picture should be modified, and that a new line, the Frenkel line, exists above the critical point and separates two states with distinct properties (see Figure 3.1) [13, 14, 20, 64]. Physically, the FL is not related to the critical point and exists in systems where the critical point is absent such as soft-sphere system ($\phi(r_{ij}) \propto \frac{1}{r_{ij}^n}$).

The main idea of the FL lies in considering how the particle dynamics change in response to pressure and temperature. Recall that particle dynamics in the liquid can be separated into solid-like oscillatory and gas-like diffusive components. This separation applies equally to supercritical fluids as it does to subcritical liquids. Indeed, increasing temperature reduces τ, and each particle spends less time oscillating and more time jumping; increasing pressure reverses this and results in the increase of time spent oscillating relative to jumping. Increasing temperature at constant pressure or density (or decreasing pressure at constant temperature) eventually results in the disappearance of the

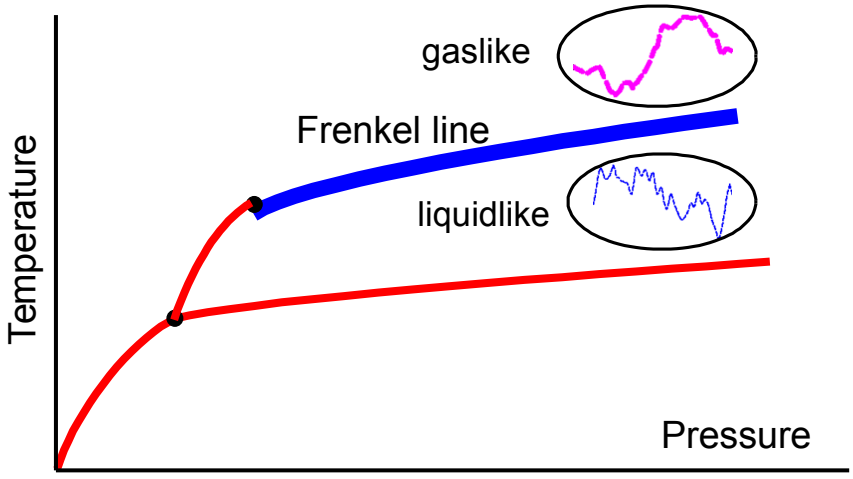

Figure 3.1: The Frenkel line in the supercritical region. Particle dynamics includes both oscillatory and diffusive components below the line, and is purely diffusive above the line. Below the line, the system is able to support rigidity and transverse modes at high frequency. Above the line, particle motion is purely diffusive, and the ability to support rigidity and transverse modes is lost at all available frequencies. Crossing the Frenkel line from below corresponds to the transition between the "rigid" liquid to the "non-rigid" gas-like fluid.

solid-like oscillatory motion of particles; all that remains is the diffusive gas-like motion. This disappearance represents the qualitative change in particle dynamics and gives the point on the FL in Figure 3.1. Most important system properties qualitatively change either on the line or in its vicinity [13, 14, 20, 64]. In a given system, the FL exists at arbitrarily high pressure and temperature, as does the melting line.

Quantitatively, the FL can be rigorously interpreted by pressure and temperature at which the minimum of the velocity autocorrelation function (VAF) disappears [14]. The VAF is defined as:

$$Z(t) = \langle v(0) \cdot v(t) \rangle \tag{3.3}$$

Above the line defined in such a way, velocities of a large number of particles stop changing their sign and particles lose the oscillatory component of motion.

Above the line, VAF is monotonically decaying as in a gas [14]. For the purposes of this discussion, the significance of the FL is that the phonon approach to liquids and Eq. (3.3) apply to supercritical fluids below the FL to the same extent as they apply to subcritical liquids. Indeed, the exisence of an oscillatory component of particle motion below the FL implies that τ is a well-defined parameter and that transverse modes propagate according to Eq. (3.1). The ability of the supercritical system to support solid-like rigidity at frequency above ω_{F} suggested the term "rigid" liquid to differentiate it from the "non-rigid" gas-like fluid above the FL [13, 14].

Therefore, the FL separates the supercritical state into two states where transverse modes can and cannot propagate. This is supported by direct calculation of the current correlation functions [65] showing that propagating and non-propagating transverse modes are separated by the Frenkel line. Interestingly, Eq. (3.3) can serve as a thermodynamic definition of the FL: the loss of the oscillatory component of particle motion at the FL approximately corresponds to $\tau \to \tau_{\mathrm{D}}$ (here, τ_{D} refers to Debye period of transverse modes) or $\omega_{\mathrm{F}} \to \omega_{\mathrm{D}}$. According to Eq. (3.3), this gives c_v of about 2. Using the criterion $c_v = 2$ gives the line that is in remarkably good agreement with the line obtained from the VAF criterion above [14].

3.3 Methods

Liquids from three important system types are considered: noble Ar, molecular CO_2 and metallic Fe. Molecular dynamics simulation package DL_POLY [31] has been used and simulated systems with 8000 Argon, 8000 Iron and 4576 CO_2 particles with periodic boundary conditions. The interatomic potential for Ar is the pair Lennard-Jones potential [38], known to perform well at elevated pressure and temperature. For CO_2 and Fe, I have used interatomic potentials

optimized and tested in the liquid state at high pressure and temperature. The potential for CO_2 is the rigid-body nonpolarizable potential based on a quantum chemistry calculation, with the partial charges derived using the Distributed Multipole Analysis method [39]. Fe was simulated using the many-body embedded-atom potential [40]. The MD systems were first equilibrated in the constant pressure and temperature ensemble at respective state points for 20 ps. System properties were subsequently simulated at different temperatures and averaged in the constant energy and volume ensemble for 30 ps.

It is my purpose to study the properties of real dense strongly-interacting liquids with potential energy comparable to kinetic energy and hence I have chosen fairly high densities: $\rho = 1.5$ g/cm^3 and $\rho = 1.9$ g/cm^3 for Ar, $\rho = 8$ g/cm^3 and $\rho = 11$ g/cm^3 for Fe and $\rho = 1.34$ g/cm^3 for CO_2. The lowest temperature in each simulation was the melting temperature at the corresponding density, T_m. The highest temperature significantly exceeded the temperature at the Frenkel line at the corresponding density, $T_{\rm F}$, taken from the earlier calculation of the Frenkel line in Ar [14], Fe [66] and CO_2 [67]. As discussed above, the temperature range between T_m and $T_{\rm F}$ corresponds to the regime where transverse modes progressively disappear and where Eq. (3.3) applies. I have simulated $100 - 700$ temperature points at each pressure depending on the system. The number of temperature points was chosen to keep the temperature step close to 10 K.

As discussed above, Eq. (3.3) applies to subcritical liquids as well as to supercritical fluids below the Frenkel line. Accordingly, my simulations include the temperature range both below and above the critical temperature. This will be discussed in more details below.

3.4 Results and discussion

3.4.1 Liquid energy and heat capacity

I have calculated ω_{F} in Eq. (3.3) from its definition in Eq. (3.1), as $\omega_{\mathrm{F}} = \frac{1}{\tau}$. τ can be calculated in a number of ways. Most common methods calculate τ as decay time of the self-intermediate scattering or other functions by the factor of e or as the time at which the mean-squared displacement crosses over from ballistic to diffusive regime [68]. These methods give τ in agreement with a method employing the overlap function depending on the cutoff parameter a_c provided $a_c = 0.3a$, where a is the inter-molecular distance [68]. The overlap function is a two-point time correlation function of local density [68, 69, 70, 71, 72, 73]. Since the relaxation times calculated from intermediate scattering function, mean squared displacement and overlap function behave very similarly, in this Chapter I use the data calculated by the overlap function.

I use the overlap function and calculate τ at 13-20 temperature points at each density depending on the system. At each density, I fit τ to the commonly used Vogel-Fulcher-Tammann (VFT) temperature dependence as showed in Eq. (3.4):

$$\tau \propto exp(\frac{A}{T - T_0}) \tag{3.4}$$

where A and T_0 are constants. I have show an example of relaxation time τ of Ar at density $\rho = 1.9$ g/cm^3 calculated by overlap function and fitted by VFT function in Figure 3.2.

I then use $\omega_{\mathrm{F}} = \frac{1}{\tau}$ to calculate the liquid energy predicted from the theory. The predicted c_v is calculated as $c_v = \frac{1}{N}\frac{dE}{dT}$ where E is given by Eq. (3.3). It

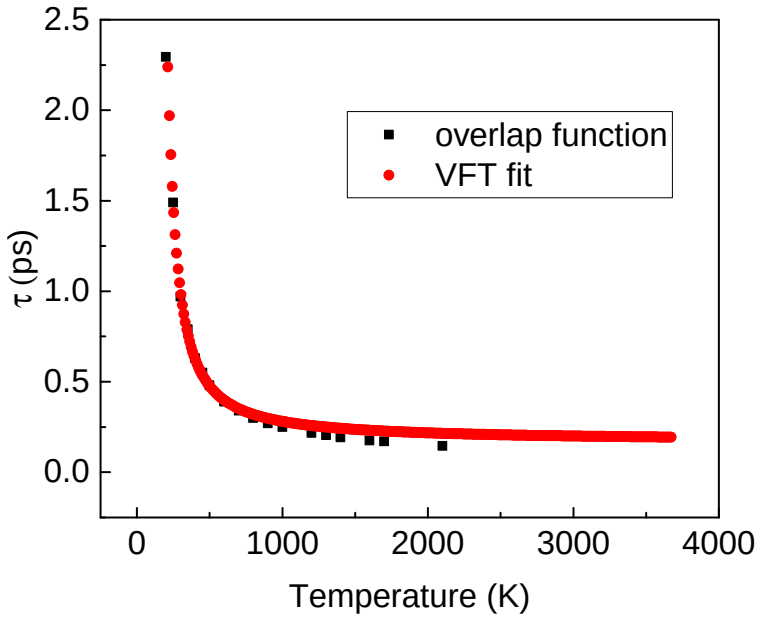

Figure 3.2: Relaxation time τ of Ar at density $\rho = 1.9$ g/cm^3 calculated by overlap function (black points) and fitted data by Vogel-Fulcher-Tammann function (red points).

should be noted that ω_F is a function of temperature T, this gives c_v as:

$$c_v = 3 - \left(\frac{\omega_{\mathrm{F}}}{\omega_{\mathrm{D}}}\right)^3 - \frac{3T\omega_{\mathrm{F}}^2}{\omega_{\mathrm{D}}^3}\frac{d\omega_{\mathrm{F}}}{dT} \tag{3.5}$$

where N is the number of atoms for Ar and Fe and the number of molecules for CO_2.

The first two terms in Eq. (3.5) give $c_v = 2$ when ω_{F} tends to its high-temperature limit of ω_{F}. The last term reduces c_v below 2 by a small amount because $\frac{d\omega_{\mathrm{F}}}{dT}$ is close to zero at high temperature [17].

I now compare the calculated energy and c_v with those directly computed in the MD simulations. It should be noted that the energy in Eq. (3.3) is the energy of thermal phonon motion, E_T, which contributes to the total liquid energy as

$$E = E_0 + E_{\mathrm{T}} \tag{3.6}$$

where E_0 is liquid energy at zero temperature and describes temperature-independent background contribution due to the interaction energy.

In comparing the calculated E_{T} in Eq. (3.3) with the energy from MD simulations, I therefore subtract the constant term from the MD energy. The comparison of $c_v = \frac{1}{N}\frac{dE}{dT}$ is performed directly because the constant term does not contribute to c_v. I have also calculated c_v using the fluctuations formula for the kinetic energy K in the constant energy ensemble: $\langle K^2\rangle - \langle K\rangle^2 = 1.5(k_{\mathrm{B}}T)^2N(1 - 1.5k_{\mathrm{B}}/c_v)$ [74]. Both methods agree well, as shown in Figures 3.3a and 3.3b.

There is only one adjustable parameter in Eq. (3.3), ω_{D}, which is expected to be close to transverse Debye frequency. ω_{F} is independently calculated from the MD simulation as discussed above. In Figures 3.3 and 3.4, I show the energy and c_v calculated on the basis of Eqs. (3.3) and (3.5) and compare them with those computed in MD simulations. Blue circle in each figure represents the critical temperature. Good agreement between predicted and calculated properties is observed in a temperature range including both subcritical and supercritical temperature. This involved using $\tau_{\mathrm{D}} \approx 0.6$ ps ($\rho = 8$ g/cm^3) and $\tau_{\mathrm{D}} \approx 0.2$ ps ($\rho = 11$ g/cm^3) for Fe, $\tau_{\mathrm{D}} \approx 0.9$ ps ($\rho = 1.5$ g/cm^3) and $\tau_{\mathrm{D}} \approx 0.3$ ps ($\rho = 1.9$ g/cm^3) for Ar and $\tau_{\mathrm{D}} \approx 0.5$ ps for CO_2, in reasonable order-of-magnitude agreement with experimental τ_{D} of respective crystalline systems as well as maximal frequencies seen in experimental liquid dispersion curves (see, e.g., [51]). It should be noted that the expected trend of τ_{D} reducing with density.

At high temperature where $\omega_{\mathrm{F}} \approx \omega_{\mathrm{D}}$, Eq. (3.5) predicts c_v close to 2, noting that the last term gives only a small contribution to c_v because ω_{F} becomes slowly varying at high temperature. Consistent with this prediction, the decrease of c_v from 3 to 2 is observed in Figures 3.3 and 3.4.

The agreement between the predicted and calculated results supports the

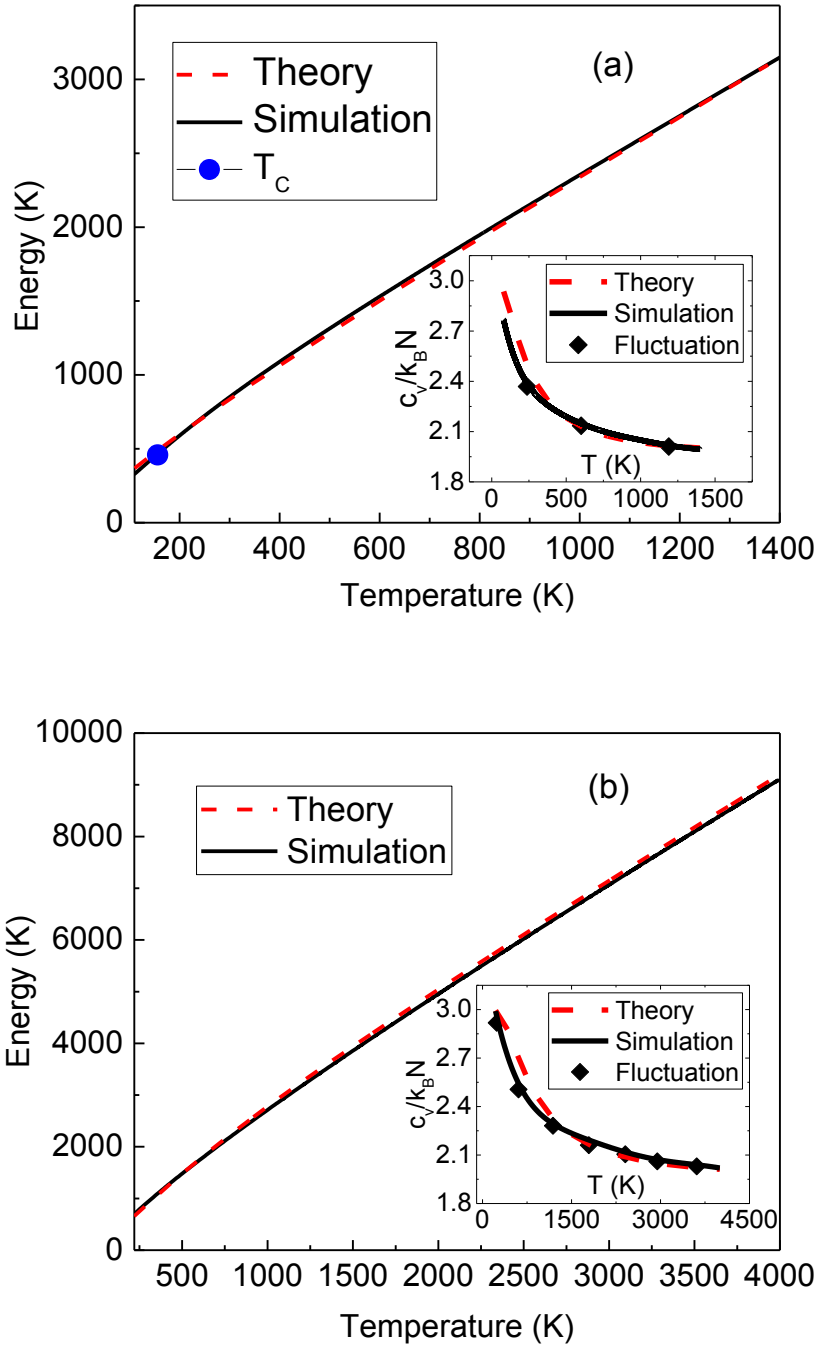

Figure 3.3: Energy per particle and specific heat of Ar at density $\rho = 1.5$ g/cm^3 (a) and $\rho = 1.9$ g/cm^3 (b). Solid and dashed lines correspond to results from simulations and theory, respectively. The large (blue) circle corresponds to critical temperature. The black solid curves in the insets show c_v calculated as $c_v = \frac{1}{N}\frac{dE}{dT}$. Solid diamonds correspond to c_v calculated from the fluctuation formula (see text). The red (dashed) line is the theoretical result for c_v.

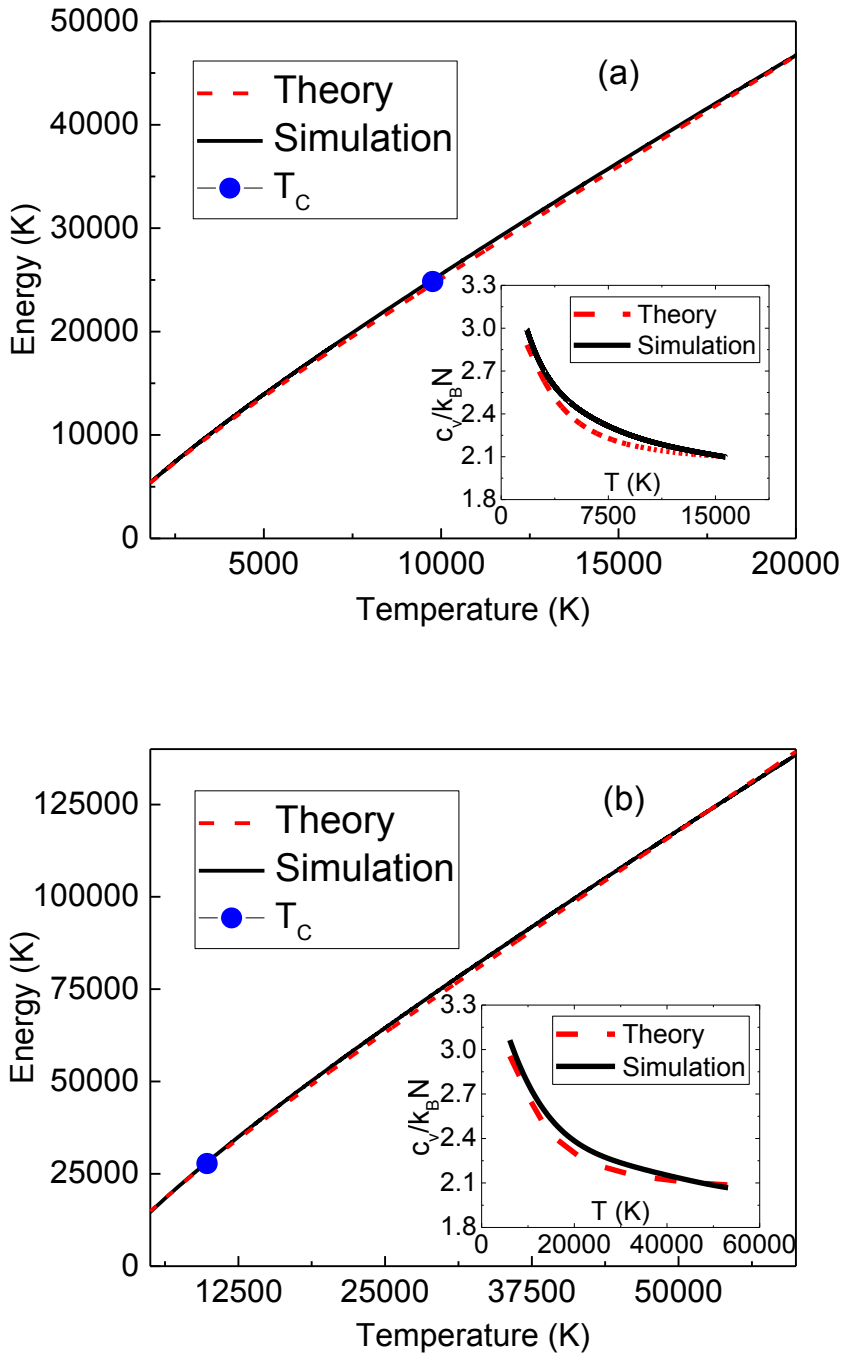

Figure 3.4: Energy per particle and specific heat of Fe at density $\rho = 8$ g/cm^3 (a) and $\rho = 11$ g/cm^3 (b). Solid and dashed lines correspond to results from simulations and theory, respectively. The large (blue) circle corresponds to critical temperature. The black solid curves in the insets show c_v calculated as $c_v = \frac{1}{N}\frac{dE}{dT}$. The red (dashed) line is the theoretical result for c_v.

interpretation of the decrease of c_v with temperature discussed above: ω_{F} decreases with temperature, and this causes the reduction of the number of transverse modes propagating above ω_{F} and hence the decrease of c_v.

For CO_2, the same mechanism operates except the degrees of freedom in a molecular system need to account for. In order to understand this, the case of solid CO_2 is considered. The MD interatomic potential treats CO_2 molecules as rigid linear units, contributing the kinetic term of 2.5 to the specific heat per molecule including 1 from the rotational degrees of freedom of the linear molecular and 1.5 from translations (here, it should be noted that CO_2 molecules librate and rotate in the solid at low and high temperature, respectively [75]). Noting the potential energy contributes the same term due to equipartition, the specific heat becomes 5 per molecule. This implies that for molecular CO_2, Eq. (3.3) modifies as $E_{\mathrm{T}} = NT\left(5 - \left(\frac{\omega_{\mathrm{F}}}{\omega_{\mathrm{D}}}\right)^3\right)$, where N is the number of molecules and ω_{F} is related to the jump frequency of molecules and which gives $c_v = 5$ in the solid state where ω_{F} is infinite. I use the modified equation to calculate the energy and c_v and compare them to those computed from the MD simulation in Figure 3.5.

Consistent with the above discussion, it is observed that c_v for CO_2 calculated directly from the MD simulations is close to 5 at low temperature just above melting. At this temperature, $\omega_{\mathrm{F}} \ll \omega_{\mathrm{D}}$, giving the solid-like value of c_v as in the case of monatomic Ar and Fe. As temperature increases, two transverse modes of inter-molecular motion progressively disappear, resulting in the decrease of c_v to the value of about $c_v = 4$, in agreement with c_v calculated from the theoretical equation for E_{T}.

It should be noted that the temperature range in which I compare the predicted and calculated properties is notably large (e.g., 200-8000 K for Ar, and 2000-55000 K for Fe). This range is 10-100 times larger than those typically considered earlier [17]. The higher temperatures for Fe might appear as

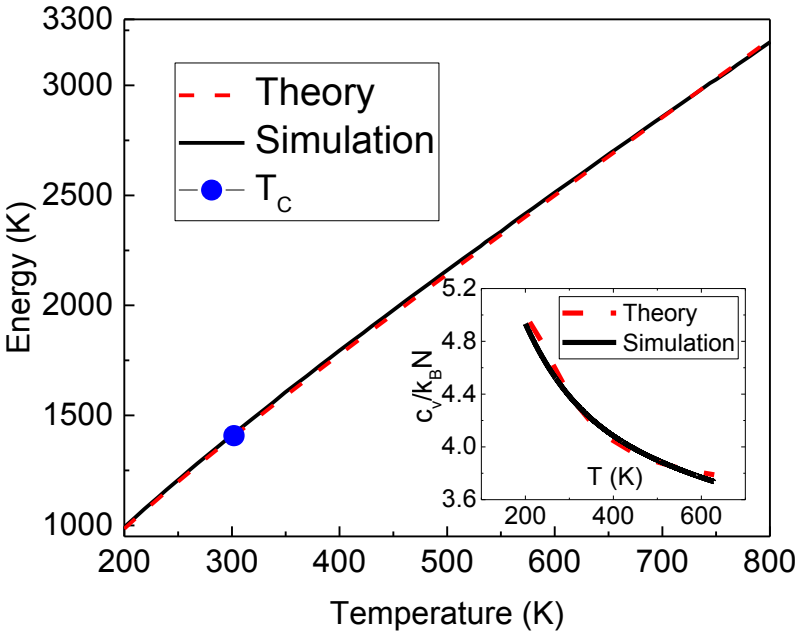

Figure 3.5: Energy per particle and specific heat of CO_2 at density $\rho = 1.34$ g/cm^3. Solid and dashed lines correspond to results from simulations and theory, respectively. The large (blue) circle corresponds to critical temperature. The black solid curves in the insets show c_v calculated as $c_v = \frac{1}{N}\frac{dE}{dT}$. The red (dashed) line is the theoretical result for c_v.

unusual, however it is noted that liquid iron as well as supercritical iron fluid remains an unmodified system up to very high temperature: the first ionization potential of Fe is 7.9 eV, or over 90,000 K. Hence the considered temperature range is below the temperature at which the system changes its structure and type of interactions.

The very wide temperature range reported here is mostly related to the large part of the temperature interval in Figures 3.3-3.5 being above the critical point where no phase transition intervenes and where the liquid phase exists at high temperature, in contrast to subcritical liquids where the upper temperature is limited by the boiling line. The agreement between predicted and calculated properties in such a wide temperature range adds support to the phonon

approach to liquid thermodynamics as proposed.

Three points are addressed below regarding the observed agreement between the calculated and predicted results. First, the collective modes contributing to the thermal energy in (3.3) are considered to be harmonic. The anharmonicity can be accounted for in the Grüneisen approximation, however this involves an additional parameter [17]. I attempted to avoid introducing additional parameters and sought to test Eq. (3.3) which contains only one parameter, ω_{D}.

Second, Eq. (3.3) involves the Debye model and quadratic density of states (DOS). This approximation is justified since the Debye model is particularly relevant for disordered isotropic systems such as glasses [12], which are known to be nearly identical to liquids from the structural point of view. Furthermore, the experimental dispersion curves in liquids are very similar to those in solids such as poly-crystals [52, 53, 54]. Therefore, the Debye model can be used in liquids to the same extent as in solids. One important consequence of this is that the high-frequency range of the phonon spectrum makes the largest contribution to the energy, as it does in solids including disordered solids. It should be noted that liquid DOS can be represented as the sum of solid-like and gas-like components in the two-phase thermodynamic model [76], and the solid-like component can be extracted from the liquid DOS calculated in MD simulations. This can provide more information about the DOS beyond Debye approximation.

Third, Eq. (3.3) assumes a lower frequency cutoff for transverse waves, $\omega_{\mathrm{F}} = \frac{1}{\tau}$, as envisaged by Frenkel in Eq. (3.1). A recent detailed analysis of the Frenkel equations shows that the dispersion relation for liquid transverse modes is $\omega = \sqrt{c_s^2 k^2 - \frac{1}{4\tau^2}}$, where c_s is the shear speed of sound and k is wavenumber [17]. This dispersion relation implies a gap in k-space $k_{gap} = \frac{1}{c\tau}$ (by a factor of 2). Here, ω gradually crosses over from 0 to its solid-like branch

$\omega = c_s k$ when $\omega \gg \omega_F = \frac{1}{\tau}$. In this sense, using a lower frequency cutoff in Eq. (3.3) might be thought of as an approximation. However, this recent PRL paper [77] has shown that the square-root dependence of ω gives the liquid energy that is identical to Eq. (3.3). This is because the k-gap ($k_{gap} = \frac{1}{c\tau}$) corresponds to $\omega = \frac{1}{\tau}$ in the Debye model ($\omega = kc$) which is the Frenkel frequency ω_F. Then, $\int_{\omega_F}^{\omega_D} kT\frac{6N}{\omega_D^3}\omega^2 d\omega$ is equal to $\int_{k_{gap}}^{k_D} kT\frac{6N}{k_D^3}k^2 dk$ [77].

3.5 Conclusions

As discussed in this Chapter Introduction, liquids have been viewed as inherently complicated systems lacking useful theoretical concepts such as a small parameter [12]. Together with recent experimental evidence and theory [17], the modelling data presented here and its quantitative agreement with predictions are beginning to change this traditional perspective. Extensive molecular dynamics simulations of liquid energy and specific heat lend support to the view that liquid thermodynamics can be understood on the basis of high-frequency collective modes. A more general implication is that, contrary to the prevailing view, liquids are emerging as systems amenable to theoretical understanding in a consistent picture as is the case in solid state theory. I have found this to be the case for several important types of liquids at both subcritical and supercritical conditions spanning thousands of Kelvin.

Chapter 4

Structural crossover and its relationship to dynamical and thermodynamic properties

In the previous Chapter, the thermodynamic crossover at the Frenkel line was studied. In this Chapter, I will discuss about the structural crossover which also happens at the Frenkel line and its relationship to the dynamical and thermodynamic crossover.

Molecular dynamics simulations can provide detailed pictures of the dynamical properties of liquids. It is learned that atoms in a liquid vibrate near the quasi-equilibrium position and then jump to the nearby equilibrium position-this is considered as vibrational-hopping regime. This can be seen by viewing the atomic trajectories in the simulation. The liquid structure and its changes can also be studied with temperature and pressure. In this Chapter, I study about the structural crossover at the Frenkel line of Ar, Fe and CO_2. Part of the material in this Chapter was previously published in Ref. [42].

4.1 Introduction

The insights into inter-relationships between structure, dynamics and thermodynamics in liquids and supercritical fluids are discussed. The results in the previous Chapter support the picture that the decrease of liquid c_v from 3 to 2 is related to reduction of the energy of transverse modes propagating above ω_{F}. $c_v = 2$ corresponds to complete disappearance of transverse modes at the FL when $\omega_{\mathrm{F}} \approx \omega_{\mathrm{D}}$ (the disappearance is supported by the direct calculation of transverse modes on the basis of current correlation functions [65]). Importantly, $c_v = 2$ marks the crossover of c_v because the evolution of different collective modes is qualitatively different below and above the FL [17]. Below the line, transverse modes disappear starting from the lowest frequency ω_{F}. Above the line, the remaining longitudinal mode starts disappearing starting from the highest frequency $\frac{2\pi c}{L}$, where L is the particle mean free path (no oscillations can take place at distance smaller than L). This gives qualitatively different behavior of the energy and c_v below and above the FL, resulting in their crossover at the FL [17].

Interestingly, the thermodynamic crossover at $c_v = 2$ implies a structural crossover. Indeed, the energy per particle in a system with pair-wise interactions is

$$E = \frac{3}{2}k_{\mathrm{B}}T + 4\pi\rho \int_0^\infty r^2 U(r) g(r) dr \tag{4.1}$$

where $\rho = N/V$ is number density, $U(r)$ is the interatomic potential and $g(r)$ is radial distribution function.

According to Eq. (3.6), the liquid energy is $E = E_0 + E_{\mathrm{T}}$, where E_{T} is given by Eq. (3.3). If the system energy undergoes the crossover at the FL where $c_v = 2$, Eq. (4.1) implies that $g(r)$ should also undergo a crossover. Therefore, the structural crossover in liquids can be predicted on the basis of

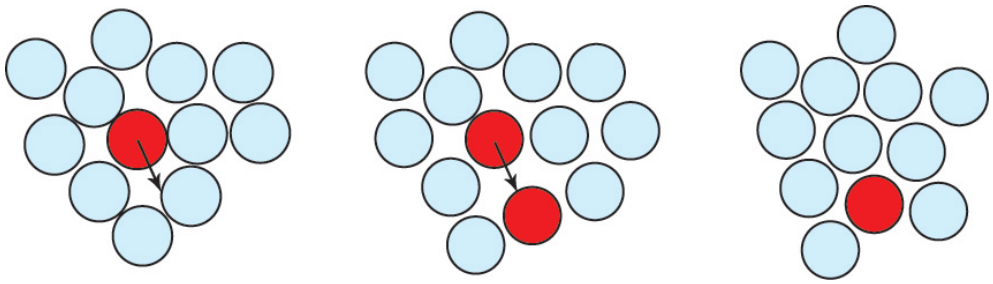

Figure 4.1: Schematic representation of a jump event in the liquid.

the thermodynamic properties.

It is also expected that the structural crossover at the FL would be related to the dynamical crossover on general grounds. As discussed above, below the FL particles oscillate around quasi-equilibrium positions and occasionally jump between them. The average time between jumps is given by liquid relaxation time, τ (Figure 4.1 schematically shows a local jump event from its surrounding "cage"). This means that a static structure exists during τ for a large number of particles below the FL, giving rise to the well-defined medium-range order comparable to that existing in disordered solids [78]. On the other hand, the particles lose the oscillatory component of motion above the FL and start to move in a purely diffusive manner as in gases. This implies that the features of $g(r)$ are expected to be gas-like. As a result, medium-range peaks of $g(r)$ are expected to have different temperature dependence below and above the FL. This behavior was observed in Ar and Fe in MD simulations [79]. More recently, the crossover in supercritical Ne and CH_4 in the medium range at the FL was ascertained on the basis of X-ray scattering experiments [80, 81]. The experimental study is extended to supercritical CO_2 by neutron scattering recently.

4.2 Supercritical Ar and Fe

4.2.1 Methods

I have used the molecular dynamics (MD) simulation package DL_POLY [31] and simulated systems with 8000 Argon and 8000 Iron particles with periodic boundary conditions. The interatomic potential for Ar is the pair Lennard-Jones potential [38] and for Fe is the many-body embedded-atom potential [40]. The MD systems were first equilibrated in the constant pressure and temperature ensemble at respective state points for 20 ps. System properties were subsequently simulated at different temperatures and averaged in the constant energy and volume ensemble for 30 ps.

I have simulated density $\rho = 1.9$ g/cm^3 for Ar and $\rho = 11$ g/cm^3 for Fe. The lowest temperature in each simulation was the melting temperature at the corresponding density, T_m. The highest temperature exceed the temperature at the Frenkel line at the corresponding density, T_{F}. Using the FL criterion $c_v = 2$ gives the temperature at the FL, T_{F}, of about 4000 K at that density of Ar, which is consistent with the criterion of the disappearance of the minimum of the velocity autocorrelation function [14]. For Fe, the corresponding T_{F} is about 50,000K. I have simulated 100 temperature points for Ar and Fe, respectively. The number of temperature points was chosen to keep the temperature step close to 10 K.

The PDF was calculated with the distance step of 0.05 Å, giving 600 PDF points for Argon and 300 PDF points for Fe.

4.2.2 Results and discussion

Before discussing about the PDF features, I show the vibrational-hopping regime in the supercritical liquids. As I have mentioned, liquid can support

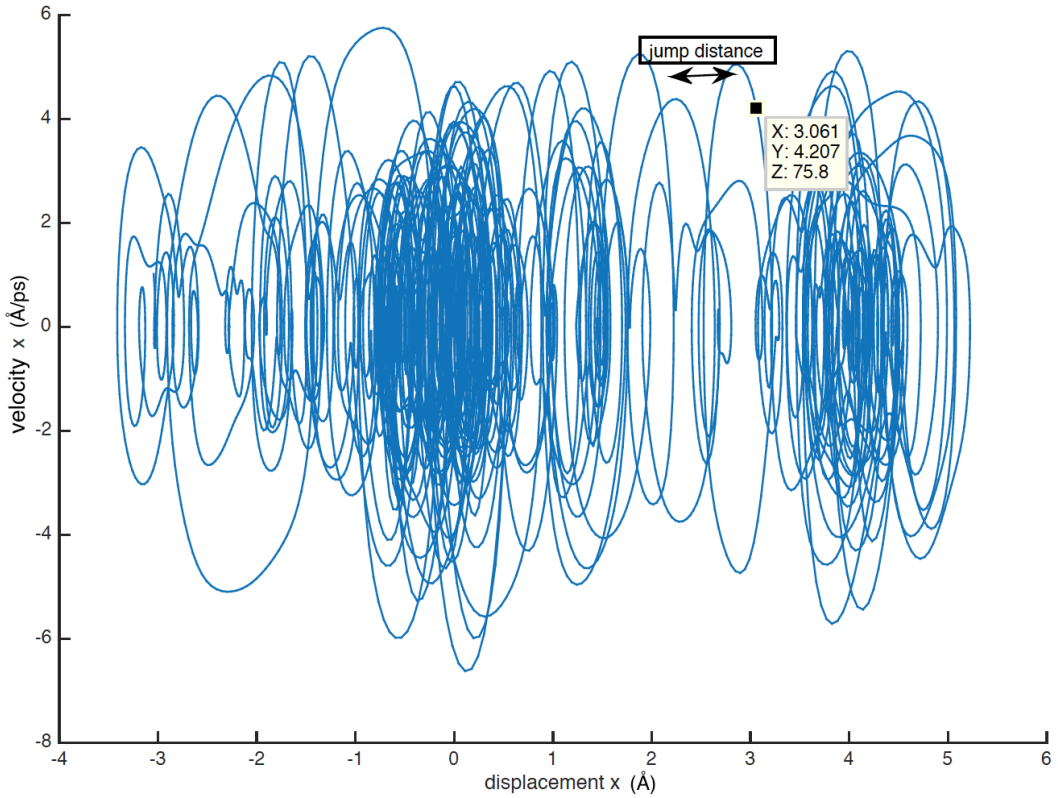

Figure 4.2: A jump event seen from x axis in simulation of liquid-like supercritical Ar below the Frenkel line.

shear waves below Frenkel line, the particles have oscillatory and diffusive motion. At the region above the FL, the particles lose the oscillatory component of motion and start to move in a purely diffusive manner as in gases. In other words, it is expected to see that particles in supercritical fluids below the FL are oscillating at the quasi-equilibrium position and then jump to its neighbourhood at low temperature. This vibrational-hopping regime is shown in Figure 4.2. The data in Figure 4.2 was obtained from the MD simulation directly and illustrates one atom's trajectory over times.

Then, the PDFs of Argon are showing in Figure 4.3 and discussed below. PDF peaks can still be observed in the medium range order up to about 20 Å at low temperature. The peaks reduce and broaden with temperature. To

study this in more details, I plot the peak heights vs temperature in Figure 4.3b. It is observed that the medium-range third and fourth peaks persist well above the critical temperature ($T_c = 151$ K for Ar): the highest temperature simulated corresponds to $53T_c$. This interestingly differs from the traditional expectation that the structure of the matter so deep in the supercritical state has gas-like features only. At temperature above T_{F}, the height of the fourth peak becomes comparable to its temperature fluctuations (calculated as the standard deviation of the peak height over many structures separated in time by 1 ps at each temperature) by order of magnitude. The fifth and higher-order peaks is observed to disappear before the highest temperature in the simulated range is reached.

The peak heights are plotted in Figure 4.3b in the double-logarithmic plot because it is expected to see an approximate power-law decay of the peak heights at low temperature. Indeed, PDF in solids can be represented as a set of Gaussian functions with peaks heights h depending on temperature as $h \propto \frac{1}{\sqrt{T}} \exp\left(-\frac{\alpha}{T}\right)$ where α is a temperature-independent factor [1, 82]. This temperature dependence of h was also quantified in MD simulations [83]. h decrease mostly due to the factor $\frac{1}{\sqrt{T}}$ whereas the effect of the exponential factor on h is small and serves to reduce the rate at which h decrease [83]. This implies that in solids, $\log h \propto -\log T$ approximately holds.

In supercritical fluids, the same relationship is expected to hold below the FL where $\tau \gg \tau_{\mathrm{D}}$, corresponding to a particle oscillating many times before diffusively moving to the next quasi-equilibrium position. Indeed, the ratio of the number of diffusing particles N_{dif} to the total number of particles N in the equilibrium state is $\frac{N_{dif}}{N} = \frac{\tau_{\mathrm{D}}}{\tau}$ [17] at any given moment of time. $\frac{N_{dif}}{N}$ is small when $\tau \gg \tau_{\mathrm{D}}$ below the FL and can be neglected. Hence, $\log h \propto -\log T$ applies to supercritical fluids at any given moment of time below the FL where $\tau \gg \tau_{\mathrm{D}}$. This also applies to longer observation times if

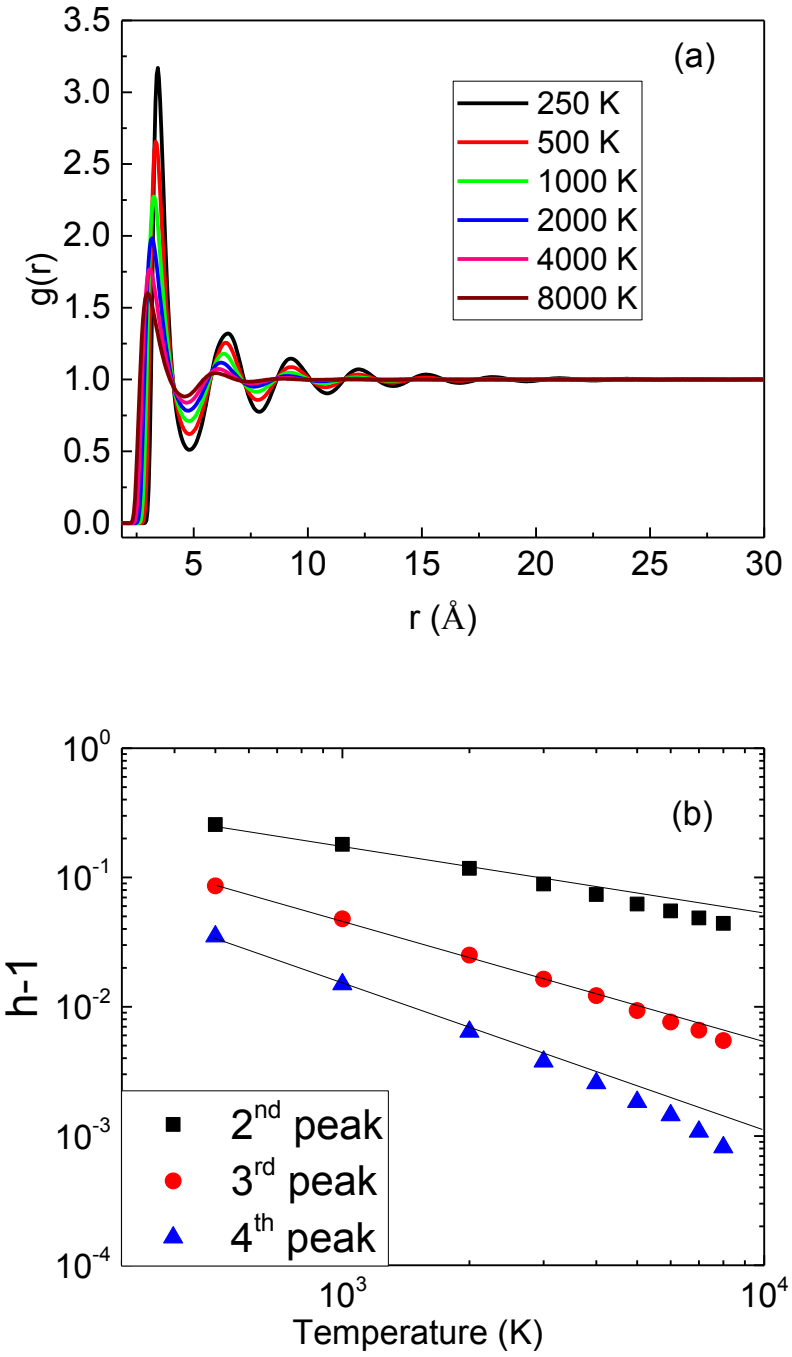

Figure 4.3: (a) Pair distribution functions of Ar at different temperatures. The temperatures correspond to the first peak decreasing from top to bottom at 250 K, 500 K, 1000 K, 2000 K, 4000 K and 8000 K; (b) $h-1$, where h are the heights of PDF peaks at different temperatures. The lines are linear fits to the low-temperature data range.

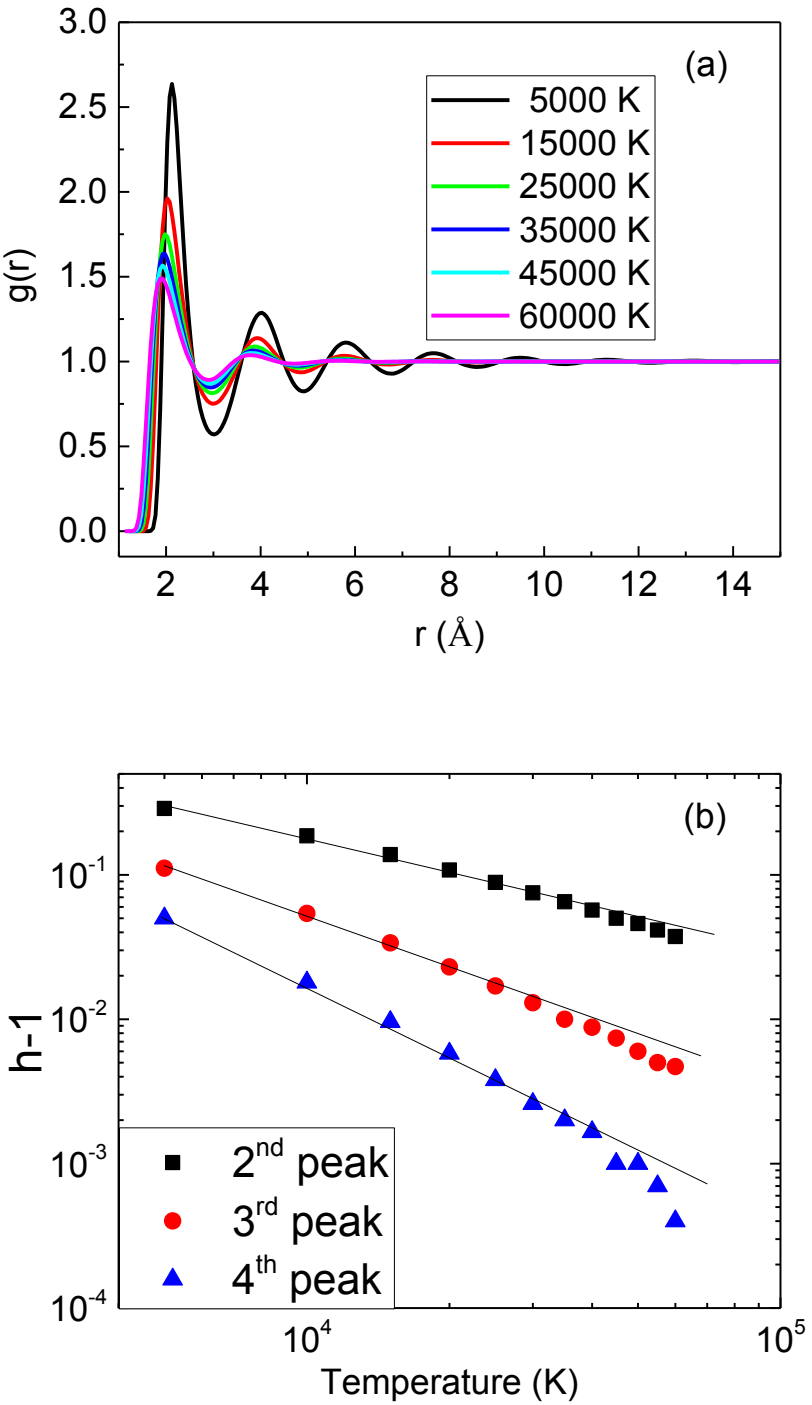

Figure 4.4: (a) Pair distribution functions of Fe at different temperatures. The temperatures correspond to the first peak decreasing from top to bottom at 5000 K, 15000 K, 25000 K, 35000 K, 45000 K and 60000 K; (b) $h-1$, where h are the heights of PDF peaks at different temperatures. The lines are linear fits to the low-temperature data range.

h is averaged over τ [17]. It should be noted that the above result, $h \propto \frac{1}{\sqrt{T}}$, involves the assumption that the energy of particle displacements is harmonic (see, e.g., Ref. [1]). Anharmonicity becomes appreciable at high temperature, however the anharmonic energy terms are generally small compared to the harmonic energy. This is witnessed by the closeness of high-temperature c_v to its harmonic result for both solids and high-temperature liquids [84, 85].

Therefore, it is expected that $\log(h-1) \propto -\log T$ approximately holds in the low-temperature range below the FL as in solids but deviates from the linearity around the crossover at the FL where $\tau \to \tau_{\mathrm{D}}$ and where the dynamics becomes gas-like (the calculated PDF in Figure 4.3a is normalized to 1 where no correlations are present at large distances; hence I plot $h-1$ in order to compare it with the theoretical result $h \propto \frac{1}{\sqrt{T}}$ which tends to zero when no correlations are present at high temperature). It should be noted that the crossover is expected to be broad because $\tau \gg \tau_{\mathrm{D}}$ applies well below the FL only. A substantial diffusive motion takes place in the vicinity of the line where $\frac{N_{dif}}{N}$ can not be neglected, affecting the linear relationship.

Consistent with the above prediction, the linear regime is observed at low temperature in Figure 4.3b, followed by the deviation from the straight lines taking place around 3000 K for the 2nd peak, 5000 K for the 3rd peak and 4000 K for the 4th peak, respectively. The smooth crossover in the 3000-5000 K range is centered around 4000 K, consistent with the temperature at the Frenkel line $c_v = 2$ discussed above.

Same behaviour is also observed in Figure 4.4 showing the PDFs of Iron. The deviation happens at around 50000 K for the 2nd peak, 40000 K for the 3rd peak and 40000 K for the 4th peak, respectively. The crossover takes place at around the Frenkel temperature 50000 K calculated from $c_v = 2$.

4.3 Supercritical CO_2

This work was stimulated by my collaborators Dr S. Marinakis and Prof A. Soper who, inspired by the idea of the FL, have recently performed neutron scattering experiments in supercritical CO2. I have simulated 4000 CO_2 molecules using the same potential as discussed earlier in this thesis at state points corresponding to the experimental conditions. The MD systems were first equilibrated in the constant pressure and temperature ensemble at respective state points for 300 ps. System properties were subsequently simulated at different temperatures and averaged in the constant energy and volume ensemble for 50 ps. I have simulated two pressures 500 and 590 kbar with temperatures from 250 K to 400 K.

The static structure factor is calculated in order to compare with the experimental data. The form of $S(k)$ is [37]:

$$S(k) = 1 + 4\pi\rho \int_0^\infty r(g(r) - 1)\frac{sinkr}{k}dr \tag{4.2}$$

where ρ is the number density and $g(r)$ is radial distribution function and $k = \frac{2\pi n}{L}$, where L is the system size.

Figure 4.5 shows S_{c-c}(k) and g_{c-c} (r) calculated at 500 kbar and 250-400 K. It is observed that the the first peak heights of S_{c-c}(k) and g_{c-c} (r) decrease with temperature. In particular, I plot the the first peak heights of S_{c-c}(k) and g_{c-c} (r) as a function of temperature in Figure 4.6. The predicted crossover temperature at the FL at 500 kbar is about 320 K [67] from VAF calculation. In Figure 4.6, the change of slope of first peak heights of S_{c-c}(k) and g_{c-c} (r) are both observed at temperature around 360 K which is close to the predicted one.

Thus, similar to the Ar and Fe system, the structural crossover is detected in supercritical CO_2 at conditions close to the FL. This is interesting because CO_2

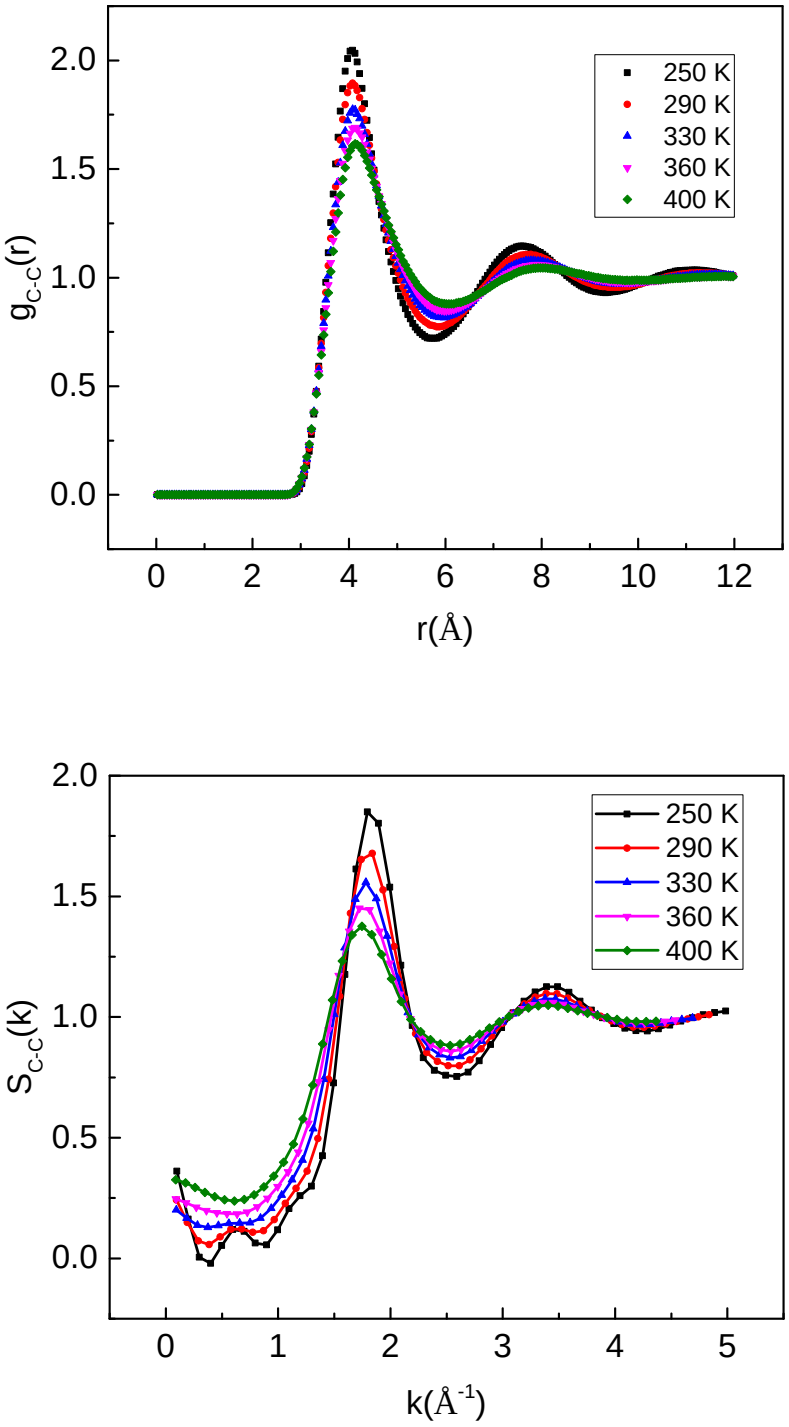

Figure 4.5: S_{c-c}(k) and g_{c-c} (r) of supercritical CO_2 at 500 kbar.

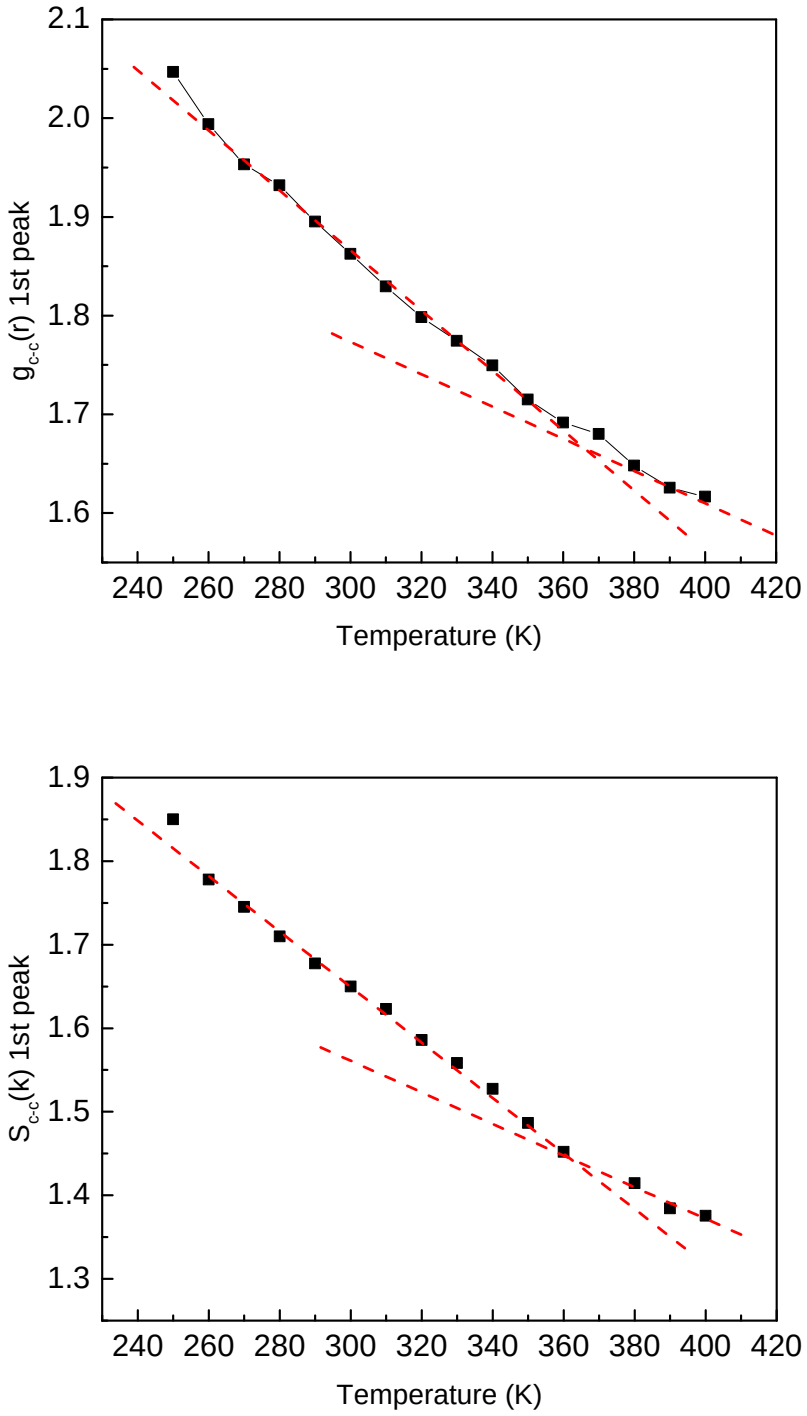

Figure 4.6: Slope changes of the first peak heights of S_{c-c}(k) and g_{c-c} (r) supercritical CO_2 at 500 kbar, red dashed lines are guides for the eye.

is an industrially important supercritical fluid widely used in, for example, extraction of caffein and making decaf coffee.

Moreover, preliminary experimental data of Dr S. Marinakis and Prof A. Soper detect the same structural crossover at the conditions close the FL. This data, in conjunction with my modelling results, is currently being prepared for publication.

4.4 Conclusions

In this Chapter, I discussed about the structural crossover at the Frenkel line and its relationship to the dynamical and thermodynamic crossover.

The vibrational-hopping regime has been shown by displaying the atom trajectories in the MD simulation. The pair distribution functions of Ar, Fe and CO_2 have been plotted and static structure factor of CO_2 has been calculated in a wide temperature range and up to the temperature above the Frenkel line. The slope change in PDFs and $S(k)$ features support the structure crossover observed at conditions close to the Frenkel line.

Chapter 5

Supercritical Grüneisen parameter and its universality at the Frenkel line

I subsequently study thermo-mechanical properties of matter at extreme conditions deep in the supercritical state, at temperatures exceeding the critical one up to four orders of magnitude. Grüneisen parameter γ is calculated and found decreasing with temperature from 3 to 1 on isochores depending on the density. This results indicate that from the perspective of thermo-mechanical properties, the supercritical state is characterized by the wide range of γ which includes the solid-like values - an interesting finding in view of the common perception of the supercritical state as being an intermediate state between gases and liquids. This result is rationalized by considering the relative weights of oscillatory and diffusive components of the supercritical system below the Frenkel line. γ is also found nearly constant at the Frenkel line above the critical point and this universality is explained in terms of pressure and temperature scaling of system properties along the lines where particle dynamics changes qualitatively. Part of the material in this Chapter was previously

published in Ref. [86].

5.1 Introduction

Dimensionless quantities play an important role in describing physical phenomena. One such parameter, the Grüneisen parameter (GP), has been proved to be very useful in the theory of lattice vibrations and thermodynamics of solids. In solid state physics, the Grüneisen parameter describes the change of system's elastic properties in response to volume change [87]:

$$\gamma = -\left(\frac{\partial \ln \omega}{\partial \ln V}\right)_T \tag{5.1}$$

where ω is the effective average frequency of particle vibrations, V is the system volume.

The Grüneisen parameter can also be related to system energy and pressure [88]:

$$\gamma = V\left(\frac{\partial P}{\partial E}\right)_V \tag{5.2}$$

Eqs. (5.1) and (5.2) are equivalent in the condensed matter systems, but the second equation is more general and applies to gases, high-temperature fluids and plasma where individual particles do not vibrate. Eq. (5.2) leads to [88]

$$\gamma = \frac{\alpha_P B_T V}{c_v} \tag{5.3}$$

where α_P is the thermal expansion coefficient, B_T is the isothermal bulk modulus and c_v is the constant volume heat capacity.

As follows from (5.1) and (5.2), γ is a thermo-mechanical quantity and it is important for thermo-mechanical effects, in particular for those involving extreme temperatures and pressures. These include shock wave effects, rapid

expansion and heating of systems absorbing nuclear radiation and so on. Often in this case, the GP becomes particularly important, the pulse duration is shorter than the timescale of acoustic transport, the induced thermal pressure is directly proportional to γ. Consequently, the GP is extensively used in analyzing the equations of state of condensed matter and plasma at extreme conditions.

The aim of this Chapter is to calculate and analyze the GP deep in the supercritical state. γ has been calculated for two common model systems (LJ model and soft-sphere model) at temperature and pressure exceeding the critical ones by orders of magnitude.

5.1.1 Typical values for the Grüneisen parameter

The main physical meaning of the Grüneisen approach and using the Grüneisen parameter lies in quantifying phonon anharmonicity. In general, anharmonicity can be complicated and non-trivial to treat, especially when perturbation theory is employed. The Grüneisen parameter for individual mode frequencies is defined as the logarithmic derivative of phonon frequencies with respect to volume change (in harmonic case, phonon frequencies do not depend on volume). Hence the larger the Grüneisen parameter, the larger anharmonicity. Once the Grüneisen parameter is defined in such a way, the contribution of anharmonicity other system properties such as energy can be calculated. In the Grüneisen approximation, the Grüneisen parameter is assumed to be temperature-independent.

For most condensed matter systems, the range of γ is $0.5 - 4$. Diamond is an "ideal" Grüneisen system with $\gamma = 1$ [89]. Systems with large pressure derivatives of B (lattice stiffens quickly with compression) often have large γ [88]. Interestingly, since B_T and C_V are positive in equilibrium, the sign of γ is

governed by the sign of α_P. Some systems such as Cu_2O and ScF_3 have small negative γ in a quite large temperature and pressure range [90], accompanied by negative α_P and softening of force constants on compression. Negative γ can also be seen in shock-wave experiments due to non-equilibrium smeared phase transformations [91].

Compared to solids, relatively little is known about the GP in liquids and dense gas states. For the ideal gas, $\gamma = \frac{2}{3}$ is a constant as follows from $E = \frac{3}{2}PV$. The same result also applies to the degenerate electron gas [92]. For the frequently discussed hard-spheres model, γ can be calculated from the Carnahan-Starling equation $Z = \frac{PV}{Nk_BT} = \frac{1+\eta+\eta^2-\eta^3}{(1-\eta)^3}$, where $\eta = \frac{\pi}{6}\rho\sigma^3$ is the packing fraction of hard spheres of diameter σ at density ρ [93]. This gives $\gamma = \frac{2}{3}f(\rho)$, where $f(\rho)$ is a function of density, implying that the GP of hard spheres is constant along isochores. For model Van del Waals system, $\gamma = \frac{2}{3} \times \frac{V}{V-Nb}$, where b is the cohesion volume, the GP diverges when the volume becomes close to the critical volume [94]. The soft-sphere interaction with weak attraction modifies the GP, and there are analytical evaluations of this effect [95, 96]. Based on certain assumptions and in reasonable agreement with simulations of noble-gas systems [97], there are numerical evaluations of the GP for the commonly-used Lennard-Jones potential [98]. For more complicated liquids such as water and mercury, the GP was calculated using Eq. (5.3) and was found to increase with pressure, in contrast to its usual decrease in crystals [99]. The GP was also calculated in liquid Ar in a small range of pressure and temperature and was found to decrease on isobaric heating [100]. In a wider temperature and pressure range, γ in Ar in the dense gas and liquid state increases on isothermal compression and is nearly constant on isochoric heating [101]. γ was also calculated from ensemble averages of fluctuations [102]. Finally, γ was evaluated using the radial distribution function of liquids with acceptable errors [103].

Notably, no studies or evaluations of γ were done significantly above the critical point of matter. As discussed above, supercritical fluids has been widely deployed in many important industrial processes [18, 19], but theoretically little is known about the supercritical state. The supercritical fluids can be thought of as high-density gases or high-temperature fluids whose properties change smoothly with temperature or pressure and without qualitative changes of properties. This picture is modified by the Frenkel line (FL) which exists above the critical point and separates two states with distinct properties [13, 14, 20, 17, 64].

In supercritical fluids, increasing temperature at constant pressure (or decreasing pressure at constant temperature) eventually results in the disappearance of the solid-like oscillatory motion of particles; all that remains is the diffusive gas-like motion. This disappearance represents the qualitative change in particle dynamics and gives the point on the FL. Another criterion for the FL which coincides with the VAF criterion is $c_v = 2k_\mathrm{B}$ [14]. Indeed, the loss of solid-like oscillatory component of motion implies the disappearance of solid-like transverse modes which, in turn, gives $c_v = 2k_\mathrm{B}$ [17]. The qualitative change of particle dynamics and $c_v = 2k_\mathrm{B}$ at the FL are two important insights that I will use below to discuss the universality of the GP at Frenkel line.

5.2 Methods

Firstly, molecular dynamics simulation package DL_POLY [31] is used to simulate the LJ model. The simulated systems have 8000 particles with periodic boundary conditions and the interatomic potential for Argon is the pair Lennard-Jones potential [38]. Five densities have been simulated : $\rho_1 = 1.20$ g/cm^3, $\rho_2 = 1.35$ g/cm^3, $\rho_3 = 1.50$ g/cm^3, $\rho_4 = 1.90$ g/cm^3 and $\rho_5 = 2.20$ g/cm^3. The temperature in each simulation varies from melting temperature

at the corresponding density up to 10000 K with the interval 10 K. The MD systems were first equilibrated in NVE ensemble for 40 ps. The data were subsequently collected at different temperatures for each density and averaged over the period of 60 ps.

The second system, soft-sphere system is simulated in a wide range of density and temperature. This part of simulation was carried out by our collaborator Dr Yu. D. Fomin (Institute for High Pressure Physics, Moscow Institute of Physics and Technology). The soft-sphere interaction potential is $U(r) = \varepsilon \left(\frac{\sigma}{r}\right)^n$, where n is the softness parameter. $n = 6$ and $n = 12$ are considered, respectively. For $n = 6$, γ is calculated using Eq. (5.2) in which energy and pressure are obtained from MD simulation. This part of the simulation work was performed using the LAMMPS MD package [110]. A system of 4000 particles in a cubic box with periodic boundary conditions is simulated. The reduced densities of the system are ρ_1*= 1.0 and ρ_2*= 1.5 and the temperatures vary from T*= 2.7 to 3.4 in the soft-sphere units. The Frenkel temperature of this system at this density is T_F*= 3.1. The equilibration and production runs involved 10^6 steps with a timestep was set to 0.0001 ps.

5.3 Results and discussion

γ is calculated by two methods. In the first method, I use V, P and E from the MD simulations, calculate γ using Eq. (5.2) and fit the resulting values to the polynomial. In the second method, I first fit V, P and E to respective polynomials and then calculate γ using Eq. (5.2). Both methods result in close curves for γ as follows from Figures 5.1 and 5.2 discussed below.

Figure 5.1 and Figure 5.2 show the γ calculated for Ar using both methods along 5 different isochors. It should be noted that the range of thermodynamic parameters used here is record-high: the highest temperature and pressure

exceed the critical ones by over one to two orders of magnitude. At each density, the arrow shows the corresponding temperature of the FL.

It is observed that γ calculated by Eq. (5.2) decreases from 2.5 to 1 with temperature at low density and from about 3 to 1.2 at high density. Notably, $\gamma = 2.5 - 3.5$ are characteristic of the solid state. Therefore, the results indicate that from the perspective of thermo-mechanical properties, the supercritical state is characterized by the range of γ which includes the solid-like values. This is an interesting finding in view of the common perception of the supercritical state as being an intermediate state between gases and liquids [18, 19].

The solid-like values of supercritical γ at low temperature can be explained by considering the relative weight of the oscillatory and diffusive components of motion in the supercritical state. This weight can be quantified by the R-parameter [17]:

$$R = \frac{\omega_{\mathrm{F}}}{\omega_{\mathrm{D}}} \tag{5.4}$$

where $\omega_{\mathrm{F}} = \frac{1}{\tau}$ and ω_{D} is Debye frequency.

Recall that the oscillatory component of particle motion disappears at the Frenkel line. However, if the supercritical system is sufficiently below the Frenkel line, particles spend most of their time oscillating, and diffusive jumps between the quasi-equilibrium positions are rare. This gives $R \ll 1$. In this case the average system energy is well approximated by the energy of the oscillatory motion [17]. This is because $\frac{N_{diff}}{N_{tot}} = \frac{\omega_F}{\omega_D} \ll 1$, where N_{diff} is the atom number with purely diffusive motion and N_{tot} is the total atom number in the system. Therefore, basic thermodynamic properties of the supercritical system below the FL are solid-like, as are the dynamical properties related to phonons. Hence γ is expected to be characterized by the solid-like values in

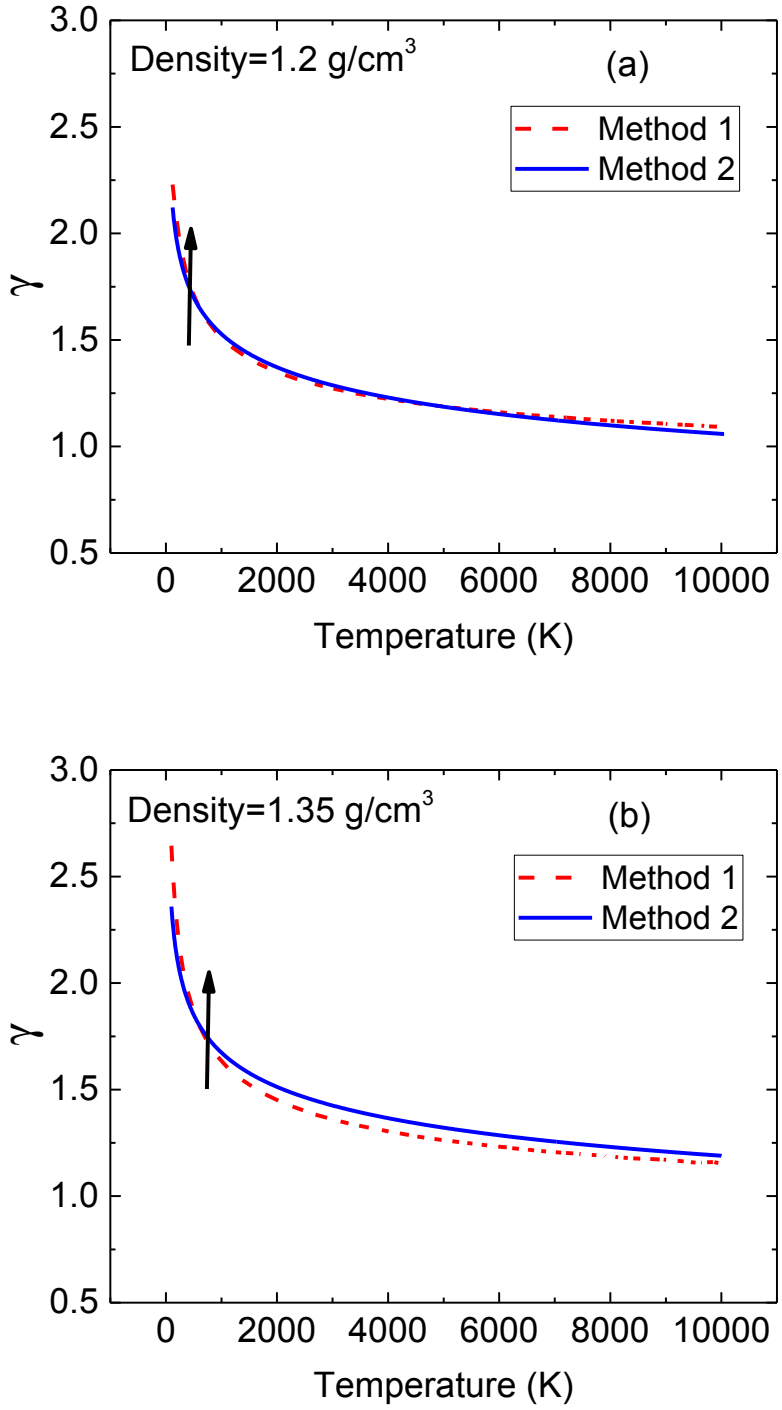

Figure 5.1: Grüneisen parameters calculated for the Lennard-Jones (Ar) system at two lower densities. The red dashed lines and blue solid lines are calculated using the two methods described in text. The arrows show the temperature at the Frenkel line.

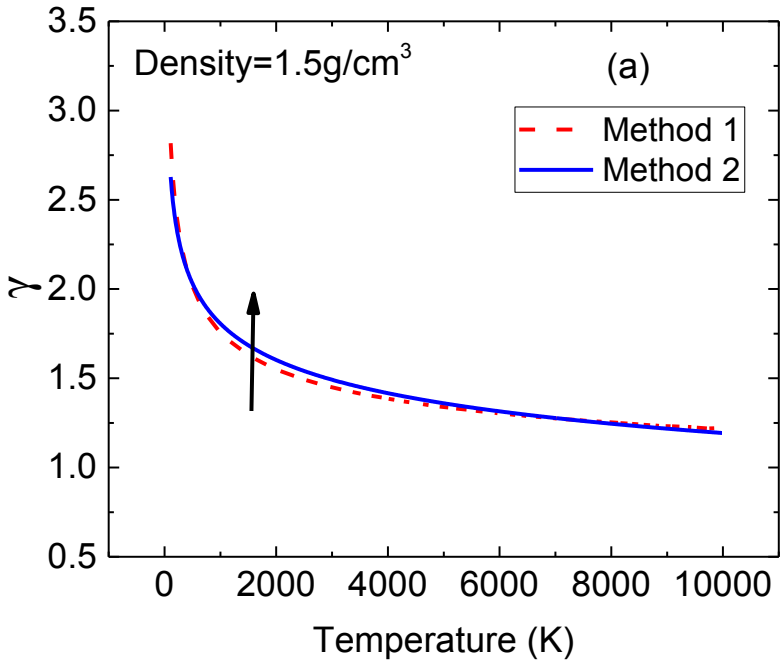
Density=1.5g/cm3
(a)
Method 1
Method 2
γ
3.5
3.0
2.5
2.0
1.5
1.0
0.5
0
2000
4000
6000
8000
10000
Temperature (K)

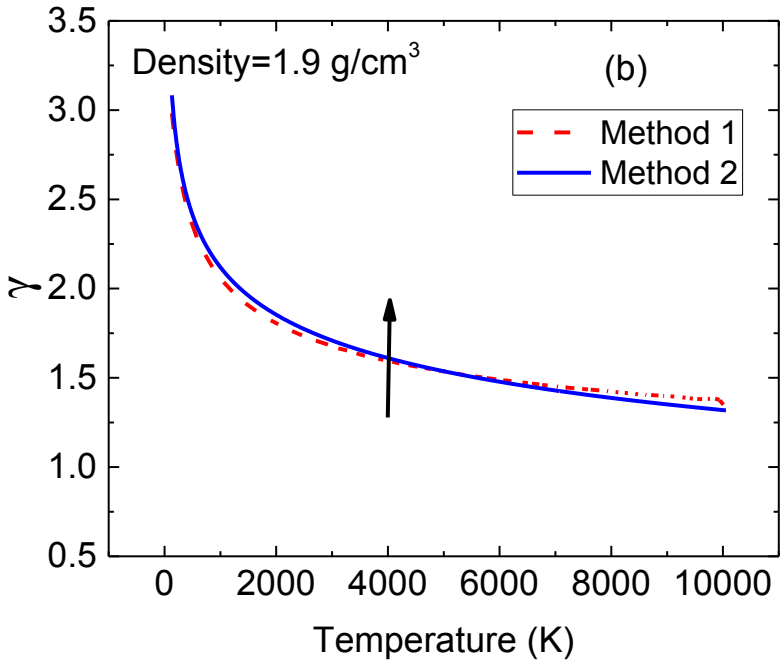
Density=1.9 g/cm3
(b)
Method 1
Method 2
γ
3.5
3.0
2.5
2.0
1.5
1.0
0.5
0
2000
4000
6000
8000
10000
Temperature (K)

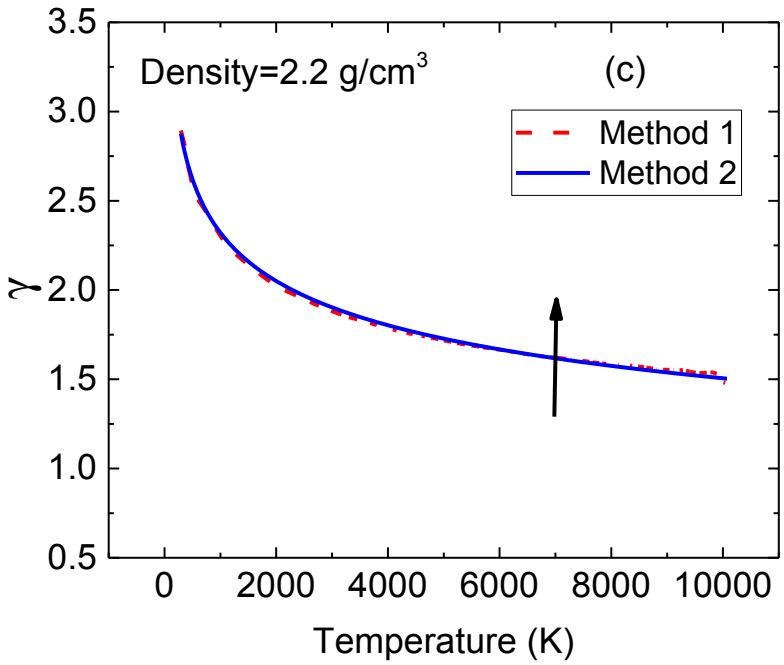

Figure 5.2: Grüneisen parameters calculated for the Lennard-Jones (Ar) system at three higher densities. The red dashed lines and blue solid lines are calculated using the two methods described in text. The arrows show the temperature at the Frenkel line.

this regime.

The similarity between γ of the supercritical systems below the FL and their solid-like values can be explored further, by using the solid-like equation in Eq. (5.1). Debye frequencies ω_{D} have been evaluated earlier for the LJ system for two supercritical densities below the FL: $\omega_{\mathrm{D}} = 7.2$ THz for $\rho = 1.50$ g/cm^3 and $\omega_{\mathrm{D}} = 18.4$ THz for $\rho = 1.90$ g/cm^3 [42]. Using these values and $\omega \propto \rho^{\gamma}$, which follows from Eq. (5.1), gives $\gamma \approx 3.8$. This is in reasonable agreement with γ calculated in the MD simulation at high density, given the approximations involved in finding ω_{D}.

I now address the behavior of γ at the FL and plot the GP at all five densities and temperatures corresponding to the FL in Figure 5.3. It should be noted that γ are plotted in the range approximately corresponding to the

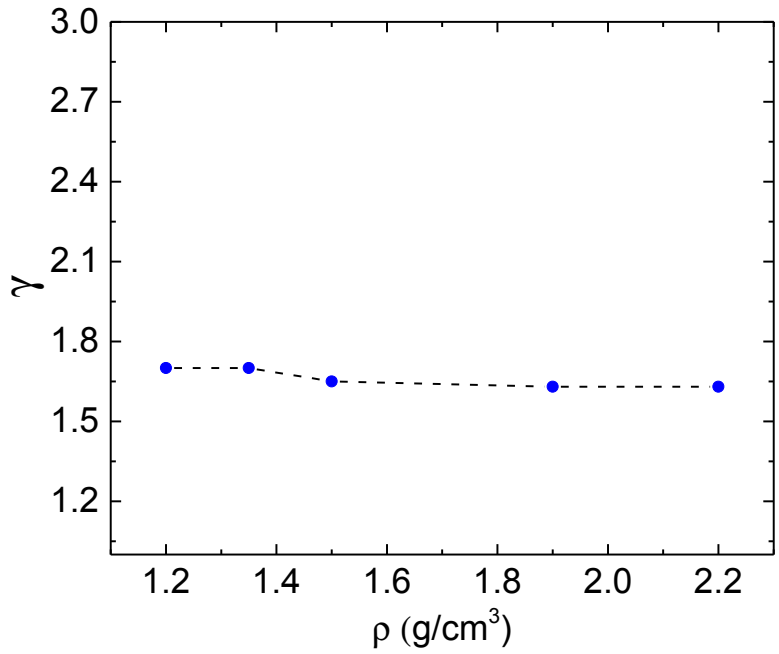

Figure 5.3: Grüneisen parameters at the Frenkel line for 5 different densities used in Figures 5.1 and 5.2. γ are plotted in the range approximately corresponding to the largest and smallest γ in Figures 5.1 and 5.2.

largest and smallest γ in Figures 5.1 and 5.2. It is observed that γ is nearly constant at the FL: $\gamma = 1.6 - 1.7$ Figure 5.3. This is an interesting result, given that the corresponding temperatures at the FL varies by more than an order of magnitude.

The following explanation is proposed for the near constancy of γ at the FL. The universality of γ is related to scaling. At high energy (e.g. high pressure or temperature), particle interactions mostly involve the repulsive part of the potential. Therefore, the interatomic potential for Ar (as well as for many other systems) becomes effectively close to the soft-sphere potential $U \propto \frac{1}{r^n}$ [104, 105], the classic example of a homogeneous potential. According to the Klein theorem [12, 106, 107], the non-ideal part of the partition function depends on density ρ and temperature as $\frac{\rho^{\frac{n}{3}}}{T}$ rather than on ρ and T separately.

The resulting relationship between temperature and pressure at the melting line is $P_m \propto T_m^{1+\frac{3}{n}}$ [107]. (Interestingly, the kinetic energy is also a homogeneous function of the second order, leading to scaling of kinetic coefficients such as viscosity and diffusion [108, 109]). Zhakhovsky extended the scaling argument [109] and noted that, more generally, scaling always exists along those lines on the phase diagram where particle trajectories are similar or change in a similar way as they do at, for example, the melting line. Recall that the Frenkel line separates the combined oscillatory and diffusive motion below the line from purely diffusive motion above the line [13, 14, 20, 17, 64]. Therefore, the scaling relationship $P_{\mathrm{F}} \propto T_{\mathrm{F}}^{1+\frac{3}{n}}$ is expected to hold at the FL as it does for the melting line. Such a relationship has been indeed ascertained in the soft-sphere system as well as LJ system at high pressure on the basis of MD simulations [14]. Then, $\gamma = V\frac{dP}{dE} = V\frac{dP}{dT}\frac{dT}{dE} \propto VT^{\frac{3}{n}}\frac{1}{c_v}$. Using the scaling relationship $V \propto T^{-\frac{3}{n}}$ from the Klein theorem, this gives $\gamma = f(n)\frac{1}{c_v}$, where $f(n)$ is the function of n only. As mentioned earlier, c_v is constant at the FL [14, 17]. Hence, γ at the FL does not depend on temperature and pressure, i.e. is a universal parameter for a system with a given n. In this picture, the constancy of the Grüneisen parameter at the Frenkel line is the result of scaling of volume and temperature as discussed above in detail.

To compare the results of the scaling argument with MD simulations further, γ is calculated for the soft-sphere system in a wide range of density and temperature. The results for $n = 6$ have been shown in Figure 5.4 for two different densities ρ^*= 1.0 and ρ^*= 1.5. Consistent with the scaling argument above (the soft-sphere system obeys the scaling argument), it is observed that γ is nearly constant at the FL.

It should be noted that γ for the soft-sphere system at the FL increases with n: using the previous data in ref [111], γ is calculated to be 1.5 for $n = 12$ at the FL. This is close to γ at the FL for the LJ system (see Figure 5.3). This

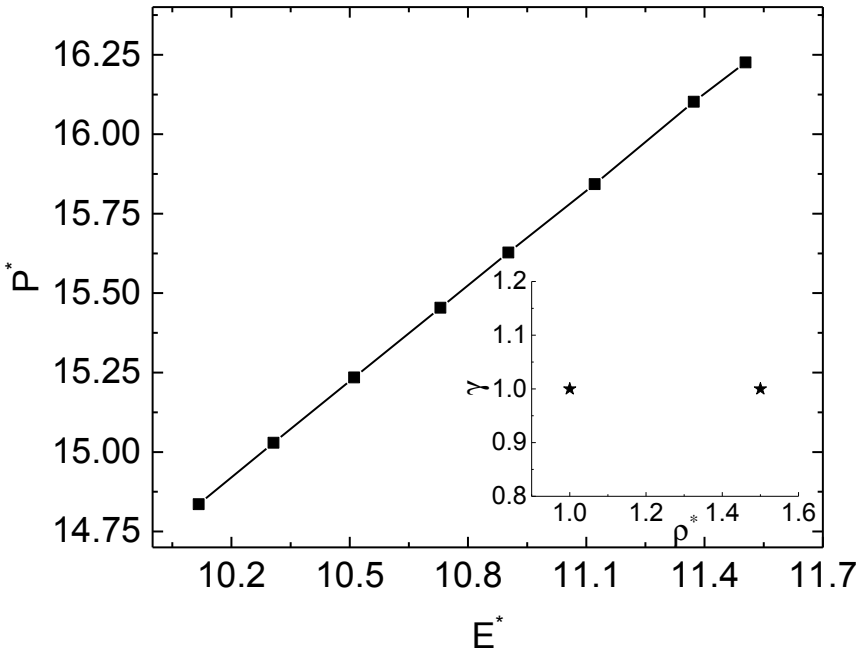

Figure 5.4: The dependence of pressure on energy for the soft sphere system with $n = 6$ at $\rho^*= 1.0$. Pressure and energy are shown in soft-sphere units. The inset shows the Grüneisen parameter at two densities at the FL: $\rho^*= 1.0$ and $\rho^*= 1.5$.

can be understood because the LJ potential becomes close to the soft-sphere potential at high pressure and high temperature as discussed above.

Before concluding, two remarks are made here. First, recall the earlier observation that γ is constant along the isochore [101]. This was related to a narrow range of pressure and temperature where the system can be approximated by a soft-sphere system with nearly constant effective radii and packing fraction and whose GP is constant along the isochore as mentioned earlier. At the same time, the results in this study involving large range of pressure and temperature indicate that γ can vary substantially, from those values typical of solids to the dense-gas ones.

Second, it will be interesting to evaluate the GP in the vicinity of the critical

point. According to Eq. (5.3), γ is governed by quantities which diverge at the critical point: compressibility, thermal expansion and heat capacity. Assuming, as is often done in the theory of critical phenomena, that the divergences of α and β_T are equivalent, γ at the critical point is governed by the behavior of c_v. For real systems, c_v has a weak power divergence at the critical point, and γ can be predicted to be close to 0. This point warrants further investigation.

5.4 Conclusions

In summary, Grüneisen parameter of supercritical matter have been calculated for two model systems in a very wide range of pressure and temperature. It has been found that γ varies in a wide range which interestingly includes the solid-like values. This result is rationalized by considering the relative weights of oscillatory and diffusive components of the supercritical system below the Frenkel line. γ is also found nearly constant along the Frenkel line and rationalize this finding using the scaling of system properties along the lines where particle dynamic changes qualitatively. It is likely that a more general statement applies: any dimensionless parameter is universal at the line where scaling operates.

Chapter 6

The nature of collective excitations and their crossover at extreme supercritical conditions

Physical properties of an interacting system are governed by collective excitations, but their nature at extreme supercritical conditions is unknown. Here, direct evidence is presented for propagating solid-like longitudinal phonon-like excitations with wavelengths extending to interatomic separations deep in the supercritical state at temperatures up to 3,300 times the critical temperature. It is observed that the crossover of dispersion curves develops at k points reducing with temperature. This effect is interpreted as the crossover from the collective phonon regime to the collisional mean-free path regime of particle dynamics and find that the crossover points are close to both the inverse of the shortest available wavelength in the system and to the particle mean free path inferred from experiments and theory. Notably, both the shortest wavelength and mean free path scale with temperature with the same power law, lending further support to these findings. The results in this Chapter was previously published in Ref. [112].

6.1 Introduction

Any system with interacting agents or particles is capable of supporting waves. The hydrodynamic approximation to liquids and gases and elastic approach to solids, collectively known as the continuum approximation, is widely used in many areas of physics. It predicts propagating long-wavelength longitudinal density fluctuations, sound. As useful as it is, the continuum approximation does not describe many important properties: for example, the solid state theory and in particular thermodynamics of solids relies on the atomistic description. The atomistic description relies, in turn, on the knowledge that the range of wavelengths λ in solids varies from approximately system size to the shortest interatomic separation a on the order of Angstroms where atomistic effects operate.

Theoretical understanding of waves in liquids remains challenging, particularly in view that widely-used perturbation approaches do not apply [12]. Until fairly recently, this difficulty extended to experimental studies as well. However, the deployment of next-generation synchrotron sources enabled physicists to make the same assertion about waves in liquids as in solids: phonon-like excitations in liquids extend up to the shortest interatomic separation as they do in solids [46, 47, 48, 50, 51, 52, 53, 54]. This solid-like property of liquids is remarkable because traditionally, liquids have been studied in the hydrodynamic approximation $\lambda \gg a$ only [43]. It suggests that liquids are amenable to understanding using solid-like concepts and their implications [17].

The recent evidence of non-hydrodynamic solid-like waves in liquids (waves with large k vectors) [17, 46, 47, 48, 50, 51, 52, 53, 54] prompts an intriguing question of whether these waves can extend to the third state of matter, gases, and thus be common to *all three states*. In familiar gases at ambient condi-

tions, this would appear impossible because the particle mean free path l is much larger than a, implying that the system can not support solid-like wavelengths close to a. l can be decreased by increasing pressure or lowering the temperature but this results in the first-order gas-liquid transition well before l approaches Angstroms. However, the supercritical state where no gas–liquid phase transition intervenes, offers more flexibility: one can change the density *continuously*, from gas-like to liquid-like values. Therefore, studying the supercritical state offers an intriguing possibility to see whether the longitudinal wave in the gas-like state (traditionally known as sound wave) can support ever-decreasing wavelengths up to the shortest solid-like atomistic lengths where λ becomes comparable to Angstroms. This would imply new unanticipated properties of waves that gas-like states can support.

The theory of dilute gases is tractable due to the concept of mean free path (MFP), based on the idea that molecules mostly move freely between binary collisions. The theory gives specific predictions for important system properties such as temperature dependence of viscosity and thermal conductivity [5]. For dense gases and fluids (loosely defined as systems where intermolecular distances are comparable to molecular sizes) at moderate temperature, this approach does not apply because a molecule continuously moves in the field of forces of others. This involves three and higher-order encounters, and treating these is of considerable difficulty. As a result, common gas theories are unable to describe important properties of dense gases such as temperature dependence of viscosity [5].

The division into dilute and dense gases has traditionally been done at moderate pressure and temperature [5]. However, experiments have been increasingly probing the matter at extreme conditions including deeply supercritical ones, calling for new theories to be developed [18]. Indeed, the supercritical state has remained poorly understood in general, despite the

wide deployment of supercritical fluids in important industrial applications [18]. This has stimulated my interest in a hitherto unexplored question: what kind of collective excitations can exist in the supercritical state of matter?

Central to my proposal is that both temperature and density (rather than density alone as traditionally assumed) are important for the concept of the mean free path to emerge. Indeed, let us consider a supercritical fluid at density close to, for example, water density at the triple point where the system would be characterized as "dense" as opposed to "dilute" in the traditional classification. If this system is at very high supercritical temperature, a molecule, even though it moves in the field of others, has enough energy to move with little deflection for a certain distance. More specifically, the high energy of the particle results in small deflection angles and small momentum transfer in the collision integrals featuring in transport properties [5]. This implies that the concept of the mean free path l emerges in dense systems provided the particle energy is high, and is not limited to dilute gases as assumed previously. In the somewhat crude picture of the mean free path in the system with particles of size a, the increase of $l \propto \frac{1}{a}$ corresponds to the decrease of effective a with temperature.

I can therefore develop and use theoretical predictions of dynamical and thermodynamic properties in dense and hot supercritical fluids in the MFP regime. Testing this idea constitutes one of the general aims of this Chapter.

Apart from the general question of the nature of collective excitations at deep supercritical conditions, the important implication is considered of the MFP regime for the wave propagation. In the MFP regime, the system cannot support an oscillatory motion with wavelengths shorter than the mean free path l. It is therefore predicted that supercritical dispersion curves should undergo a *crossover* from the phonon regime at small k vectors to the MFP regime where no phonons exist with wavelengths shorter than l.

In this Chapter, I perform extensive molecular dynamics (MD) simulations and obtain direct evidence for propagating solid-like longitudinal modes with short wavelengths deep in the supercritical state at temperatures up to 3,300 times the critical temperature. It is subsequently observed that the crossover of dispersion curves develops at k points reducing with temperature and this effect as the crossover from the phonon to the MFP regime is interpreted on the basis of (a) closeness of the crossover points to those corresponding to the shortest available wavelength in the system; (b) closeness of the crossover points to those corresponding to the particle mean free path; and (c) the same power-law temperature dependence of the shortest wavelength and the mean free path.

It should be noted that traditionally, the supercritical state was thought to disallow any difference between a gas and a liquid [18]. As discussed above, it was proposed that the supercritical state can be separated into the gas-like and liquid-like properties by the Frenkel line (FL) [13, 14, 20]. Above the line, particle dynamics are purely diffusive as in gases, in contrast to dynamics below the line where particles both diffuse and oscillate. This property is related to the ability to sustain different types of waves: only one longitudinal mode exists above the line, whereas two transverse modes disappear [113, 114]. Hence the Frenkel line provides a guide as to where on the supercritical phase diagram it is expected to find a gas-like state with the longitudinal mode only. In this Chapter, the evolution of the longitudinal modes with temperature is studied.

6.2 Simulation and results

I have performed extensive molecular dynamics (MD) simulations [31] of supercritical liquid Ar [42] using the Lennard-Jones (LJ) potential and constant

volume and energy ensemble. The simulated temperature starts from 500 K (just above the FL temperature) and increases to very high temperatures deep in the supercritical state up to 500,000 K, corresponding to over 3,000 times the critical temperature (Ar critical temperature is 151 K). The simulated densities are 0.4, 0.65 and 0.8 g/cm^3. I simulated 8,000 atoms in the system. The time step varies between 1 fs at low temperature and 0.1 fs at high temperature to account for faster dynamics.

The reason for simulating high temperature (the highest temperature is in excess of the Ar ionization energy) is that, as discussed below, l is a slowly-varying function of temperature at constant density. This is due to two competing mechanisms: on one hand temperature increases l but on the other hand the buildup of pressure with temperature at constant density decreases l.

I have calculated the longitudinal current correlation functions [6] in order to address the evolution of longitudinal collective modes directly:

$$C_L(k,t) = (k^2/N)\langle J_x(\mathbf{k},t)\cdot(J_x(-\mathbf{k},0)\rangle \tag{6.1}$$

where $J(\mathbf{k},t) = \sum_{j=1}^{N} \mathbf{v}_j(t)e^{-i\mathbf{k}\cdot\mathbf{r}_j(t)}$ is the longitudinal current, N is the number of particles, $\mathbf{v}$ is the particle velocity, and the wave vector $\mathbf{k}$ is along the x axis. k-points were sampled as $k = 2\pi n/L$, where L is the system size.

The spectra of longitudinal currents are calculated by the Fourier transform of $C_L(k,t)$. In order to reduce the noise in calculating the spectra, I have repeated my simulations 20 times for each temperature by using different starting velocities and then the current results is averaged [77]. Examples of intensity maps of $\tilde{C}_L(k,\omega)$ are shown in Figure 6.1.

It is observed that the mode frequency increases with k up to large k-points corresponding to wavelengths comparable to interatomic separations as is the case in solids. In fact, the spectra look remarkably similar to those in solids.

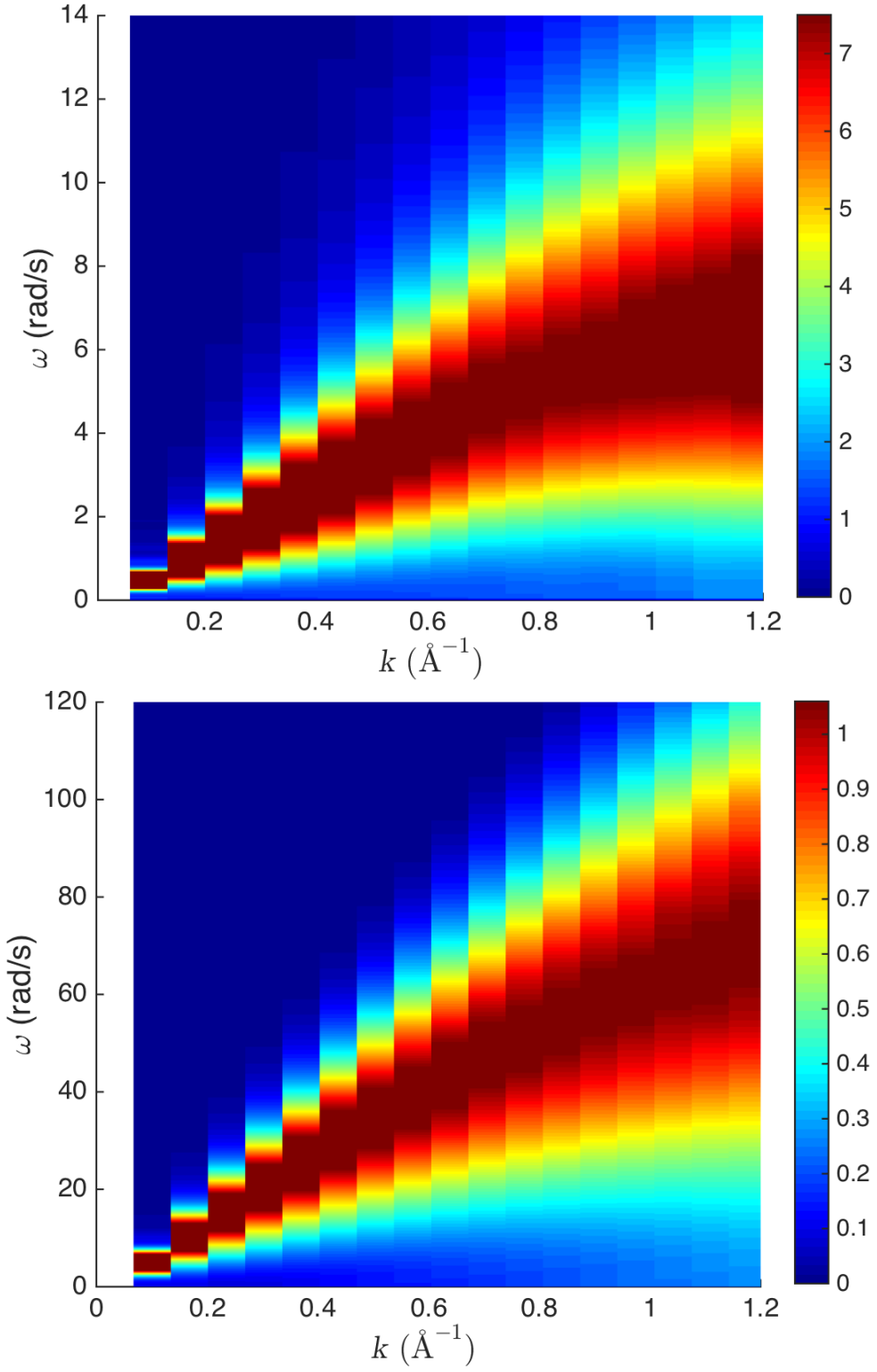

Figure 6.1: Intensity map of $C_L(k,\omega)$ for supercritical Ar at (top panel) 500 K and (bottom panel) 100,000 K. The maximal intensity corresponds to the middle points of the dark red areas and reduces away from them.

The similarity of liquid and solid phonon spectra was noted earlier at low temperature [52]. Figure 6.1 shows that this similarity extends to very high temperature deep into the supercritical state.

The frequency at which the intensity is maximal corresponds to the mode frequency at the corresponding k-point. Examples of $\tilde{C}_L(k,\omega)$ at different k are shown in Figure 6.2. The ratio of the peak width at half-height Γ to the peak frequency ω is 1.1-1.3 for the intensity peaks considered in this work, including in the examples shown in Figure 6.2. This is consistent with the experimental findings reporting propagating modes in liquids (see, e.g., Ref. [117]). The calculated $\frac{\Gamma}{\omega}$ satisfies the condition $\frac{\Gamma}{\omega} < \sqrt{3}$ for propagating modes derived theoretically [118].

I now focus on detailed examination of longitudinal dispersion curves and their change with temperature. The maxima of Fourier transforms $\tilde{C}_L(k,\omega)$ give the frequencies of longitudinal excitations [6]. The resulting dispersion curves are shown in Figure 6.3. The slope of the linear part of the dispersion curve at small k gives the speed of sound, c, which can be compared with experiments probing the speed of sound at small k and ω. As follows from Figure 6.4, the calculated c agrees with the experimental c available at low temperature [120] well. The increase of c with temperature is due to large pressure buildup in the system at constant density. For example, the pressure increases to 46 GPa, 80 GPa and 103 GPa at the highest simulated temperature at three simulated densities (0.4, 0.65 and 0.8 g/cm^3).

It is observed that the regime of collective phonon excitations starts to deviate from linearity in Figure 6.3. This crossover takes place at temperatures well above the FL. This is expected because, as discussed above, crossing the FL from below corresponds to the regime of diffusive particle motion where the concept of the MFP applies.

Importantly, the crossover of dispersion curves takes place at k points

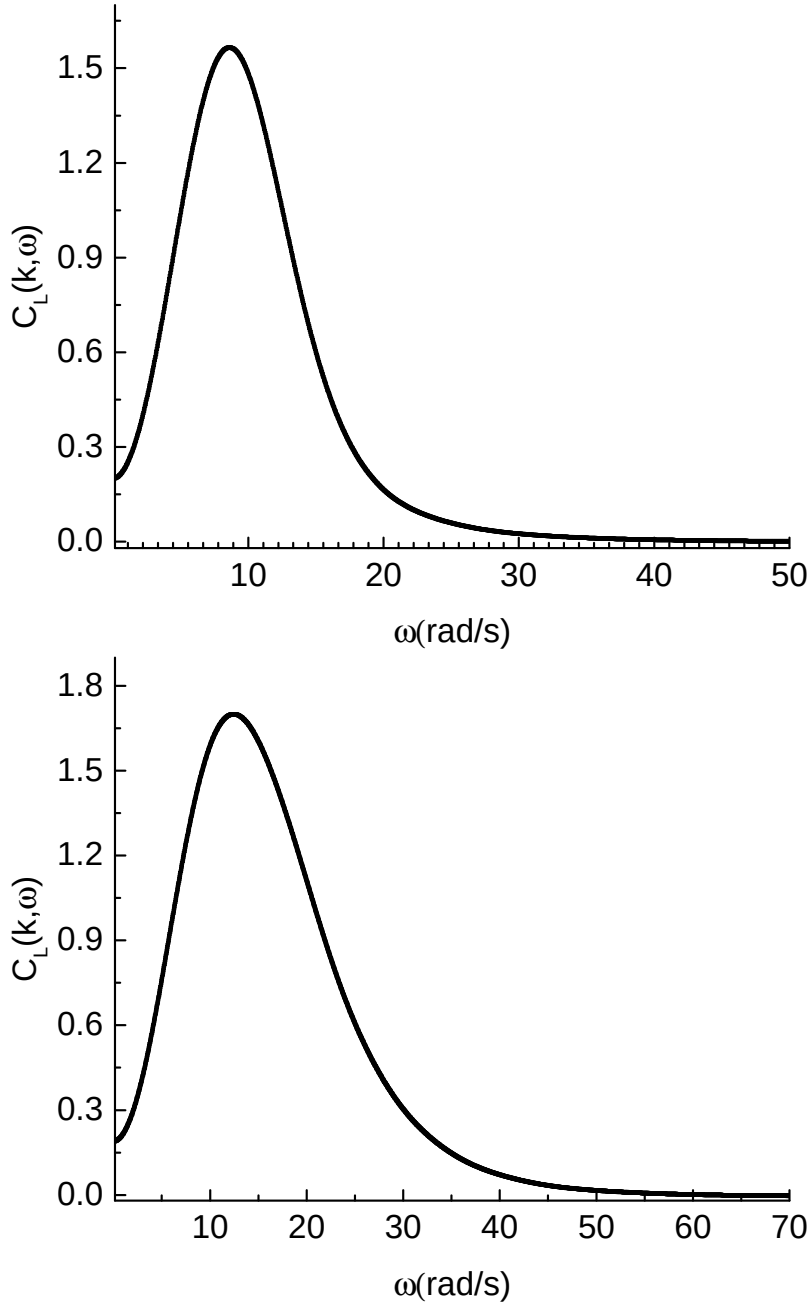

Figure 6.2: Examples of $C_L(k,\omega)$ calculated at density 0.65 g/cm^3 and $T = 500$ K and shown at $k = 0.67$ Å^{-1} (top) and $k = 1.34$ Å^{-1} (bottom).

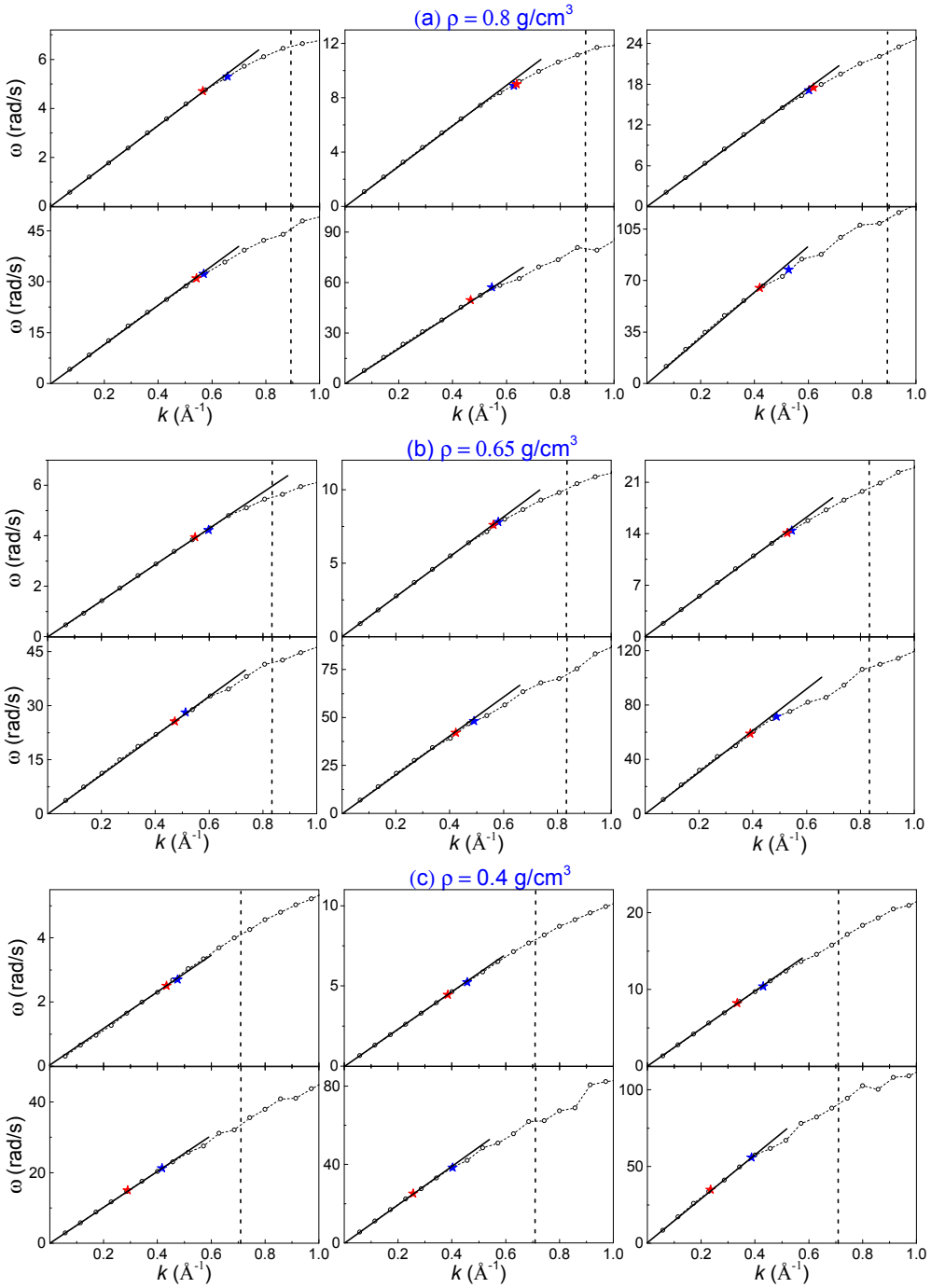

Figure 6.3: Phonon dispersion curves of supercritical Ar at density $\rho_1 = 0.8$ g/cm^3 (top panel), $\rho_2 = 0.65$ g/cm^3 (middle panel) and $\rho_3 = 0.4$ g/cm^3 (bottom panel). The corresponding temperatures are (from left to right, top to bottom of each density) are 500 K, 2000 K, 10000 K, 50000 K, 200000 K and 500000 K, respectively. The blue star points are $k^\star$ calculated by Eq.(6.3). The red star points are k-points calculated as $\frac{\pi}{l}$, where the mean-free path l is evaluated from experimental gas-like viscosity. The dashed vertical lines mark the first pseudo-Brillouin zone boundary calculated as $k_{ZB} = \left(6\pi^2 \frac{N}{V}\right)^{\frac{1}{3}}$ [12]. The straight lines starting from (0,0) guide the eye showing the linear slope.

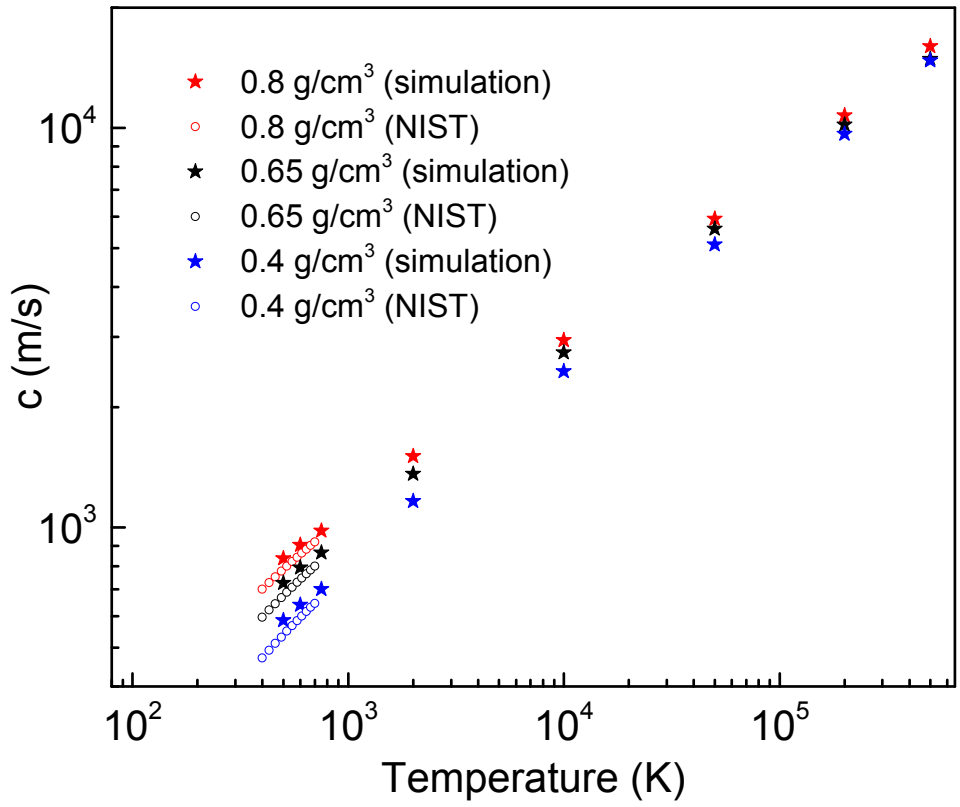

Figure 6.4: The calculated speed of sound (stars) and the experimental [120] speed of sound (open symbols) at three simulated densities.

which decrease with temperature. This behavior is consistent with previous hypothesis: in the MFP regime above the FL where atoms move freely up to distance l on average, the increase of l with temperature implies that the shortest wavelength of the longitudinal phonons increases, resulting in the decrease of their largest k points. It should be noted that the MFP regime (and the corresponding slope of ω vs k) is intermediate between the sound regime at small k and free-particle regime at large k discussed later.

6.3 Discussion: three methods

This interpretation is supported by three quantitative estimates. I start with evaluating λ and note that one straightforward evaluation involves a rela-

tionship between λ and specific heat c_v. Indeed, free motion of atoms up to distances comparable to l in the MFP regime contributes only to kinetic energy but not to the potential term. Then, the energy of the system with one longitudinal mode only is the sum of the kinetic term $\frac{3}{2}NT$ ($k_B = 1$) and the potential energy of the longitudinal mode with wavelengths longer than the shortest wavelength in the system $\lambda = l$. Using the Debye model, this gives the energy as [115]:

$$E = \frac{3}{2}NT + \frac{1}{2}NT\frac{a^3}{\lambda^3} \tag{6.2}$$

where a is interatomic separation.

Eq. (6.2) gives specific heat $c_v = \frac{3}{2} + \frac{1}{2}\frac{a^3}{\lambda^3}$ (the variation of λ with temperature is neglected due to the very slow increase of $l(T)$ as discussed below). This gives λ as

$$\lambda = \frac{a}{(2c_v - 3)^{1/3}} \tag{6.3}$$

Eq. (6.3) applies to the regime above the Frenkel line where $c_v < 2$ [13, 14, 20] (under this condition, Eq. (6.3) implies $\lambda > a$ as required). I have calculated $c_v = \frac{1}{N}\frac{dE}{dT}$ in a wide temperature range corresponding to the decrease of c_v from about 2 to its gas-like value $\frac{3}{2}$ (see Figure 6.5). It is observed that c_v decreases very slowly at high temperature. According to Eq. (6.3), λ is predicted to vary similarly slowly at high temperature. This will be discussed later.

Using the calculated c_v, I have evaluated the shortest wavelength λ using Eq. (6.3). Some care is needed to find the corresponding k. In Eq. (6.2), the shortest λ is assumed to be a, corresponding to $E = 2NT$ and $c_v = 2$ [115]. For specific evaluations of λ, recall that the shortest wavelength in the system with the shortest length scale a is $2a$, therefore k at the crossover from the sound to

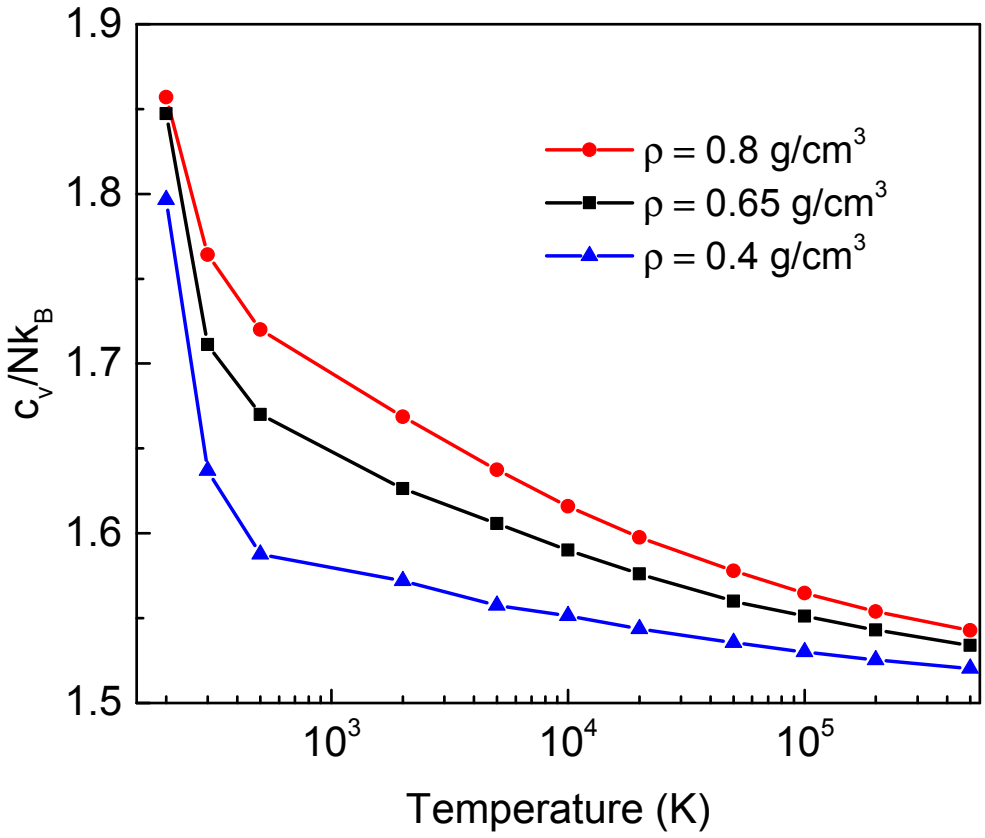

Figure 6.5: Specific heat as a function of temperature for three simulated densities.

the MFP regime, $k^\star$, is $k^\star = \frac{2\pi}{2\lambda} = \frac{\pi}{a}\left(2c_v - 3\right)^{\frac{1}{3}}$. I plot $k^\star$ in Figure 6.3 as blue stars and observe that in most cases (particularly at higher density) $k^\star$ lies close to the deviation of the sound regime from linearity. This constitutes my *first* quantitative evidence in support to previous hypothesis that the crossover of dispersion curves is related to the shortest wavelength available in the system.

$k^\star$ is plotted as a function of temperature in double-logarithmic plot in Figure 6.6. It should be noted that Figure 6.6 shows that $k^\star$ and λ obey the power law

$$\begin{aligned} k^\star &\propto \frac{1}{T^\alpha} \\ \lambda &\propto T^\alpha \end{aligned} \tag{6.4}$$

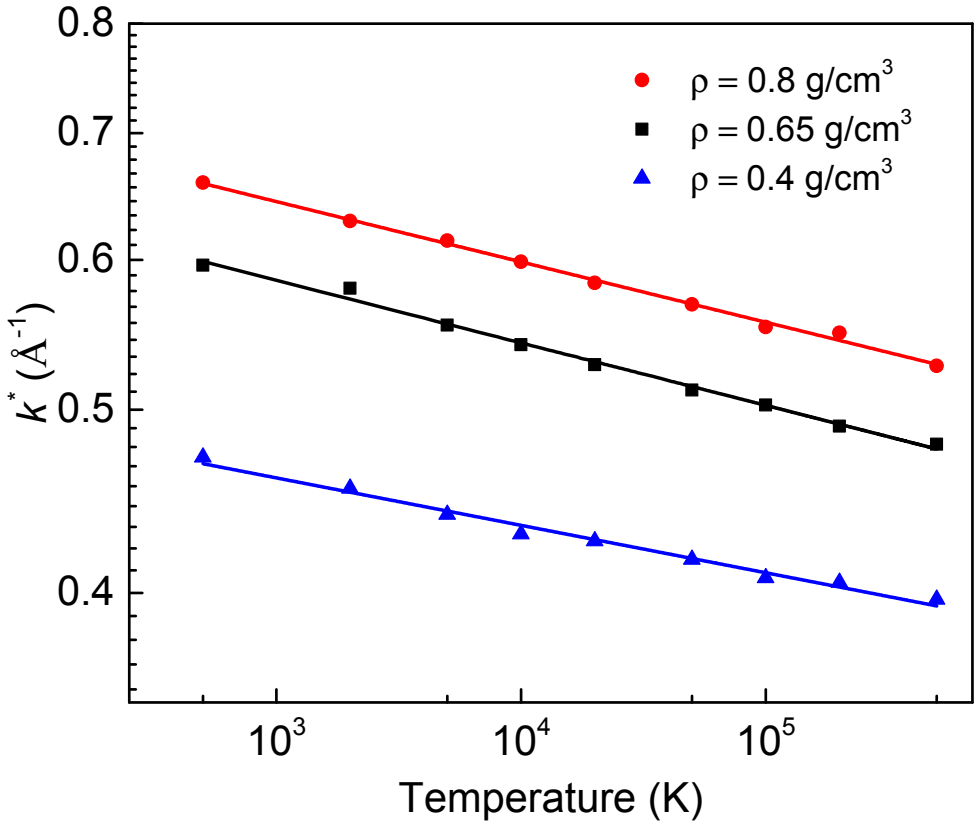

Figure 6.6: Dependence of $k^{\star}$ on temperature. The lines are fits to the power-law dependence.

where α is about 0.1.

The existence of a power law is important because it often implies an underlying dynamical process leading to universal scaling relationships, as it does in, for example, the phase transitions area. I will re-visit this point below in my evaluation of l.

As proposed above, the crossovers in Figure 6.3 are related to the shortest wavelength of the system governed by the mean free path l. l can be directly evaluated from viscosity in the mean-free path regime: $\eta = \frac{1}{3}\rho\bar{v}l$, where ρ is density and $\bar{v}$ is average velocity. Using experimental η from the NIST database [120] at 500 K, I calculate l and the corresponding k-point as $\frac{\pi}{l}$. I plot the calculated k points as red stars in Figure 6.3 and observe that they

lie close to both $k^\star$ calculated on the basis of Eq. (6.3) and to the crossover of dispersion curves. The NIST database does not extend to high temperature, and so I fit the experimental low-temperature viscosity to the power law (see the discussion below) and extrapolate η to high temperature. Similarly to 500 K, the calculated k-points from extrapolated viscosity remain close to $k^\star$ calculated on the basis of Eq. (6.3) and to the crossover of dispersion curves. The increase of the distance between red and blue stars at high temperature compared to low can be related to the reduced reliability of extrapolation to high temperature.

The proximity of k-points evaluated from λ in Eq. (6.3) and the mean free path l to each other and to the crossover of dispersion curves constitutes my *second* quantitative evidence in support to the previous hypothesis that the crossover of dispersion curves is related to the crossover from the phonon regime to the MFP regime where the mean-free path limits the shortest available wavelength as $\lambda = l$.

Importantly, the small value of α we observe for λ in Eq. (6.4) is the same as the temperature exponent of the mean free path l in both experiment and theory. Experimentally, evaluating l from the experimental supercritical gas-like viscosity gives $l \propto T^\alpha$ with α close to 0.1 [115].

Interestingly, the same result $l \propto T^\alpha$ with α close to 0.1 follows from the kinetic gas theory. Approximating the Enskog series by the first term and considering the interatomic interaction in the form of the inverse-power law $U \propto \frac{1}{r^m}$ gives viscosity η as [5]

$$\begin{aligned} \eta &\propto T^s \\ s &= \frac{1}{2} + \frac{2}{m-1} \end{aligned} \tag{6.5}$$

The temperature dependence of l can be predicted using Eq. (6.5) and

viscosity in the MFP regime $\eta = \frac{1}{3}\rho\bar{v}l$ and noting that $\bar{v} \propto T^{0.5}$. This gives $l \propto T^{s-0.5}$.

In the limit of large m corresponding to the hard sphere system, (6.5) predicts $s = \frac{1}{2}$ and, therefore, temperature-independent l. In this limit, l is governed by density only. Some care is needed to evaluate s for the LJ potential used in this work. Recall that the function describing the repulsive part of the LJ potential is governed by both repulsive $\frac{1}{r^{12}}$ and attractive $\frac{1}{r^6}$ terms. The net result is that the effective repulsive function varies as $U \propto \frac{1}{r^m}$ with $m = 18$–20 [125]. Using this m in (6.5) gives $s \approx 0.6$. Using $l \propto T^{s-0.5}$ gives $l \propto T^{0.1}$, and I obtain the same exponent calculated for λ in (6.4).

The coincidence of the temperature behavior of λ and l as power law $\propto T^{\alpha}$ with the same exponent α constitutes my *third* quantitative evidence in support to previous hypothesis that the crossover of dispersion curves is related to the crossover from the sound to the MFP regime and $\lambda = l$. Taken together, the three quantitative estimates support the interpretation of the crossover to the MFP regime, rather than a trivial deviation of dispersion curves from linearity close to the zone boundary.

It should be noted that at larger k, the mean free path regime is followed by the free-particle regime. Indeed, very large k and ω correspond to particles moving short distances at short times, i.e. the regime of free particles and the dispersion $\omega = vk$, where v is particle velocity (this also applies to crystals where large k correspond to scattering from both free particles and phonons in higher Brillouin zones). I have calculated the dispersion relation for large ω and k and show examples in Figure 6.7. The calculated slope at large k agrees with the most probable thermal speed $v_p = \sqrt{2k_{\mathrm{B}}T/m}$ within 9–13% for different densities. Hence, the MFP regime considered earlier is intermediate between the sound regime and the free-particle regime in terms of k-values.

I make a remark regarding the values of l. The shortest wavelengths

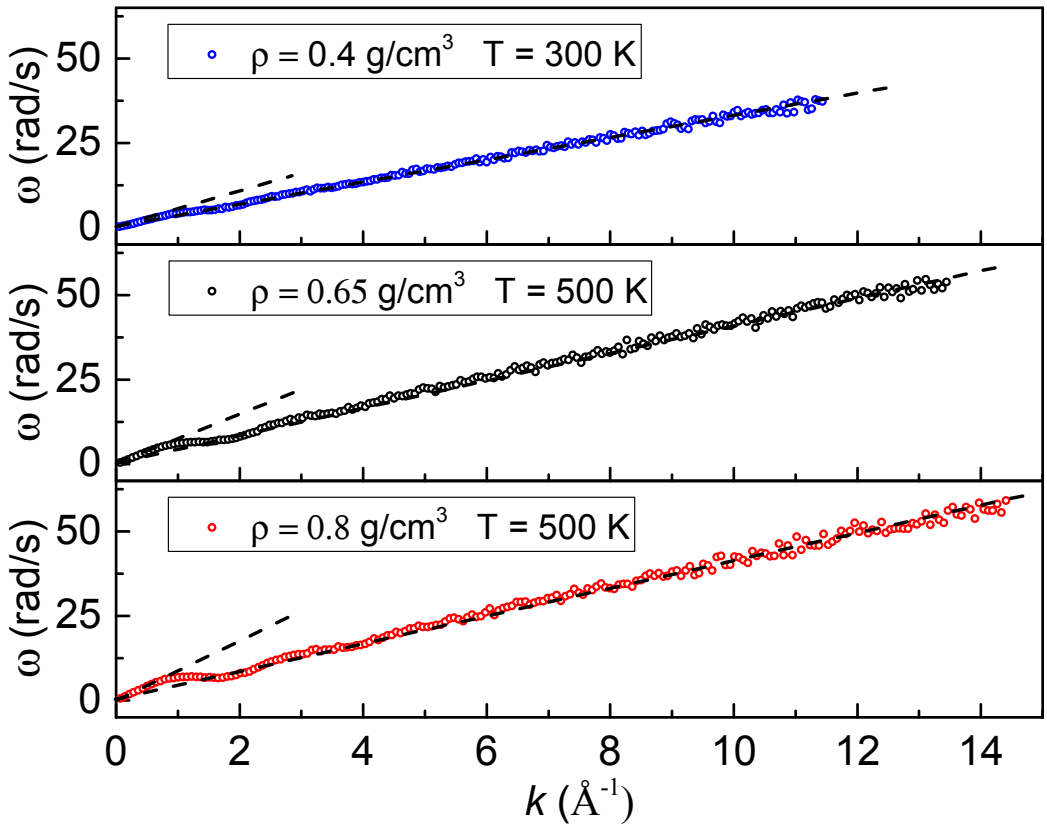

Figure 6.7: Phonon dispersion curves of supercritical Ar at large k at different density and temperature. Dashed lines are guides for the eye and show the speed of sound at small k and thermal velocity at large k.

at k-points in Figure 6.6 and the corresponding l are approximately 10–15 Å, or about 3–4 interatomic separations (the small range of l is due to its slow decrease on the isochores as discussed earlier). This is shorter than l generally envisaged in the kinetic theory of gases and is to be expected for dense supercritical fluids as compared to dilute gases [5]. This can explain why the slope of ω vs k differs from thermal velocity in the MFP regime (thermal velocity is recovered at large k as discussed above).

Even though l is short, it is nevertheless important from the thermodynamic point of view because it cuts off phonons with largest frequencies which contribute most to the system energy [17]. As a result, c_v decreases from about

2 at the Frenkel line (this value has contributions from the kinetic term $\frac{3}{2}$ and the potential term of the longitudinal mode $\frac{1}{2}$) to the value close to c_v of the ideal gas, $\frac{3}{2}$. This is seen in Figure 6.5. Short l also implies that, since l is an average property, its relative fluctuations around the mean value may be non-negligible, which could explain that in some cases λ and l may deviate from the observed crossover of dispersion curves in Figure 6.3.

Before concluding, it should be noted that high temperatures were required to detect the decreasing k at the crossover at fixed density. Although these temperatures might seem unusually high, there are three reasons why they are relevant to real systems and experiments. First, liquid argon remains an unmodified system up to fairly high temperature: the first ionization potential of condensed liquids is on the order of 10^5 K. Hence most of my temperature range where the dispersion relations and crossovers are seen corresponds to the unmodified non-ionized argon describable by the LJ potential. Second, performing experiments at realistic constant pressure, rather than constant density used here, lowers the crossover temperature significantly due to faster increase of the mean free path when volume increases. Third, performing the experiments in systems with lower critical point such as Ne implies that the crossover temperature is lower: the crossover at the largest temperature simulated here is predicted to be lower by the ratio of Ar and Ne critical temperatures, or over 3 times.

We note that there is a similarity between the observed crossover of collective excitations and the Ioffe-Regel (IR) crossover. The IR crossover was intensely studied in disordered systems (see, e.g., Shintani and Tanaka, Nature Materials 2008). The IR crossover corresponds to the crossover between propagating and non-propagating phonons and was originally introduced to describe the completely non-propagating case where the phonon mean free path becomes comparable to the interatomic spacing, so that no phonons

propagate. In the case of longitudinal modes discussed here, the crossover is partial: propagating to non-propagating crossover takes place at a distance equal to the mean-free path l, and phonons with wavelengths above and below l become propagating and non-propagating, respectively.

6.4 Conclusions

In summary, I presented evidence for propagating solid-like longitudinal phonons deeply in the supercritical regime, with wavelengths extending to interatomic separations and observed the crossover of dispersion curves. By studying temperature dependence of the shortest available wavelength and mean free paths, I related this effect to the crossover from the collective phonon to the collisional mean-free path regime of particle dynamics.

Chapter 7

Thermodynamic heterogeneity and crossover in the supercritical state of matter

A hallmark of a thermodynamic phase transition is the qualitative change of system thermodynamic properties such as energy and heat capacity. On the other hand, no phase transition is thought to operate in the supercritical state of matter and, for this reason, it was believed that supercritical thermodynamic properties vary smoothly and without any qualitative changes. Here, I perform extensive molecular dynamics simulations in a wide temperature range and find that a deeply supercritical state is thermodynamically heterogeneous, as witnessed by different temperature dependence of energy, heat capacity and its derivatives at low and high temperature. The evidence comes from three different methods of analysis, two of which are model-independent. I propose a new definition of the relative width of the thermodynamic crossover and calculate it to be in the fairly narrow relative range of 13-20%. On the basis of these results, the crossover is related to the supercritical Frenkel line. The results in this Chapter has been submitted to Journal of Physics: Condensed

matter.

7.1 Introduction

Transitions between different phases and properties of those transitions have been one of central themes of condensed matter physics. Ideas and methods developed in this field are applied to other wide-ranging areas, including geology, chemistry, quantum field theory and cosmology. First and second-order phase transitions and related critical phenomena are best-studied [121]. A first-order transition takes place across the boiling line. The line finishes at the critical point where the transition becomes second-order.

Phase transitions involve phases traditionally defined as physically uniform and homogeneous states or regions of space and which have qualitatively different properties such as different temperature or pressure dependencies of system characteristics. Interestingly, an absence of a phase transition in a certain range of thermodynamic parameters (pressure, temperature) does not necessarily imply that no qualitatively different states exist in that range. In other words, a transition between two states with qualitatively different properties can still take place even when the states belong to the same phase in the traditional definition of this term. When this occurs, we are dealing with a thermodynamic non-uniformity (heterogeneity) where a smeared transformation or a crossover takes place between the two states, rather than a phase transition. Compared to phase transitions, crossovers are less understood in general, not least because they are more subtle and are more difficult to detect, but also because their understanding is not developed from a general theoretical standpoint.

One example of what is believed to be a physically uniform and homogeneous state is the supercritical state of matter. Supercritical fluids are

increasingly deployed in a number of important applications but their theoretical understanding is not developed [18]. The supercritical state is loosely defined to be above the range of thermodynamic parameters above the critical point. It was widely thought that no qualitative differences exist between gases and liquids, or any physical states, in the supercritical regime [121, 18]. This belief implied that thermodynamic properties vary smoothly and without any qualitative changes. Guided by a theoretical consideration of particle dynamics and modelling results [13, 14, 20], it has been recently proposed that two qualitatively different states with gas-like and liquid-like properties exist in the supercritical state and are separated by a crossover centered at the Frenkel line (FL). Recently, structural and dynamical changes at the FL have been experimentally confirmed in supercritical neon [80], methane [81] and CO_2 [122]. Here, I focus on important *thermodynamic* properties of this crossover and discuss the evidence for the thermodynamic crossover seen as the change of central system properties such as energy, heat capacity and its derivatives.

I start by recalling the main idea of the Frenkel line in the supercritical state, based on the qualitative change of particle dynamics. At low temperature, the dynamics of liquid particles combine small-amplitude solid-like oscillatory motion around quasi-equilibrium positions and large-scale diffusive jumps between neighbouring positions, the picture introduced by Frenkel [1]. This motion is quantified by the liquid relaxation time τ, the average time between particle's jumps. τ is directly related to viscosity and other important liquid properties. The FL proposal is based on considering how τ changes with temperature (pressure). Below the critical point, τ decreases with temperature until the liquid crosses the phase transition line and boils. Above the critical point where no phase transition intervenes, τ continuously decreases with temperature until it reaches its limiting value comparable with the shortest

(Debye) transverse oscillation period τ_D. When $\tau \approx \tau_D$, a particle spends about the same time oscillating as diffusing, at which point the oscillatory component of particle motion is lost. The crossover from combined oscillatory and diffusive particle motion to purely diffusive is the crossover at the FL.

The dynamical crossover can be operationally defined from the disappearance of minima of velocity autocorrelation function (VAF), corresponding to monotonic VAF decay as in a gas [14]. This gives the FL on the phase diagram which coincides with $c_v = 2$, where c_v is specific heat and $k_B = 1$. There is a good reason for this coincidence because $c_v = 2$ signifies a particular dynamical and thermodynamic state of the system as discussed below.

Frenkel predicted [1] that at short times $t < \tau$ or high frequency $\omega > \frac{1}{\tau}$ (by a factor of 2π), the liquid behaves like a solid and therefore supports two solid-like transverse modes. The range in which transverse modes propagate shrinks with temperature, starting from the lowest frequency (or, to be more precise, from the smallest k-point or largest wavelength as discussed in detail later). Eventually, the liquid exhausts the frequency range at which it can support transverse modes, the result confirmed by direct molecular dynamics simulations [113]. At this point, liquid potential energy is given by the potential energy of one remaining longitudinal mode only, or $\frac{T}{2}$ per particle. Together with the kinetic contribution $\frac{3T}{2}$, the energy per particle becomes $2T$, giving the specific heat $c_v = 2$ [17]. On further temperature increase, it is now the longitudinal mode that starts shrinking in range, starting from the shortest wavelength because the wavelength can not be shorter than the particle mean free path [17, 115].

Therefore, different collective modes evolve with temperature *differently* below and above the FL. This provides the key to predicting the thermodynamic crossover at the FL: since each mode contribute the energy T per particle to the total energy of the supercritical system, the energy and its derivatives are

predicted to have different temperature dependence below and above the FL (below I give specific equations for the system energy below and above the FL), i.e. exhibit a crossover around $c_v = 2$. However, there has been no detailed study of actual functional dependencies of the energy, c_v and its derivatives below and above the FL and the associated crossover from its low-temperature to high-temperature regime. Another important open question is how wide is the thermodynamic crossover? Is the crossover range comparable to the entire range of variation of thermodynamic functions, or is it localised around the predicted $c_v = 2$?

In this Chapter, I perform extensive molecular dynamics simulations of supercritical system in a very wide temperature range and analyze the functional dependence of energy, c_v and its derivatives below and above the FL. Two of my analysis methods are model-independent and do not rely on any prior knowledge related to a crossover. The analysis shows that the supercritical state is thermodynamically heterogeneous, with different temperature dependence of energy, c_v and its derivatives at low and high temperature. I find that the thermodynamic crossover corresponds to the Frenkel line, and is of a fairly narrow relative width of 13-20%.

7.2 Methods

I have performed extensive parallel molecular dynamics (MD) simulations of supercritical liquid Ar using the Lennard-Jones (LJ) potential and constant volume and energy ensemble using two densities, 1.5 and 1.9 g/cm^3. The simulated temperature starts from just above the melting temperature and increases to very high temperatures deep in the supercritical state up to 50,000 K, corresponding to 215 times the critical temperature. In this work I study energy derivatives, c_v and its derivative. This is often done by fitting the energy

points and subsequently differentiating the fit. I find that the resulting c_v and its derivatives can depend on the type of fit used. For this reason, I do not fit the energy. Instead, I simulate 510 temperature points for each density using a high-performance computing cluster. Each run involves 30 ps of equilibration and further 50 ps of production runs during which the calculated properties are averaged. Each temperature simulation is repeated 20 times using different starting conditions, and the calculated energy at each temperature is further averaged over 20 different runs. This averaging was found to be essential in order to reduce fluctuations of energy derivatives, particularly large at high temperature. In total, I performed 20,000 MD runs, equivalent to over 100,000 processor-hours or over 11 processor-years.

7.3 Results and discussion

This study focuses on temperature dependence of energy E, $c_v = \frac{1}{N}\frac{dE}{dT}$ and its derivatives. c_v at two densities is shown in Figure 7.1. As discussed above, the predicted crossover of thermodynamic properties takes place at temperature corresponding to $c_v = 2$. This corresponds to the temperature range of about 1000-4000 K at both densities. This temperature range corresponds to approximately $10 - 30T_c$ (Ar critical temperature is $T_c = 151$ K) and hence the crossover can not be attributed to the Widom line, the line of persisting near-critical anomalies [22] which disappears after about $3T_c$ [123, 124].

It should be noted that the crossover at $c_v = 2$ assumes that each mode contributes $\frac{T}{2}$ to the energy as in the harmonic case. Intrinsic anharmonicity, present in experiments and MD simulations, can alter c_v somewhat [17], implying that the crossover of c_v takes place around $c_v = 2$ but not exactly at it.

Three methods of analysis are performed. In the *first*, model-independent

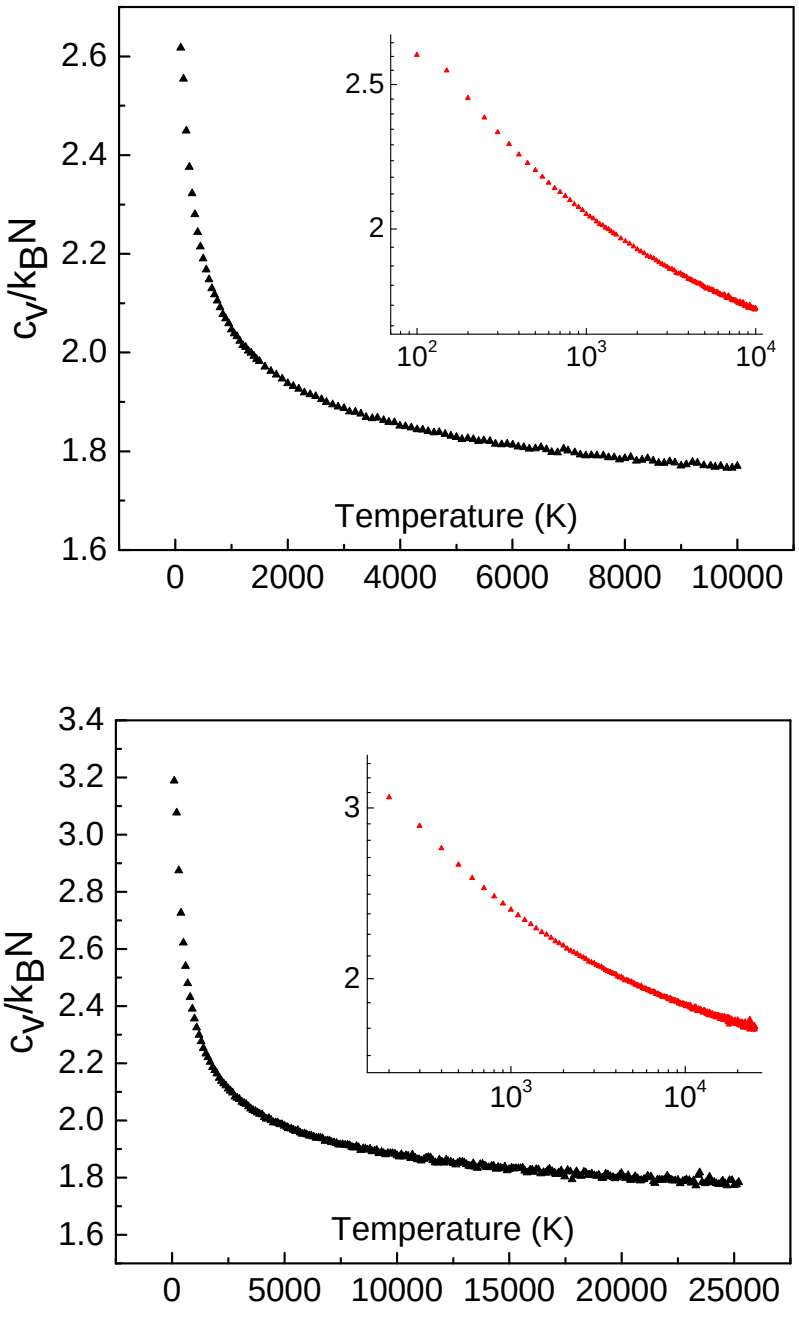

Figure 7.1: c_v calculated for density 1.5 g/cm^3 (top) and 1.9 g/cm^3 (bottom).

method, I focus on temperature dependence of the system energy and fit the low-temperature and high-temperature parts of the energy to the simplest three-parameter function with a varying power exponent, $E = A + BT^C$. The high-temperature fitting range starts from temperature 3000 K above the predicted crossover range so that the analysis is not affected by the prior knowledge of the crossover temperature and finishes at 50,000 K, over ten times the crossover temperature. The low-temperature fitting range starts from just above the critical temperature and finishes 1000 K below the crossover range. The coefficient of determination related to the goodness of the fit, R^2, is significantly higher if the fit is performed for low- or high-temperature range as compared to the entire range: in the first case $1 - R^2$ is 10-100 times larger than in the second case. I define and calculate the difference parameter D:

$$D = (E - E_h)^2 + (E - E_l)^2 \tag{7.1}$$

where E_h and E_l are fitted energies in the high- and low-temperature range, respectively.

D can be used to study whether a given curve represents one or two different functional dependencies. If $E(T)$ is described by a single function, D is zero or a small value related to fitting errors. If low and high-temperature dependence of $E(T)$ is given by two different functions, E_l and E_h will make zero contributions to D at low and high T, respectively and, conversely, large contributions to D at high and low T. This, together with D being positive, implies that D has a minimum. Large D at either low or high T indicates that this temperature is far away from the crossover between the two functions. At the minimum, neither E_h nor E_l fit the function as well as they do on the asymptotes but do not make a large contribution to D. Hence, the minimum of D approximately corresponds to the crossover between the two functions.

I plot D for two densities in Figure 7.2 and make two important observations. First, a very deep minimum of D is observed for both densities. Second, the minimum develops at temperatures around 1000 K and 4000 K at both densities. It is observed that these are the temperatures at which $c_v = 2$ at both densities in Figure 7.1, corresponding to the crossover at the Frenkel line.

Similarly to the first method, my *second* method of analysis is model-independent and deals with c_v and its derivaties. It is observed that c_v changes slowly at high temperature in Figure 7.1 and crosses over to a much steeper function at low temperature. The double-logarithmic plot of c_v is not linear (see the inset to Figure 7.1), implying that the temperature dependence of c_v can not be described by a power law. To address the change of slope of c_v in more detail, I calculate $\frac{dc_v}{dT}$ using the data in Figure 7.1 and observe a slow and nearly constant behavior at high temperature which crosses over to a much steeper dependence at low temperature. The crossover from the small to large slope is in the range of about 1000-3000 K for both densities. This is close to the temperature range at which $c_v = 2$ in Figure 7.1, corresponding to the crossover at the FL.

Next, I fit $\frac{dc_v}{dT}$ and show the fit in Figure 7.3a (the inset shows the semi-logarithmic plot highlighting the low-temperature range with the large slope). Using the fit, I calculate the second derivative $\frac{d^2c_v}{dT^2}$ and plot it in Figure 7.3b, together with the semi-logarithmic plot highlighting the low-temperature range with the steep slope). A similar behavior of the second derivative is observed: the crossover from slow high-temperature to steep low-temperature behavior. The crossover is in the range 1000-2000 K for both densities and is close to the temperature range where $c_v = 2$ at the FL.

In view of the very wide temperature range considered in Figure 7.1, the closeness of the crossover temperatures of first and second derivatives to temperatures where $c_v = 2$ is particularly encouraging.

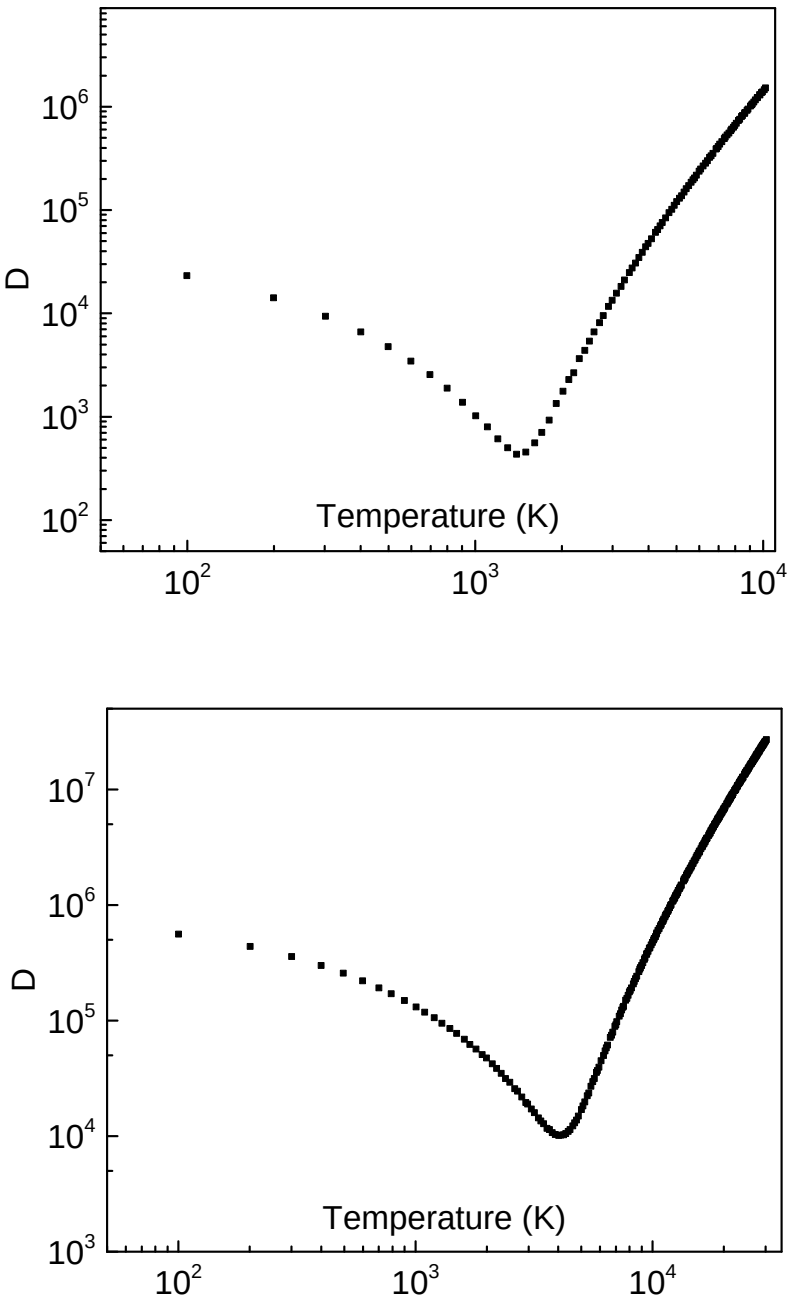

Figure 7.2: Difference parameters D calculated for density 1.5 g/cm^3 (top) and 1.9 g/cm^3 (bottom).

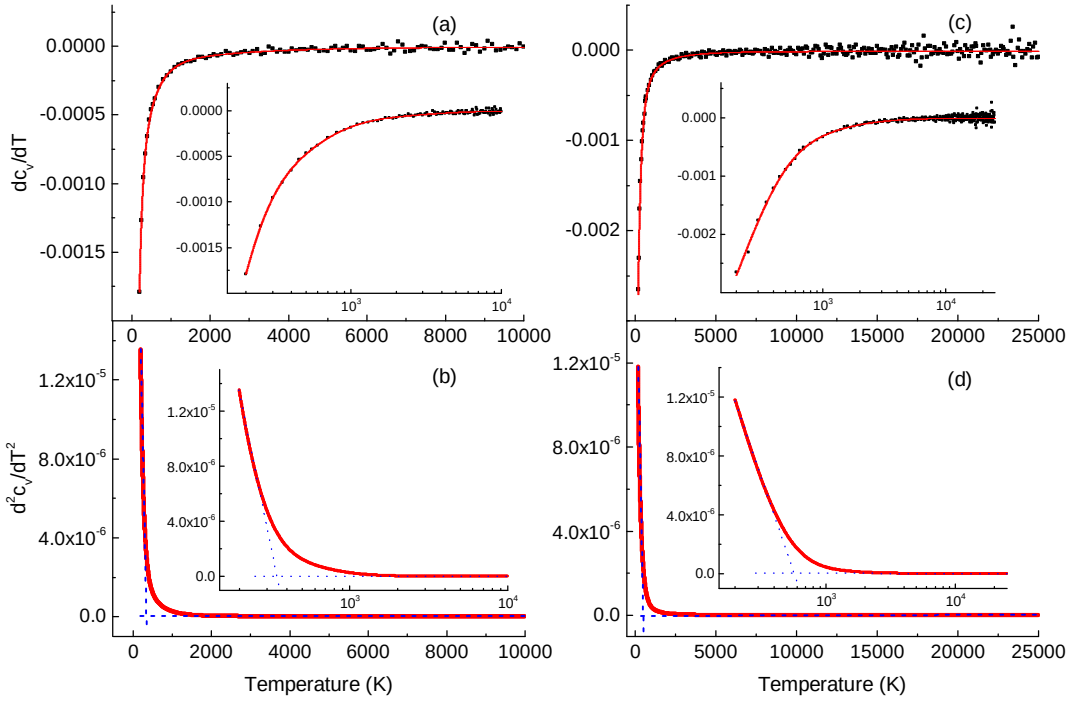

Figure 7.3: (a) shows $\frac{dc_v}{dT}$ and its fit for density 1.5 g/cm^3; (b) shows $\frac{d^2c_v}{dT^2}$ calculated as the derivative of the fit in (a), with the dashed lines showing straight-line approximations to the low- and high-temperature range. The insets show the same graphs in the semi-logarithmic plots to highlight the low-temperature range with steep slopes. (c) and (d) show the same for density 1.9 g/cm^3.

On the basis of Figure 7.3, the width of the thermodynamic crossover, W, is discussed. There is no universal approach to defining the crossover width. If low and high-temperature range of a function in question (or its certain transformation) are close to straight lines, the crossover width is given by the difference between temperatures at which deviations from the straight lines are seen. However, this definition is not unique and depends on the path chosen on the phase diagram (I have chosen the constant-volume path for convenience of calculating c_v). Indeed, a constant-pressure path gives a different W: density decrease with temperature results in faster temperature decrease of τ below the FL and faster increase of the mean free path l above the FL and, therefore, gives a smaller W.

In order to alleviate the issues related to the dependence of the crossover width on the path on the phase diagram, I propose a definition of the crossover that is based on c_v itself (or functions of c_v) rather than on thermodynamic parameters such as temperature or pressure. The relative width of the specific heat crossover is defined as

$$W = \frac{c_v^l - c_v^h}{c_v^{cr}} \tag{7.2}$$

where c_v^l and c_v^h are values of c_v corresponding to the deviation of c_v or its function from their low- and high-temperature behavior and $c_v^{cr} = 2$ is the value of c_v at the FL crossover.

Observing that low- and high-temperature range of $\frac{d^2 c_v}{dT^2}$ can be approximated by the straight lines, c_v^l and c_v^h are obtained by taking the deviation temperatures from Figure 7.3b,d and subsequently finding the corresponded c_v from Figure 7.1. It should be noted that there is a slight ambiguity in finding the deviation temperatures related to how one chooses to draw the straight-line approximation, particularly in the low-temperature range. Whereas this may affect the deviation temperature, the corresponding variation of c_v in Figure 7.1 is insignificant. I find $c_v^l = 2.15$ and $c_v^h = 1.895$ for low density and $c_v^l = 2.3$ and $c_v^h = 1.9$ for high density. Eq. (7.2) gives W of 13% and 20% at low and high density, respectively. The smaller W is close to the width of the experimental *structural* crossover of 10-12 % in supercritical Ne [80].

In my *third* method of analysis, I continue to analyze the temperature dependence of the system energy. This method is based on linearizing the energy by transforming the energy functions into linear dependencies using recent theoretical predictions. This method of analysis might be viewed as a less general analysis method, however it is widely used in the analysis of experimental and modelling data. The key to calculating the energy below the

FL is accounting how the range of solid-like transverse modes shrinks with temperature. In the Frenkel picture where transverse modes propagate above frequency $\omega_{\mathrm{F}} = \frac{1}{\tau}$, the energy of transverse modes per particle is calculated to be [17] $E_t = 2T\left(1 - \left(\frac{\omega_{\mathrm{F}}}{\omega_{\mathrm{D}}}\right)^3\right)$, where ω_{D} is Debye frequency. A more detailed analysis [17] gives the dispersion relation of transverse modes as $\omega = \sqrt{c^2k^2 - \frac{1}{\tau^2}}$, which implies the gap in k-space, $k_g = \frac{1}{c\tau}$. Ascertained on the basis of direct modelling results [77], the gap implies that the range of transverse modes shrinks with temperature because τ increases. E_t can be calculated as either the integral over k-space or frequency, and gives the same E_t as above [77, 114]. As shown previously [17], adding the energy of the remaining longitudinal mode and the kinetic energy gives the total liquid energy per particle as discussed previously:

$$E = E_0 + T\left(3 - \left(\frac{\omega_{\mathrm{F}}}{\omega_{\mathrm{D}}}\right)^3\right) \tag{7.3}$$

where E_0 is the temperature-independent term giving the energy at zero temperature.

Using Eq. (7.3), the energy below the FL can be linearized as follows. Using the commonly considered Vogel-Fulcher-Tammann (VFT) law for temperature dependence of $\omega_{\mathrm{F}} = \omega_{\mathrm{D}} e^{-\frac{U}{T-T_0}}$, where U and T_0 are VFT parameters, f_l is introduced as $f_l = \frac{1}{\ln\left(3 - \frac{E-E_0}{T}\right)}$. According to Eq. (7.3), $f_l = -\frac{T-T_0}{3U}$. Hence, f_l is predicted to be a linear function of temperature.

Calculating the energy above the FL involves considering how the remaining longitudinal mode changes with temperature. Recall that above the Frenkel line, the oscillatory component of particle motion is lost and only the gas-like diffusive motion remains. As temperature increases, the particle mean free path l grows. Because the system can not oscillate at wavelengths shorter than l, l sets the smallest wavelength of the remaining longitudinal wave in the

system. As shown previously [17, 115], adding the energy of this mode to the kinetic energy of atoms gives the total energy per particle of the supercritical fluid above the FL as:

$$E = E_0 + \frac{3}{2}T + \frac{1}{2}T\left(1 + \frac{\alpha T}{2}\right)\left(\frac{a}{l}\right)^3 \tag{7.4}$$

where a is the interatomic separation and α is the coefficient of thermal expansion that makes an anharmonic contribution to the mode energy, significant at high temperature above the FL.

Using Eq. (7.4), the energy above the FL can be linearized by introducing $f_h = \frac{E - E_0 - \frac{3}{2}T}{1 + \frac{1}{2}\alpha T}$. According to Eq. (7.4), $f_h = \frac{1}{2}T\left(\frac{a}{l}\right)^3$. l can be calculated from the gas-like viscosity as $\eta = \frac{1}{3}\rho\bar{v}l$, where ρ is density and $\bar{v}$ is average velocity. Using experimental η, it has been shown earlier that l depends on temperature as power law, $l \propto T^{\alpha}$ [115]. The same result follows from the kinetic gas theory: approximating the Enskog series by the first term and considering the interatomic interaction in the form of the inverse-power law $U \propto \frac{1}{r^m}$ gives viscosity η as $\eta \propto T^s$, where $s = \frac{1}{2} + \frac{2}{m-1}$ [5]. Combining it with $\eta = \frac{1}{3}\rho\bar{v}l$, I get $l \propto T^{\frac{2}{m-1}}$ because $\bar{v} \propto T^{\frac{1}{2}}$. Hence, $f_h = \frac{1}{2}T\left(\frac{a}{l}\right)^3$ follows the power law and is the linear function in the double-logarithmic plot.

To calculate f_h, α needs to determine first. Since my energy calculations are at constant density, I perform new calculations at constant pressure enabling the calculation of $\alpha = \frac{1}{V_0}\frac{V - V_0}{T}$. α depends on pressure which increases with temperature in the constant-density simulations used for energy calculations. To calculate α, I used the pressure in the middle of the pressure range in constant-density simulations. The calculated α as a function of temperature is shown in Figure 7.4. Interestingly, it is observed that α in the gas-like regime above the FL decreases approximately as inverse power law, as expected from the ideal gas equation of state. Using $\alpha(T)$ from Figure 7.4, f_h is calculated at

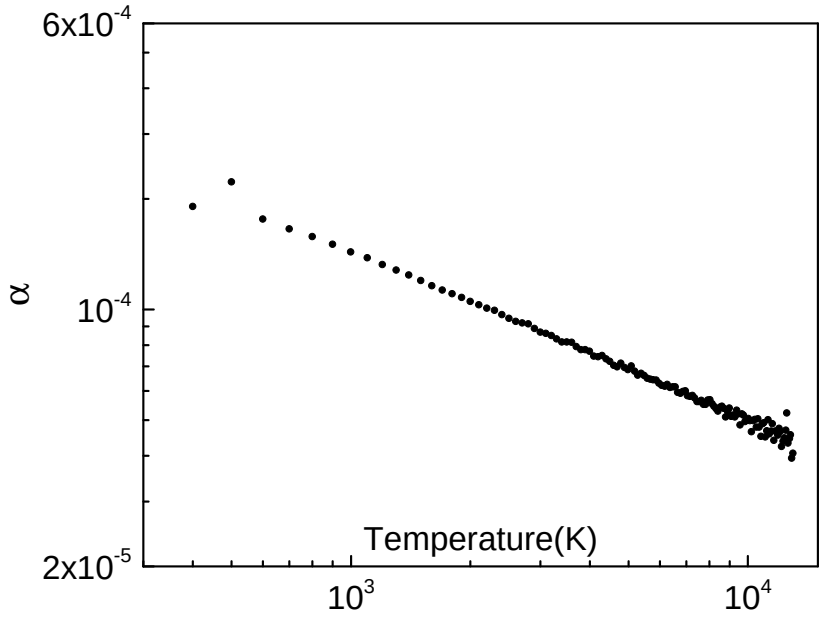

Figure 7.4: Thermal expansion coefficient calculated at 50 kbar for Ar at density ρ =1.9 g/cm^3.

each temperature.

I plot f_l and f_h at two densities in Figure 7.5. Consistent with theoretical predictions, we observe a linear temperature dependence of f_l in the low-temperature range and linear slope of f_h in the high-temperature range in the double-logarithmic plot. Deviations from the linearity are seen and take place at temperatures close to the crossover temperature at both densities. This is expected because the theoretical results Eq. (7.3) and Eq. (7.4) are designed to work for $2 < c_v < 3$ and $1.5 < c_v < 2$, respectively. The important insight from this analysis is that linearizing the energy using a theoretical model works for either low- or high-temperature range but not both. This provides further support to the previous results that there are two supercritical regimes characterized by different temperature dependencies of the energy, with an accompanying thermodynamic crossover.

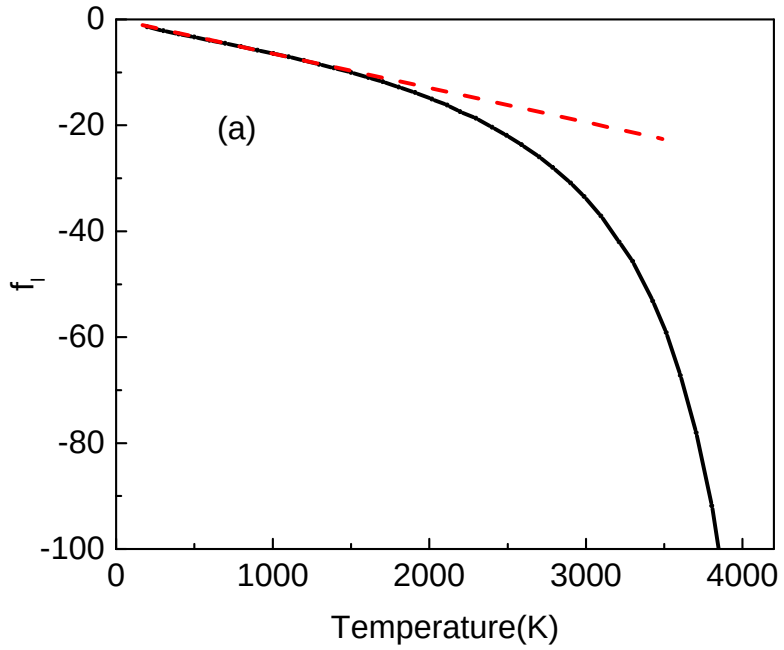
0
-20
-40
-60
-80
-100
(a)
f_l
0
1000
2000
3000
4000
Temperature(K)

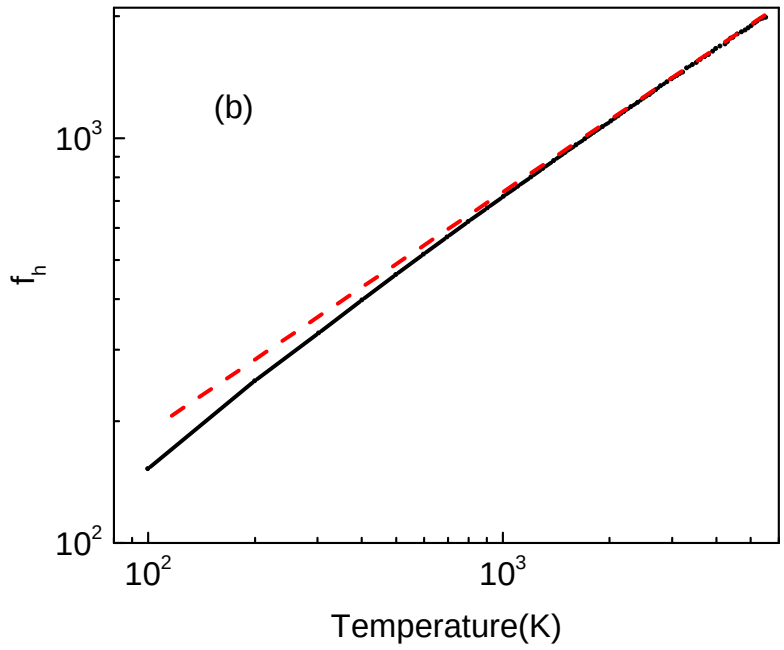
(b)
10^3
10^2
f_h
10^2
10^3
Temperature(K)

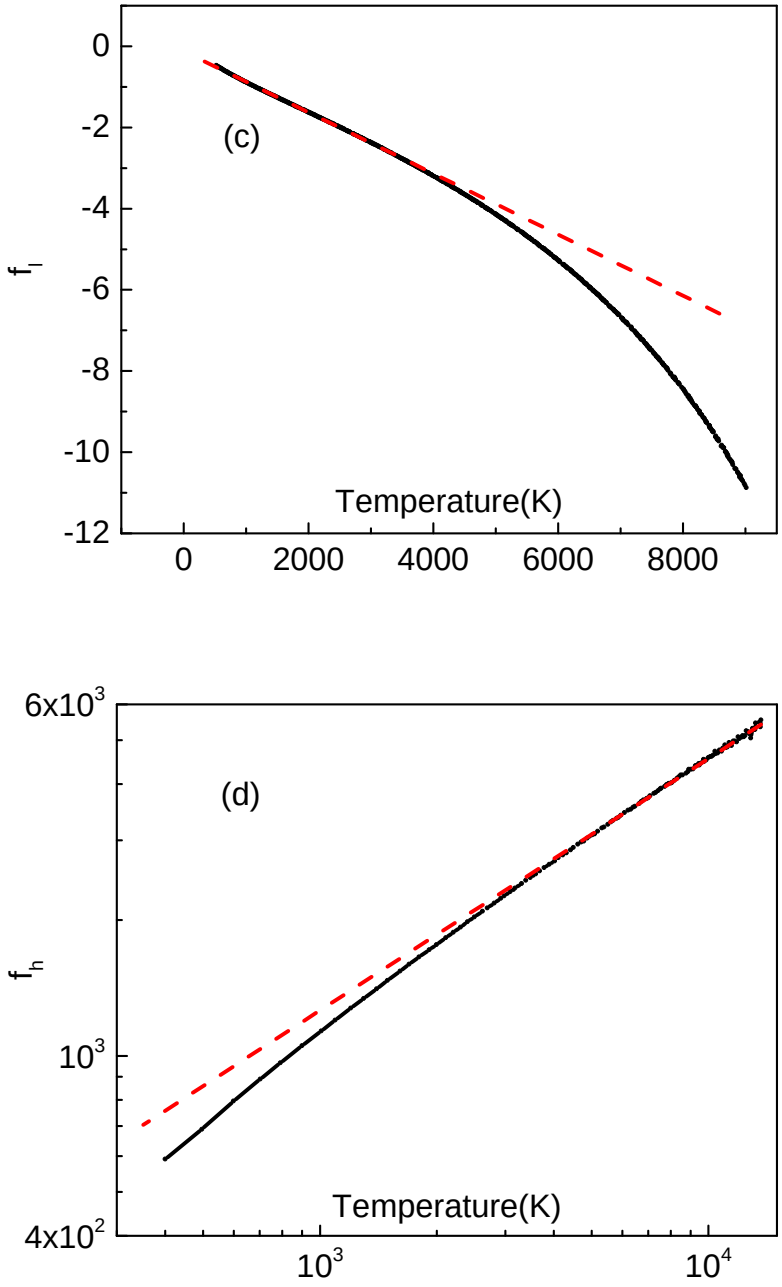

Figure 7.5: f_l and f_h shown at low density 1.5 g/cm^3 in (a)-(b) and high density 1.9 g/cm^3 in (c)-(d). The dashed lines show the linear regimes at low and high temperature, respectively.

In addition to linearizing energy functions, Eqs. (7.3) and (7.4) provide a physical explanation for why c_v has two different functional dependencies at low and high temperature and its very different slopes in particular. The physical properties of interest are ω_{F} in Eq. (7.3) and l in Eq. (7.4). ω_{F} in Eq. (7.3) increases faster-than-exponential with temperature, namely as the VFT law discussed above. This gives fast disappearance of transverse modes with temperature and large slope of c_v and its derivatives in Figure 7.3. On the other hand, l in Eq. (7.4) is a slow function of temperature. Indeed, $l \propto T^{\alpha}$ with α close to 0.1, as followed from the experimental gas-like viscosity $\eta = \frac{1}{3}\rho\bar{v}l$ [115]. The same result follows from the kinetic gas theory [5] as mentioned earlier: $l \propto T^{\frac{2}{m-1}}$, where m is the exponent of the interaction potential $U \propto \frac{1}{r^m}$. Recall that the function describing the repulsive part of the LJ potential is governed by both repulsive $\frac{1}{r^{12}}$ and attractive $\frac{1}{r^6}$ terms, with the net result that the effective m is 18-20 [125]. Consistent with the previous result, this gives α close to 0.1, explaining why c_v and its derivative are slow functions of temperature.

7.4 Conclusions

In summary, I have established thermodynamic heterogeneity of the supercritical state using three different methods of analysis. The associated thermodynamic crossover has the relative width in the range 13-20 % and corresponds to the Frenkel line. My results do not preclude the existence of a phase transition in a narrow temperature range close to $c_v = 2$ and call for a more detailed investigation of this point.

Chapter 8

Conclusions

In this thesis, I addressed a challenging problem of understandings thermodynamic and dynamical properties of liquids and supercritical fluids.

I started with revisiting the solid-like approach to liquid thermodynamics based on collective modes. This was extended to calculating the energy and the heat capacity in liquid-like supercritical state which is the area below the Frenkel line in the phase diagram. Extensive molecular dynamics simulations of liquid energy and specific heat showed that liquid thermodynamics can be understood on the basis of high-frequency collective modes. A more general implication is that, contrary to the prevailing view, liquids are emerging as systems amenable to theoretical understanding in a consistent picture as is the case in solid state theory. I have found this to be the case for several important types of liquids at both subcritical and supercritical conditions spanning thousands of Kelvin.

I subsequently addressed the structural crossover at the Frenkel line and its relationship to the dynamical and thermodynamic crossover. Pair distribution functions of Ar and Fe plotted in a wide temperature range show the structural crossover and I found different slopes of PDF heights below and above the Frenkel line. My preliminary results show a similar effect for supercritical

CO_2.

I have calculated the Grüneisen parameter of supercritical matter for two model systems in a very wide range of pressure and temperature and found that γ varies in a wide range which interestingly includes the solid-like values. This result was rationalized by considering the relative weights of oscillatory and diffusive components of the supercritical system below the Frenkel line. I also found that γ is nearly constant along the Frenkel line and explained this finding using the scaling of system properties along the lines where particle dynamic changes qualitatively.

I presented evidence for propagating solid-like longitudinal phonons deeply in the supercritical regime, with wavelengths extending to interatomic separations and observed the crossover of dispersion curves. By studying temperature dependence of the shortest available wavelength and mean free paths, I related this effect to the crossover from the collective phonon to the collisional mean-free path regime of particle dynamics.

Finally, I have established thermodynamic heterogeneity of the supercritical state using three different methods of analysis. The associated thermodynamic crossover has the relative width in the range 13-20 % and corresponds to the Frenkel line.

There are several interesting immediate questions to explore in the future work.

First, it would be interesting to see more experimental work on the structural crossover, in addition to Ne, CH_4 and CO_2.

Second, future experiments can address the crossover of longitudinal excitations from the sound-like dispersion to the mean-free-path regime.

Third and finally, both modelling and experiments should address the issue of the thermodynamic crossover in the supercritical systems at cv=2. This should be done with finer temperature revolution. This will enable us to

calculate the width of the crossover more precisely and answer an important question of whether a phase transition operated at the Frenkel line.

Appendix A

Publication list

1. L. Wang, C. Yang, M. T. Dove, Yu. D. Fomin, V. V. Brazhkin and K. Trachenko. Direct links between dynamical, thermodynamic, and structural properties of liquids: Modeling results. Physical Review E 95, 032116 (2017)

2. L. Wang, M. T. Dove, K. Trachenko, Yu. D. Fomin and V. V. Brazhkin. Supercritical Grüneisen parameter and its universality at the Frenkel line. Physical Review E 96, 012107 (2017)

3. L. Wang, C. Yang, M. T. Dove, A. V. Mokshin, V. V. Brazhkin and K. Trachenko. The nature of collective excitations at extreme supercritical conditions. Scientific Reports, 9, 755 (2019)

4. L. Wang, C. Yang, M. T. Dove, V. V. Brazhkin and K. Trachenko. Thermodynamic heterogeneity and crossover in the supercritical state of matter. (under review)

5. S. Marinakis, L. Wang, K. Trachenko and A. Soper, Experimental evidence of the Frenkel line in supercritical CO2. (In preparation)

Bibliography

[1] J. Frenkel, Kinetic Theory of Liquids (Oxford University Press, 1947).

[2] J. P. Boon and S. Yip, Molecular Hydrodynamics (Courier Dover Publications, 1980).

[3] N. H. March, Liquid Metals (Cambridge University Press, 1990).

[4] N. H. March and M. P. Tosi, Atomic Dynamics in Liquids (Dover Publications, 1991).

[5] S. Chapman and T. G. Cowling, The Mathematical Theory of Non-uniform gases (Cambridge University Press, 1995).

[6] U. Balucani and M. Zoppi, Dynamics of the Liquid State (Oxford University Press, 1995).

[7] J. M. Ziman, Models of disorder (Cambridge University Press, 1995).

[8] R. Zwanzig, Non-Equlibrium Statistical Mechanics (Oxford University Press, 2001).

[9] J. L. Barrat and J. P. Hansen, Basic Concepts for Simple and Complex Fluids (Cambridge University Press, 2003).

[10] T. E. Faber, Introduction to the Theory of Liquid Metals (Cambridge University Press, 2010).

[11] J. P. Hansen and I. R. McDonald, Theory of Simple Liquids (Elsevier, 2013).

[12] L. D. Landau and E. M. Lifshitz, Statistical Physics (Pergamon Press, 1969).

[13] V. V. Brazhkin, Yu. D. Fomin, A. G. Lyapin, V. N. Ryzhov and K. Trachenko, Phys. Rev. E **85**, 031203 (2012).

[14] V. V. Brazhkin, Yu. D. Fomin, A. G. Lyapin, V. N. Ryzhov, E. N. Tsiok and K. Trachenko, Phys. Rev. Lett. **111**, 145901 (2013).

[15] G. Grimvall, Phys. Scripta **11**, 381 (1975).

[16] D. C. Wallace, Phys. Rev. E **57**, 1717 (1998).

[17] K. Trachenko and V. V. Brazhkin, Rep. Prog. Phys. **79**, 016502 (2016).

[18] E. Kiran, P. G. Debenedetti and C. J. Peters, Supercritical Fluids: Fundamentals and Applications, NATO Science Series E: Applied Sciences (Kluwer Academic Publishers, Boston, 2000).

[19] J. McHardy and S. P. Sawan, Supercritical Fluid Cleaning: Fundamentals, Technology and Applications (Westwood, Noyes Publications, 1998).

[20] V. V. Brazhkin and K. Trachenko, Physics Today **65(11)**, 68 (2012).

[21] Yu. D. Fomin, V. N. Ryzhov, E. N. Tsiok, V. V. Brazhkin, K. Trachenko, arXiv:1411.6849

[22] L. Xu, P. Kumar, S. V. Buldyrev, S.-H. Chen, P. H. Poole, F. Sciortino, and H. E. Stanley, PNAS **102**, 16558 (2005).

[23] G. G. Simeoni, T. Bryk, F. A. Gorelli, M. Krisch, G. Ruocco, M. Santoro and T. Scopigno, Nat. Phys. **6**, 503 (2010).

[24] M. P. Allen and D. J. Tildesley, Computer Simulation of Liquids (Oxford Science Publications, New York, 1987).

[25] B. J. Alder and T. E. Wainwright, J. Chem. Phys. **27**, 1208 (1957).

[26] B. J. Alder and T. E. Wainwright, J. Chem. Phys. **31**, 459 (1959).

[27] A. Rahman, Phys. Rev. A **136**, 405 (1964).

[28] F. H. Stillinger and A. Rahman, J. Chem. Phys. **60**, 1545 (1974).

[29] J. A. McCammon, B. R. Gelin and M. Karplus, Nature (Lond.) **267**, 585 (1977).

[30] I. T. Todorov and W. Smith, Phil. Trans. R. Soc. (Lond.) A **362**, 1835 (2004).

[31] I. T. Todorov, W. Smith, M. T. Dove and K. Trachenko, J. Mater. Chem. **16**, 1911 (2006).

[32] W. Smith, Comput. Phys. Commun. **62**, 229 (1991).

[33] W. Smith, Theoretica. Chim. Acta. **84**, 385 (1993).

[34] M. R. S. Pinches, D. Tildesley and W. Smith, Molecular Simulation **6**, 51 (1991).

[35] D. C. Rapaport, Comput. Phys. Commun. **62**, 217 (1991).

[36] D. Fincham, Molecular Simulation **8**, 165 (1992).

[37] M. T. Dove, Introduction to Lattice Dynamics (Cambridge University Press, 1993).

[38] J. L. Yarnell, M. J. Katz, R. G. Wenzel and S. H. Koenig, Phys. Rev. A **7**, 2130 (1973).

[39] M. Gao, A. M. Misquitta, C. Yang, I. T. Todorov, A. Mutters and M. T. Dove, Mol. Syst. Des. Eng. **2**, 457-469 (2017).

[40] A. B. Belonoshko, R. Ahuja and B. Johansson, Phys. Rev. Lett. **84**, 3638 (2000).

[41] P. P. Ewald, Annalen der Physik. **369**, 253?287 (1921).

[42] L. Wang, C. Yang, M. T. Dove, Yu. D. Fomin, V. V. Brazhkin and K. Trachenko, Phys. Rev. E **95**, 032116(2017).

[43] L. D. Landau and E. M. Lifshitz, Fluid Mechanics (Butterworth-Heinemann, 1987).

[44] J. R. D. Copley and J. M. Rowe, Phys. Rev. Lett. **32**, 49 (1974).

[45] W. C. Pilgrim, S. Hosokawa, H. Saggau, H. Sinn and E. Burkel, J. Non-Cryst. Sol. **250-252**, 96 (1999).

[46] E. Burkel, Rep. Prog. Phys. **63**, 171 (2000).

[47] W. C. Pilgrim and C. Morkel, J. Phys.: Condens. Matt. **18**, R585 (2006).

[48] T. Scopigno, G. Ruocco and F. Sette, Rev. Mod. Phys. **77**, 881 (2005).

[49] G. Ruocco and F. Sette, J. Phys.: Condens. Matt. **11**, R259 (1999).

[50] S. Hosokawa, M. Inui, Y. Kajihara, K. Matsuda, T. Ichitsubo, W.-C. Pilgrim, H. Sinn, L. E. González, D. J. González, S. Tsutsui and A. Q. R. Baron, Phys. Rev. Lett. **102**, 105502 (2009).

[51] S. Hosokawa, M. Inui, Y. Kajihara, S. Tsutsui and A. Q. R. Baron, J. Phys.: Condens. Matt. **27**, 194104 (2015).

[52] V. M. Giordano and G. Monaco, PNAS **107**, 21985 (2010).

[53] V. M. Giordano and G. Monaco, Phys. Rev. B **84**, 052201 (2011).

[54] S. Hosokawa, S. Munejiri, M. Inui, Y. Kajihara, W.-C. Pilgrim, Y. Ohmasa, S. Tsutsui, A. Q. R. Baron, F. Shimojo and K Hoshino, J. Phys.: Condens. Matt. **25**, 112101 (2013).

[55] A. Cunsolo, G. Pratesi, R. Verbeni, D. Colognesi, C. Masciovecchio, G. Monaco, G. Ruocco and F. Sette, J. Chem. Phys. **114**, 2259 (2001).

[56] M. Grimsditch, R. Bhadra and L. M. Torell, Phys. Rev. Lett. **62**, 2616 (1989).

[57] F. Scarponi, L. Comez, D. Fioretto and L. Palmieri, Phys. Rev. B **70**, 054203 (2004).

[58] E. Pontecorvo, M. Krisch, A. Cunsolo, G. Monaco, A. Mermet, R. Verbeni, F. Sette and G. Ruocco, Phys. Rev. E **71**, 011501 (2005).

[59] A. Cunsolo, G. Pratesi, R. Verbeni, D. Colognesi, C. Masciovecchio, G. Monaco, G. Ruocco and F. Sette, Phys. Rev. B **85**, 174305 (2012).

[60] K. Trachenko, Phys. Rev. B **78**, 104201 (2008).

[61] A. R. Dexter and A. J. Matheson, Trans. Faraday Soc. **64**, 2632 (1968).

[62] D. C. Wallace, Phys. Rev. A **25**, 3290 (1982).

[63] F. Puosi and D. Leporini, J. Chem. Phys. **136**, 041104 (2012).

[64] V. V. Brazhkin, A. G. Lyapin, V. N. Ryzhov, K. Trachenko, Yu. D. Fomin, E. N. Tsiok, Physics-Uspekhi **55(11)**, 1061 (2012).

[65] Yu. D. Fomin, V. N. Ryzhov, E. N. Tsiok, V. V. Brazhkin and K. Trachenko, J. Phys.: Condens. Matt **28**, 43LT01 (2016).

[66] Yu. D. Fomin, V. N. Ryzhov, E. N. Tsiok and V. V. Brazhkin, Sci. Rep. **4**, 7194 (2014).

[67] C. Yang, V. V. Brazhkin, M. T. Dove and K. Trachenko, Phys. Rev. E **91**, 012112 (2015).

[68] S. Sengupta, F. Vasconcelos, F. Affouard and S. Sastry, J. Chem. Phys. **135**, 194503 (2011).

[69] C. Dasgupta, A. V. Indrani, S. Ramaswamy and M. K. Phani, Europhys. Lett. **15**, 307 (1991).

[70] S. C. Glotzer, V. N. Novikov and T. B. Schrøder, J. Chem. Phys. **112**, 509 (2000).

[71] N. Lacevic, F. W. Starr, T. B. Schrøder and S. C. Glotzer, J. Chem. Phys. **119**, 7372 (2003).

[72] C. Donati, S. Franz, S. C. Glotzer and G. Parisi, J. Non-Cryst Solids **307**, 215224 (2002).

[73] S. Karmakar, C. Dasgupta and S. Sastry, Proc. Natl. Acad. Sci. U.S.A. **106**, 3675 (2009).

[74] D. Frenkel and B. Smit, Understanding molecular simulation: from algorithms to applications (Academic press, 2001).

[75] S. Liu, M. A. Doverspike and M. S. Conradi, J. Chem. Phys. **81**, 6064 (1984).

[76] S. Lin, M. Blanco and W. A. Goddard III, J. Chem. Phys. **119**, 11792 (2003).

[77] C. Yang, M. T. Dove, V. V. Brazhkin and K. Trachenko, Phys. Rev. Lett. **1**18, 215502 (2017).

[78] P. S. Salmon, R. A. Martin, P. E. Mason and G. J. Cuello, Nature **435**, 75 (2005).

[79] D. Bolmatov, V. V. Brazhkin, Yu. D. Fomin, V. N. Ryzhov and K. Trachenko, J. Chem. Phys. **139**, 234501 (2013).

[80] C. Prescher, Yu. D. Fomin, V. B. Prakapenka, J. Stefanski, K. Trachenko and V. V. Brazhkin, Phys. Rev. B **9**5, 134114 (2017).

[81] D. Smith, M. A. Hakeem, P. Parisiades, H. E. Maynard-Casely, D. Foster, D. Eden, D. J. Bull, A. R. L. Marshall, A. M. Adawi, R. Howie, A. Sapelkin, V. V. Brazhkin, and J. E. Proctor, Phys. Rev. E. **96**, 052113 (2017).

[82] A. A. Maradudin, E. W. Montroll, G. H. Weiss and I. P. Ipatova, Theory of Lattice Dynamics in the Harmonic Approximation (Academic, New York, 1971).

[83] S. O. Yurchenko, N. P. Kryuchkov and A. V. Ivlev, J. Chem. Phys. **143**, 034506 (2015).

[84] E. I. Andritsos, E. Zarkadoula, A. E. Phillips, M. T. Dove, C. J. Walker, V. V. Brazhkin and K. Trachenko, J. Phys. Condens. Matt. **25**, 235401 (2013).

[85] D. Bolmatov and K. Trachenko, Phys. Rev. B **84**, 054106 (2011).

[86] L. Wang, M. T. Dove, K. Trachenko, Yu. D. Fomin and V. V. Brazhkin, Phys. Rev. E **96**, 012107 (2017).

[87] L. A. Girifalco, Statistical mechanics of solids, (Oxford University Press, New York, 2000).

[88] N. L. Vocadlo and G. D. Price, Phys. Earth Planet. Inter. **82**, 261-270 (1994).

[89] F. Occelli, P. Loubeyre and R LeToullec, Nature Materials **2**, 151-154 (2003).

[90] M. T. Dove and H. Fang, Rep. Prog. Phys. **79**, 066503 (2016).

[91] V. V. Brazhkin, A. G. Lyapin, V. N. Ryzhov, K. Trachenko, Yu. D. Fomin and E. N. Tsiok, Phys. Usp. **55**, 773 (2012).

[92] V. Gospodinov, Int. J. Mod. Phys. B **28**, 1450196 (2014).

[93] N. F. Carnahan and K. E. Starling, J. Chem. Phys. **51**, 635 (1969).

[94] M. de. Souza, P. Menegasso, R. Paupitz, A. Seridonio and R. E. Lagos, Eur. J. Phys. **37**, 055105 (2016).

[95] J. W. Shaner, J. Chem. Phys. **89**, 1616 (1988).

[96] J. W. Shaner, High Pressure Research **4**:1-6, 561 (1990).

[97] J. B. Lurie, J. Low Temp. Phys. **10** 751 (1973).

[98] A. M. Krivtsov and V. A. Kuz'kin, Mech. Solids **46**, 387 (2011).

[99] L. Knopoff and J. N. Shapiro, Phys. Rev. B **1**, 3893 (1970).

[100] S. K. Kor, U. S. Tandon and B. K. Singh, Phys. Lett. **38**A, 187 (1972).

[101] J. Amoros, J. R. Solana and E. Villar, Mater. Chem and Phys. **20**, 255 (1988).

[102] I. H. Umirzakov, Journal of Engineering Thermophysics, V.**11**, N**3**, 265-273 (2002).

[103] J. S. Emampour, A. Morsali, S. A. Beyramabadi, M. R. Bozorgmehr and K. Khakzadan, Int. J. Phys. Sci. **6** (24) 5731-5737 (2011).

[104] S. M. Stishov, JETP **130**, 276 (2006).

[105] J. Hansen, Phys. Rev. A **2**, 221 (1970).

[106] T. H. Berlin and E. W. Montroll, J. Chem. Phys. **20**, 75 (1952).

[107] S. M. Stishov, Sov. Phys. Usp. **17**, 625 (1975).

[108] Y. Hiwatari, H. Matsuda, T. Ogava, N. Ogita and A. Ueda, Prog. Theor. Phys. **52**, 1105 (1974).

[109] V. V. Zhakhovsky, JETP **105**, 1615 (1994).

[110] S. Plimpton, J. Comp. Phys, **117**, 1-(1995), http://lammps.sandia.gov/index.html.

[111] Yu. D. Fomin, V. N. Ryzhov and V. V. Brazhkin, J. Phys.: Condens. Matt. **25**, 285104 (2013).

[112] L. Wang, C. Yang, M. T. Dove, A. V. Mokshin, V. V. Brazhkin and K. Trachenko, Scientific Reports **9**, 755 (2019)

[113] Yu. D. Fomin, V. N. Ryzhov, E. N. Tsiok, V. V. Brazhkin and K. Trachenko, J. Phys.: Condens. Matt. **28**, 43LT01 (2016).

[114] Yu. D. Fomin, V. N. Ryzhov, E. N. Tsiok, J. E. Proctor, C. Prescher, V. B. Prakapenka, K. Trachenko and V. V. Brazhkin, J. Phys.: Condens. Matt. **30**, 134003 (2018).

[115] D. Bolmatov, V. V. Brazhkin and K. Trachenko, Nat. Comm. **4**, 2331 (2013).

[116] V. M. Giordano and G. Monaco, PNAS **107**, 21985 (2010).

[117] V. M. Giordano and G. Monaco, Phys. Rev. B **84**, 052201 (2011).

[118] S. O. Yurchenko et al, J. Chem. Phys. **148**, 134508 (2018).

[119] N. P. Bailey, U. R. Pedersen, N. Gnan, T. B. Schrøder and J. C. Dyre, J. Chem. Phys. **129**, 184507 (2008).

[120] NIST database Thermophysical properties of fluid systems, see http://webbook.nist.gov/chemistry/fluid.

[121] S. K. Ma, Modern theory of critical phenomena (Westview Press, 2000).

[122] S. Marinakis et al (in preparation).

[123] V. V. Brazhkin, Yu. D. Fomin, A. G. Lyapin, V. N. Ryzhov and E. N. Tsiok, J. Phys. Chem. B **115**, (48) 14112 ((2011).

[124] V. V. Brazhkin and V. N. Ryzhov, J. Chem. Phys. **135**, 084503 (2011).

[125] N. P. Bailey, U. R. Pedersen, N. Gnan, T. B. Schrøder and J. C. Dyre, J. Chem. Phys. **129**, 184507 (2008).